Arbeitsgruppe für Strahlenmedizininische Forschung
und
WHO-Kollaborationszentrum für Strahlenunfallmanagement
an der
Universität Ulm

Leiter: Prof. (em.) Dr. med. Dr. hc. mult. T.M. Fliedner

Simulation of Radiation Effects Using Biomathematical Models of the Megakaryocytic Cell Renewal System

Dissertation zur Erlangung des Doktorgrades der Humanbiologie
der Medizinischen Fakultät der Universität Ulm

Vorgelegt von

Dieter Hans Gräßle
aus Lauingen an der Donau
2000

Amtierender Dekan:	Prof. Peter Gierschik
1. Berichterstatter:	Prof. Theodor M. Fliedner
2. Berichterstatter:	Prof. H. Wolff
Tag der Promotion:	14.07.2000

Contents

ABBREVIATIONS

$\mathbb{R}$	Set of Real Numbers
^{3}HDFP	Tritium Labeled Diisopropylfluorophosphate
^{3}H-thymidine	Tritium Labeled Thymidine
5-FU	5-Fluorouracyl
AChE	Acetylcholinesterase
API	Application Program Interface
APS	Anti Platelet Serum
BFU-Mk	Burst Forming Unit - Megakaryocyte
C1	Early Committed Progenitors (Model)
C2	Late Committed Progenitors (Model)
CC	Committed (Progenitor) Cells
CD34	Cluster of Differentiation 34
CFU-GEMM	Colony Forming Unit - Granulocyte Erythrocyte Megakaryocyte Monocyte
CFU-GM	Colony Forming Unit- Granulocyte Monocyte
CFU-Mk	Colony Forming Unit - Megakaryocyte
CFU-S	Colony Forming Unit - Spleen
DBMS	Database Management System
DNA	Deoxyribonucleic Acid
EMB	Endoreduplicating Progenitors and Megakaryoblasts (Model)
GUI	Graphical User Interface
LET	Linear Energy Transfer
METREPOL	Medical Treatment Protocols
Mk	Megakaryocytes
MKi	Megakaryocytes (Model)
MkMass	Megakaryocyte Mass
NC	Noncommitted Progenitor Cells (Model)
ODE	Ordinary Differential Equation

PC	Personal Computer
PS	Pluripotent Stem Cells
PSinj	Injured Stem Cells
RC	Response Category
Reg	Regulator
SC	Stem Cells
SQL	Standard Query Language
TBI	Total Body Irradiation
TH	Thrombocytes (Model)

Chapter 1

Introduction and Overview

Mathematical biology is one of the fast growing areas of interdisciplinary research. The use of mathematics in biology and medicine increases as research in biological and medical science becomes more and more quantitative and complex. On the other hand, mathematics and computer science have developed new mathematical and computational methods to solve complex mathematical problems. Thus, the basis was created to apply mathematical formalisms to describe the complex processes of various systems in biology and other scientific disciplines.

1.1 Interaction of Mathematics and Biomedical Research

Looking at the development of sciences in the past years it can be recognized that the different disciplines of research are successively tearing down separating walls and are starting to cooperate in order to solve problems, or even grow together. Especially in medicine the connection of biology and mathematics produced new approaches to generate knowledge. The basic element in application of mathematics to other sciences is the "model", which is used to translate "nonmathematical" realities into mathematical formalisms. The best known example is epidemiology, which connects research on health and statistic models to produce new insights on the spread of diseases and to implement the results in health policy making. Another area of medical research in which mathematical flow models were early recognized to be the appropriate method is pharmakokinetics. There, the key problem is to describe the distribution of substances in the organ systems of the body as a function of time.

Mathematical models can support research in many ways:

- Models can help to understand complex systems by representation of the knowledge in a closed and uniform way.

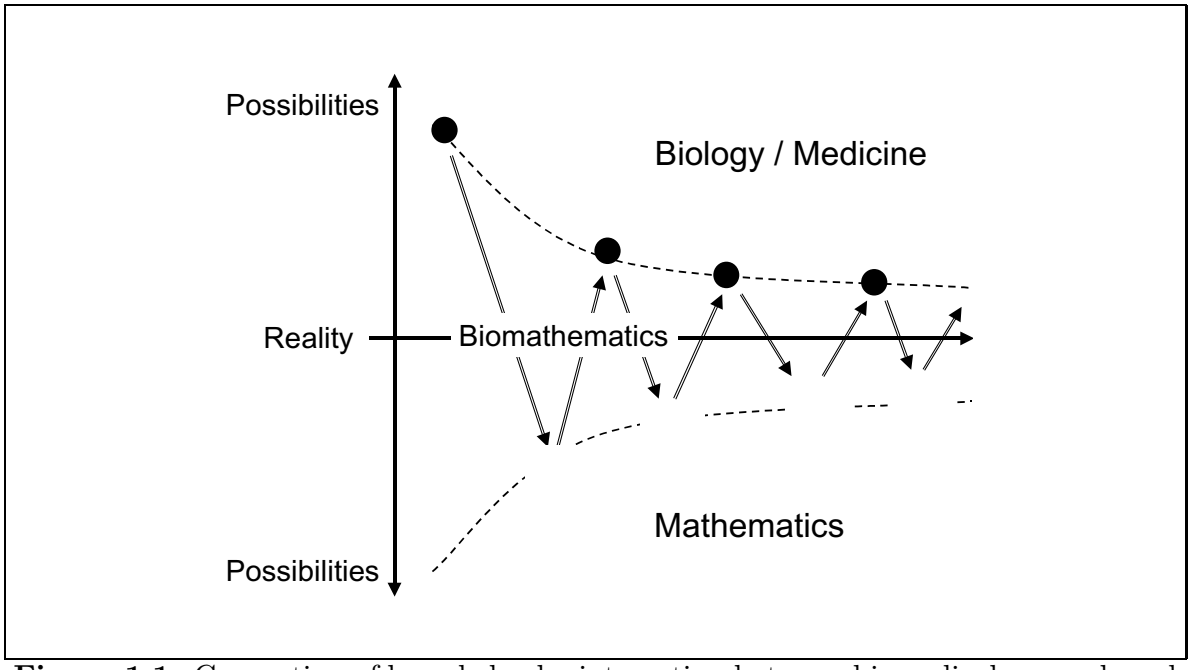

Figure 1.1: Generation of knowledge by interaction between biomedical research and mathematics.

- Models can help to find gaps of knowledge and to build new hypothesis.
- Models can identify demand for experiments and help to design the setup.
- Models can indirectly produce information on parameters, which are biologically hard to determine.
- Models can give medical assistance in diagnosis, prognosis and therapy.

The work done by biomathematics should not be seen only as simply combining biological facts and mathematical methods for calculations. Biomathematics should be a permanent interaction between biomedical research and mathematics. For example, mathematical models can help to give explanatory approaches and to set up new hypothesis. These hypothesis can be proved or rejected by biology and medicine and then improve the models. On the other hand, mathematical research is stimulated by the demand of methods and applications. This way the search for "reality" is an interacting process from two complementary sides, like vizualized in figure 1.1.

As can be seen mathematics have been established now in many areas of biomedical research. However, the development of interdisciplinary sciences such as biomathematics is still in progress.

1.2 Biomathematical Models and Hematopoietic Radiation Effects

In the case of accidental acute or chronic irradiation of humans one of the basic problems for diagnosis and therapy is the assessment of the degree of damage to the hematopoietic system. Often diagnosis and therapy is based on radiophysical dose estimations. But these are not very helpful for the medical management of patients in the first days after a radiation accident as not much is known about the course of the events, the radiation quality, and the absorbed dose. Furthermore, physical information on exposure doses are not sufficient for valid conclusions on the effects to the organism. Basis for the assessment and therapy of radiation accident victims should rather be clinical indicators, which do not depend on complicated physical dose evaluations and individual radiation sensitivities.

The Radiation Medicine Research Group of the University of Ulm, which also has the mandate of a WHO-Collaborating Center for Radiation Accident Management, investigates the effects of ionizing irradiation to the human organism. The objective of this group is to elaborate methods of diagnosis and therapy for the management of radiation accident victims. This research work is based on the evaluation of patient data stored in a database on radiation accidents of the past.

One of the essential tasks after or during radiation exposure is the assessment of the degree of damage to the hematopoietic stem cell system. If the damage of the stem cell pool can be recognized early to be reversible, a therapy with blood substitutes can be sufficient to bridge a critical phase. In the irreversible case, a stem cell transplantation therapy has to be applied. This restoration of the hematopoietic system is a decisive factor for the prognosis and therapy, since damages of the stem cell system can result in life threatening low peripheral blood cell numbers. For example, the granulocyte and platelet nadirs lead to infections and bleedings.

Direct diagnosis of the degree of damage of the stem cell pool is very difficult. The bone marrow is distributed throughout the whole skeleton and thus local inhomogenities of bone marrow damage can disturb diagnostic methods. On the other hand, one can recognize characteristic patterns in the blood cell numbers after irradiation as a

function of time. An exact understanding of the cell production mechanisms of hematopoiesis is the prerequisite for the analysis of the effects of ionizing irradiation to the stem cell pool and the resulting disturbances of cell numbers in the peripheral blood. An appropriate representation of this understanding of hematopoietic mechanisms is the closed representation of the knowledge and assumptions about hematopoiesis in the form of a biomathematical model.

1.3 Objectives of the Presented Thesis

The work presented in this thesis are mathematical model based approaches for the analysis of radiation effects on the hematopoietic and in particular on the thrombocytopoietic system. The methods developed are supposed to give explanations for the dynamics of the hematopoietic system under certain irradiation patterns. In particular, the following questions are points of interest:

- Is it possible to reflect the process of thrombocytopoiesis in a biomathematical model representing the development from the pluripotent stem cell to the thrombocyte?
- Is it possible to simulate, with appropriate model extensions, the effects of acute irradiation to hematopoiesis?
- Is it possible to estimate the surviving fractions of pluripotent stem cells after irradiation based on blood counts and model based estimation methods?
- How is the surviving fraction after irradiation of pluripotent stem cells related to the severity of the hematological manifestation of the acute radiation syndrome?
- Is it possible to simulate the effects of chronic irradiation to hematopoiesis?
- In which way does permanent excess cell loss caused by chronic irradiation influence the hematopoietic stem cell system?
- How are microdosimetric hits on the cellular level correlated with the excess cell loss rate under chronic radiation exposure?

To answer these questions, biomathematical methods for calculation of model parameters have to be developed and the biological realities and mathematical techniques for modeling have to be combined. Thus, relevant biological and mathematical backgrounds, which are necessary for developing a biomathematical model of thrombocytopoiesis, have to be identified. Mathematical methods for the evaluation of results of biological experiments have to be selected or developed. A basic mathematical model of thrombocytopoiesis has to be constructed and validated. To simulate the effects of acute and chronic irradiation on the thrombocytopoietic system, it is necessary to set up the appropriate model extensions for reduced and injured stem cell populations, and permanent excess cell loss.

An estimation routine for remaining and injured stem cell numbers after acute irradiation has to be developed and implemented.

In the case of chronic irradiation, an estimator for radiation induced excess cell loss rates has to be set up.

These estimation problems require the construction of least-square estimators based on the extended models and nonlinear optimization routines.

Microdosimetric calculations based on linear energy transfers in tissue and photon energies have to be performed for the comparison of estimated excess cell loss to particle traversals on the cellular level.

1.4 Overview on the Thesis

This thesis shows the application of mathematical models in the analysis of the effects of acute and chronic radiation exposure to the hematopoietic system.

Chapter 2 *Material and Methods* explains the relevant backgrounds of biology, mathematics, computer science, and data processing. In particular it shows the methods applied to construct the model of thromobocytopoiesis.

Chapter 3 *Results* describes the constructed model of thrombocytopoiesis in rodents and the results of the application of extended models to data of animal irradiation experiments and humans who were involed to radiation accidents.

Chapter 4 *Discussion* compares the constructed model and the applications to previous work done by different authors. The methods developed for the application of extended and modified models to radiation effects are discussed regarding their application in research and clinical use.

Chapter 5 *Summary* comprises the most important steps of development, validation, modification, and application of the modeling work. In addition, further developments and future goals are outlined.

Chapter 2

Material and Methods

Contents

2.1 Biological and Radiological Aspects

For understanding and modeling the process of thrombocytopoiesis a detailed knowledge of some biological aspects is necessary. This chapter gives a short introduction to the most important aspects regarding the cell physiological backgrounds of hematopoiesis and thrombocytopoiesis in particular and of experimental techniques to study the relevant parameters of cell turnover.

2.1.1 The Physiology of Hematopoiesis and Thrombocytopoiesis

The basic elements of hematopoiesis and thrombocytopoiesis are cells with their physiological characteristics. Mostly all experimental techniques and modeling approaches as well as radiation effects on hematopoiesis take place on the cellular level. The first step for modeling the dynamics of cellular tissues is to understand the "life cycle" of the cell.

2.1.1.1 Cell Cycle

The term cell cycle is generally used to characterize the series of phases that occur as a sequence of events in the process of cellular division like (figure 2.1). Some of these phases are characteristic for proliferating (dividing) cells, and thus by counting the frequency by which these phases occur one can assess the proliferative activity of a cell population. The cell cycle phases can be described by the following items:

- Interphase

  This phase denotes the time between ("inter") two mitoses and can be substructured into:

  - G_1 phase (Gap1, presynthetic phase, postmitotic phase)

    In this phase the cell performs its specific functional activities, like synthesis of proteines and RNA. The time spent in this phase is extremely variable and depends on many factors, like organ, stimulation, and inhibition. Strongly proliferating cells show a short G_1 phase, nonproliferating cells a very long one.

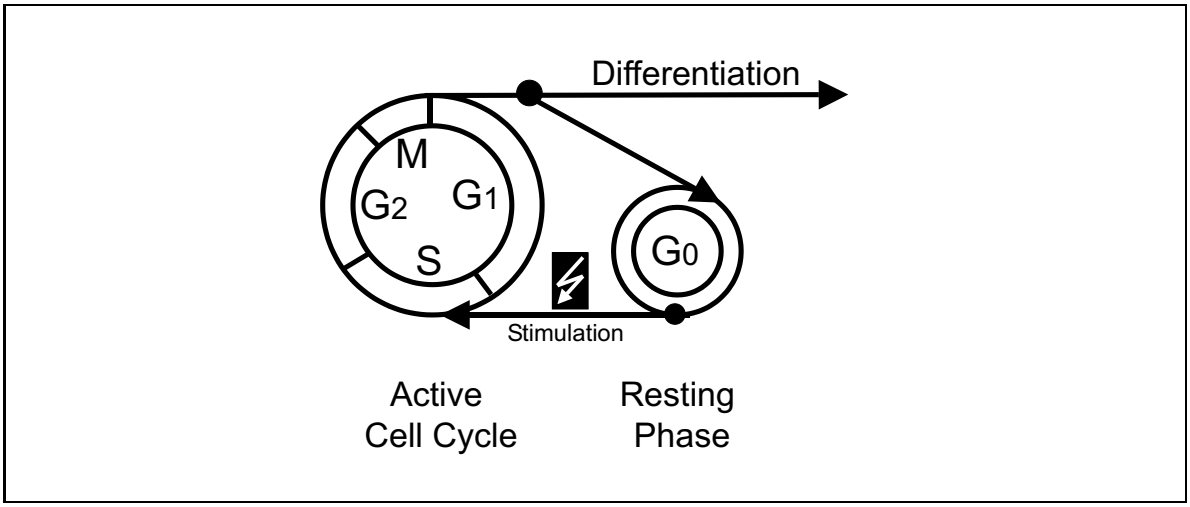

Figure 2.1: Subdivision of of cells in resting and actively proliferating cells by cell cycle characteristics.

- S phase (DNA synthesis)

  In this phase the cell synthesizes DNA (Deoxyribonucleic Acid) for the duplication of the cell nucleus. The time interval needed for the S phase is approximatly constant within one species. For measuring DNA synthesis times, cells can be labeled by incorporation of radioactive DNA precursors such as ^{3}H-thymidin.

- G_2 phase (Gap2, postsynthetic phase)

  A short period before subsequent division.

- M (mitotic phase, phase of cell division)

  Within this phase the cell performs nucleus and cell division including identical replication of the chromosomes.

- G_0 phase (resting phase)

  Some cells are able to become proliferatively inactive within the G_1 phase and get "arrested" in the so called G_0 phase, until they are activated again ("triggered") by a special stimulus. This feature is characteristic for the stem cells.

Reviews on this topic can be found in [46] [27].

If one knows the times or the time ratios of the different phases, especially the durations of the S phase and the cell generation cycle, information on the proliferation and maturation of cell populations can be derived, for example, by single cell autoradiography [4] [25].

2.1.1.2 Biological Model of Hematopoiesis

The cells of the peripheral blood are nearly completely produced in the bone marrow, which is located in the cavities of the bones of the skeleton. Bone marrow can be differentiated into the red and the yellow bone marrow. The red bone marrow is the part that is actively participating in the production of blood cells and is colored red by erythrocytes and their precursors. The yellow bone marrow contains mainly fat cells and is normally not involved in hematopoiesis. It can be activated and changed to active hematopoietic tissue on demand. The blood producing cells are embedded in a cellular bone marrow matrix, the stroma.

The stem cells, their progenitors, and the precursors of the different cell lineages of the blood (erythrocytes, granulocytes, thrombocytes, and lymphocytes) reside in the bone marrow. According to the names of the several blood cell populations the cell renewal processes of these lines are called erythropoiesis, granulocytopoiesis, thrombocytopoiesis, and lymphocytopoiesis.

Todays knowledge of on the structure of hematopoiesis can be summarized in a "biological" model of hematopoiesis (figure 2.2) following Heimpel and Pruemmer [38]. This model is derived from morphological observations, microkinematographic techniques, cell colony experiments, labeling experiments and others. Following this model all blood cells derive from the pluripotent stem cell pool. The term "pluripotent" means the ability to generate all blood cell lines and the potential of live long (unlimited) self replication. During their development from the pluripotent stem cells to fully differentiated cells they perform multiple divisions and differentiations. With increasing differentiation they loose the pluripotent features and become continously more committed to a certain cell line and will finally differentiate into peripheral blood cells. Hematopoietic cells can be structured into pluripotent stem cells, noncommitted progenitor cells (cells which are capable to generate mixed colonies of different hematopoietic cell lines), committed progenitor cells (cells which are determined to develop into one certain cell line), precursor cells and differentiated cells [74].

The circles in figure 2.2 mark the steps of thrombocytopoieis, which is the basic biological model used for building the mathematical model.

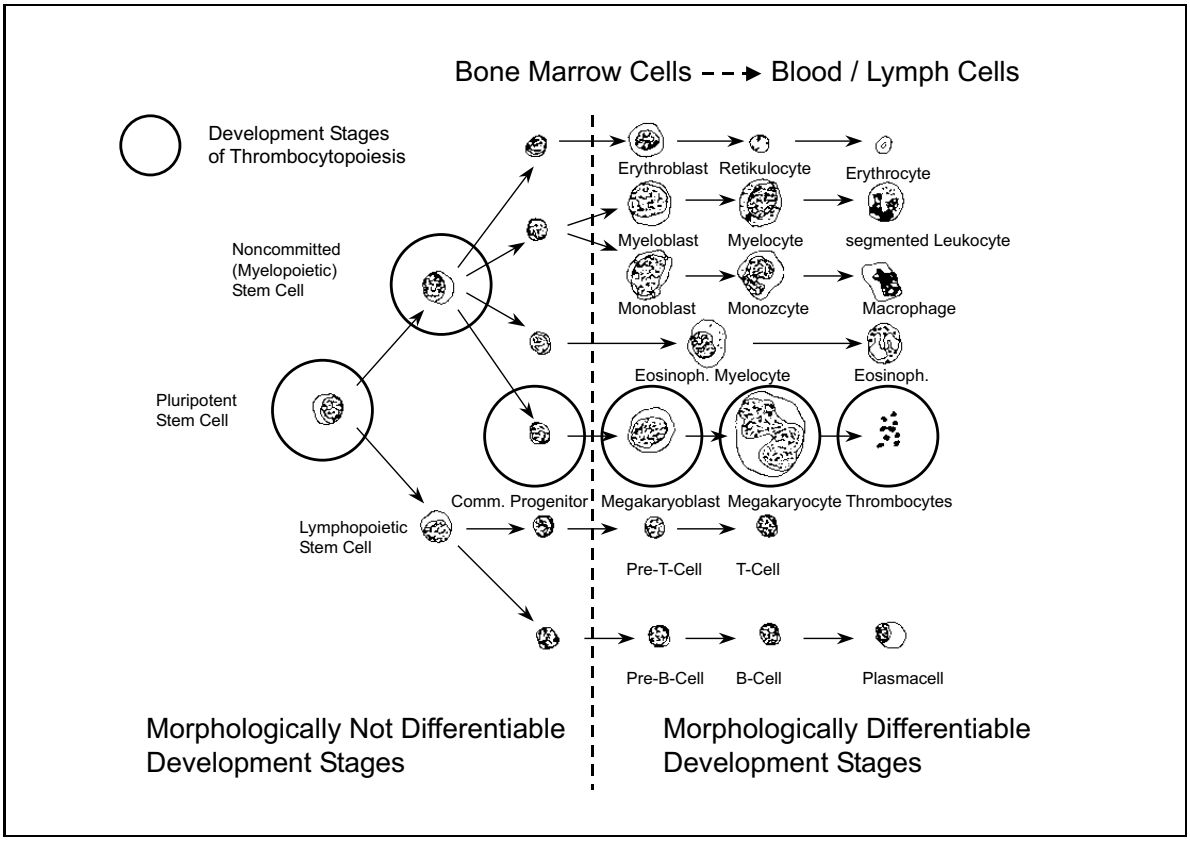

Figure 2.2: The biological model of hematopoiesis in mammalians and humans following Heimpel and Pruemmer [38].

2.1.2 Cell Development Stages of Thrombocytopoiesis

The term thrombocytopoiesis summarizes the process of the production of blood platelets in the mammalian organism. This process follows different stages of cellular development (figure 2.2), starting at the level of the pluripotent stem cells.

2.1.2.1 Pluripotent Stem Cells (PS)

Following todays knowledge on hematopoiesis it must be assumed, that the source of all blood and lymphatic cells are the pluripotent stem cells (PS), which are found mainly in the bone marrow and at comparatively low concentrations in the blood. In rodents, stem cells are also found in the spleen. Pluripotent stem cells are morphologically not recognizable and can not be differentiated exactly by labeling techniques. As pluripotent stem cells have the capability of unlimited self replication, they are able to maintain their own cell population and the blood cell production of the organism for its whole life time (unless severe disturbances occur) [74]. In the steady state system on average every second cell leaves the stem cell compartment for differentiation, the

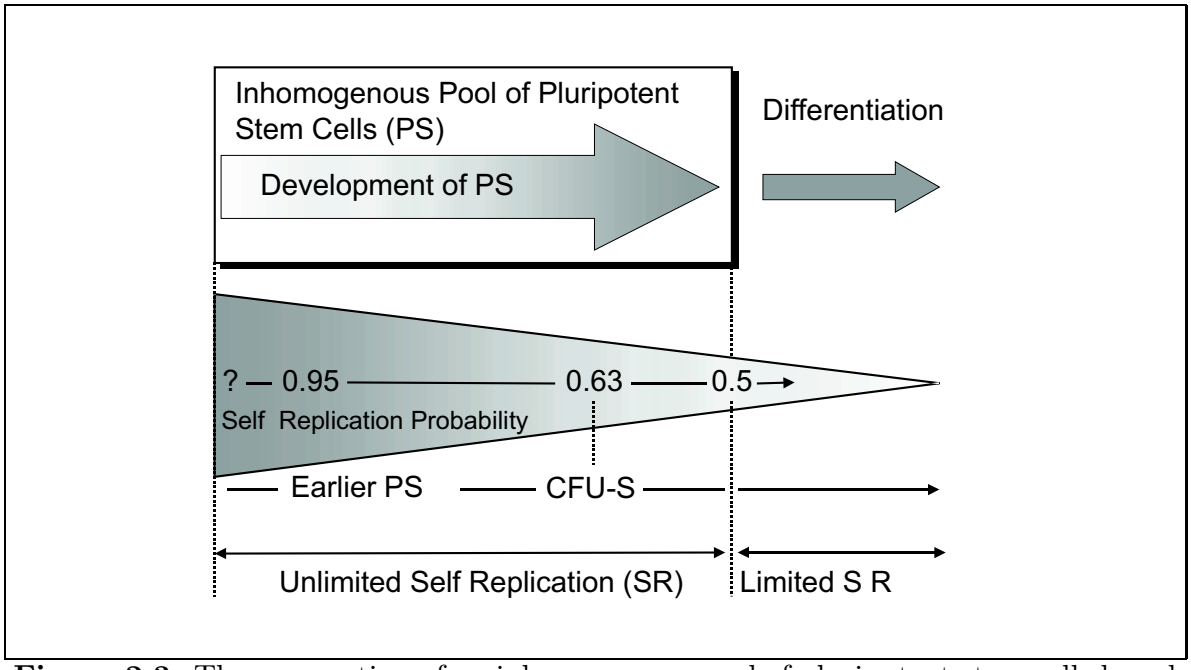

Figure 2.3: The assumption of an inhomogenous pool of pluripotent stem cells based on a continously changing self replication probability.

other remains to maintain the number of pluripotent stem cells at a constant level (asymmetric divisions). Estimations of the concentration of earliest pluripotent stem cells in bone marrow are in the area of about 10^{-5} [95]. Only about 10% of these cells are active in cell cycle [41], the rest remains in a resting phase, until they are triggered into activity [32]. This shows the great redundancies of the hematopoietic system. Self replication probabilities for different kinds of pluripotent stem cell populations are estimated to be 0.5-0.63 [70] for the murine CFU-S (Colony Forming Unit - Spleen) cells, which are histogenetically near to the pluripotent stem cells, by a method developed by Vogel [97]. For fetal liver cells of dogs self replication probabilites of 0.5-0.95 are estimated [31]. CFU-S are in general observed with a frequency of about 5-30 $\cdot 10^{-5}$ in bone marrow cells of mice [70].

The different self replication probabilities and other experimental results summarized by Metcalf [70] show that the pool of pluripotent stem cells itself is a heterogenous population of cells regarding the self replication probability. It is assumed, that within the stem cell population the self replication probability is a size which decreases continously with the development of the cell. Figure 2.3 shows the assumed inhomogeneity in the pool of the pluripotent stem cells, the location of the CFU-S in the scale of possible self replication probabilities and the resulting ability of unlimited or limited self replication.

2.1.2.2 Noncommitted Progenitor Cells

The next known development stage of hematopoiesis are noncommitted progenitor cells. These cells are not able of unlimited self replication like the pluripotent stem cells, but can produce two or more different blood cell lines in one clone. One population of uncommitted progenitor cells, which are able to produce all blood cell lines in one clone are usually called myelopoietic stem cells [38]. Lymphocytopoietic cells are assumed to derive from another early progenitor cell (see figure 2.2). An in vitro example for this cell population is the CFU-GEMM (Colony Forming Unit - Granulocyte, Erythrocyte, Monocyte, Megakaryocyte) which can produce the given four cell lines. Their plating efficiency is estimated to be about $0 - 4 \cdot 10^{-5}$ [69] in bone marrow cells. Other uncommitted progenitor cells are found to produce granulocytes and macrophages [95] and many other combinations [90].

2.1.2.3 Committed Progenitor Cells

The committed progenitor cells have lost the potential to differentiate into different blood cell lines and can only develop into one special cell line. They form colonies in the bone marrow, from which the different terminal blood cells derive. In the case of the thrombocytopoietic line these cells are called CFC-Mk (Colony Forming Cells - Megakaryocyte). In vitro examples are the CFU-Mk (Colony Forming Unit - Megakaryocyte) [65] and the earlier BFU-Mk (Burst Forming Unit - Megakaryocyte) [65]. Like most "early stage" cells they can not be identified morphologically, cytochemically or immunologically [67]. In experiments concentrations of about 1-2.4 $\cdot 10^{-4}$ [99] and $3.67 \cdot 10^{-4}$ for CFU-Mk [65] and $7.3 \cdot 10^{-5}$ for BFU-Mk [65] were found.

2.1.2.4 Precursor Cells

The terms "precursor cells" and "progenitor cells" are not strictly separated and are used in an "overlapping" manner. For example, on the one hand CFU-Mk are called megakaryocytic precursors and on the other hand (in connection with stem cell research) they are termed committed progenitors.

2.1.2.5 Transitional Cells

Between the committed progenitors and the morphologically recognizable megakaryocytic precursors there is a "transitional stage" of cell development. It is assumed, that in this phase the cells change their mitotic activity from proliferation to endoreduplication which proceeds in the morphologically recognizable megakaryoblast stage [77]. Identifyable cells in this phase could be the small acetylcholinesterase positive (AChE+) cells [63] [66].

2.1.2.6 Megakaryoblasts

Megakaryoblasts are the direct progenitors of the megakaryocytes. They are observed to endoreduplicate and become morphologically recognizable at a ploidy value of about 4N to 8N [77] (see next chapter).

2.1.2.7 Megakaryocytes

The megakaryocytes are very large bone marrow cells, which are easy to distinguish morphologically from other cells. For this reason this development stage is very well known and explored regarding cell kinetic dynamics. The second very characteristic feature of the megakaryocytes is polyploidy (i.e. multiple sets of chromosomes). Polyploid cells are more powerful in the production of cytoplasm compared to normal mononuclear cells [46]. Shifting ploidy is an important reaction mechanisms of the platelet system to disturbances. Endomitotic duplications of nuclei were observed directly with the help of microkinematographic techniques by Boll [3]. The most frequent ploidy classes are 8N, 16N, 32N and 64N, where the xN numbers denote the number of (haploid) chromosome sets. After maturation the megakaryocytes break into many little fragments, the blood platelets or thrombocytes. During this fragmentation phase they form strings, the proplatelets, which brake into single platelets. At the end of this process the naked nucleus remains, which has lost mostly all of its cytoplasm. Estimations for the platelet productivity vary from 1500 to 4000 platelets per megakaryocyte [2] [28].

Megakaryocytes can be subdivided into several differentiation stages. These stages are difficult to handle since they differ in terminologies and biological criteria for the

groups are used by different authors and thus are in general not easy to compare. For this reason it was avoided to use these differentiation stages as far as possible.

2.1.2.8 Thrombocytes

The thrombocytes or blood platelets are not complete cells but disk shaped cell fragments without nuclei. The platelets fulfill an important function in homeostasis. If the platelet level decreases under certain levels (less than about 10%) bleeding can not be stopped by the organism. Even spontaneous bleedings which are typical for a severe acute radiation syndrome can appear. The platelets are renewed with a turnover time of 8-10 days in man and 4 days in rodents [5].

2.1.3 Compensation Mechanisms of Thrombocytopoiesis

For maintainance and reconstitution of hemostasis the organism actively controles physiological processes to correct deviations after disturbances. In hematopoiesis this is done by different mechanisms, which are explained in the following paragraphs.

2.1.3.1 General Reaction Mechanisms of Cell Populations to Disturbances

Cell populations with fast cell turnover are able to react to disturbances in certain ways:

- Enhancement of the fraction of actively proliferating cells
  Cellpools, which have high reserves in their production potential normally keep a part of cells in an inactive phase, the G_0 phase, which can be activated on demand.

- Variation of the number of cellular divisions in a certain stage
  In every development stage a certain average number of divisions is performed per time unit. Enhancement of this number increases cell production.

- Variation of differentiation times
  Cells can develop slower or faster into the following stage by decreasing and increasing their maturation "speed".

- Variation of cell numbers

  Cell numbers can be controlled to vary cell production or to repopulate damaged cell pools.

2.1.3.2 Special Reaction Mechanisms of the Stem Cells

Pluripotent stem cells and stem cells with limited replicative potential can alter their self replication probability. This probability determines the average replication rate of stem cells and thus how many cells leave the stem cell pool and how many cells remain for maintainance of the pool or its reconstitution after damage. In the steady state this replication probability amounts 0.5. This means, that for every cellular division one cell remains in the pool. Thus, the total amount of cells is held at a constant level [74]. For reconstitution of the pool the replication probability can be raised to a higher value depending on the special type of the stem cells regarded(CFU-S, fetal liver cells ...) [97] [70] [72] [31].

2.1.3.3 Special Reaction Mechanisms of the Megakaryocytes

One special mechanism of megakaryocytes to react to disturbances in the thrombocyte count of the peripheral blood has its roots in the polyploidy. If the thrombocyte renewal system is stressed such as by exchange transfusion with platelet poor blood, the megakaryocytes react by shifting their ploidy distribution. In the case of thrombocytopenia the modal ploidy number is shiftet against higher values, in the case of thrombocytosis against lower [75] [78] [36] [60]. Additionally, a shift of the mean megakaryocyte volume within ploidy classes is observed [22] [36].

2.1.4 Hematological Experiments

The structure of the mathematical model follows the biological model of thrombocytopoiesis. The parameters of the model are derived and calculated from experimental results.

2.1.4.1 The Meaning of "in vivo" and "in vitro" Techniques

The most principal distinction of experimental techniques in cell biological research is given by the terms "in vivo" (Latin, "in the living") and "in vitro" (Latin, "in the glass"). "In vivo" experiments are performed in the living organism and results show information about cells in the (in the ideal case) undisturbed system. Typical examples are the single cell autoradiography techniques with ^{3}H-thymidin. "In vitro" experiments are performed with cells outside of the body and thus results are allways endangered to be so called artefacts, which are not reflecting the reality in the organism. These difficulties and dangers always should be considered when in vitro results are interpreted.

2.1.4.2 Labeling Experiments in General

One group of methods in cell research is the labeling of (certain) cells with different techniques. In the case of chemical or surface markers, labeling can simply be used for cell counting. With the help of DNA labeling more sophisticated experimental designs are possible, such as tracing cells via several development stages or observing cell turnover dynamics. For example, fast decrease of radioactivity would support the assumption of short turnover times. In the opposite, slow decrease would support long turnover times. Here the emptying dynamics are used. Sometimes it is possible to consistently label cells in a certain precursor development stage and observe the occurence of the marker in the following stages. Here the filling (and emptying) dynamics are used for evaluation. However, common basis for all labeling experiments is selective labeling of certain types of cells, cell cycle phases or cell development stages [70].

2.1.4.3 DNA Labeling with Radioactive DNA Precursors

Labeling of cells is done by radioactive labeled precursors of DNA, which after injection into the organism are available for a short time (about 30 minutes) and are incorporated into the DNA of cells which are in the S-phase during this availability time. A so called "flash labeling" of the DNA synthesizing cells is done. One example for this kind of techniques is the single cell autoradiography with ^{3}H-thymidine (tritium labeled thymidine). Following the radioactivity in the DNA of cells, the labeling can

be detected by high resolution autoradiography of single cells and by radiochemical analysis of tissue samples. As a consequence, the labeling can be observed at a cellular and subcellular level, which makes it possible to estimate turnover times and flow rates in cell renewal systems such as the bone marrow or the blood. Serial sampling of such tissues allows one to follow the cohort of labeled cells from the proliferating pool through the maturing and functional pools. By estimating the percentage of labeled cells and counting the number of grains in the autoradiographic photo emulsion per cell certain kinetic parameters of cell populations can be derived. Thus, autoradiography provides a method to calculate flow and production rates of various cell pools. The following determinations have been established:

- Flow of labeled cells through mitosis

  A method for determining cell generation times is the observation of the appearance and dissappearance of labeled mitoses as a function of time after flash labeling with tritiated thymidin. By correct interpretation this provides a method for determination of cell generation times in tissues.

- Labeling index

  The labeling index I_l is defined as the total number of labeled cells N_S (cells in S-phase) divided by the total number of cells in the population N. Under ideal conditions I_l equals the DNA synthesis time t_S divided by the average cell generation time t_G:

  $$I_l = \frac{N_S}{N} = \frac{t_S}{t_G} \tag{2.1}$$

- Grain count reduction

  In a (idealized) self-sustaining cell population the time for halving of the mean grain count would equal the average cell generation time. Under real conditions normally one has to deal with concatenated cell pools. As a consequence, the grain count reduction is mainly determined by the cell pool with the longest turnover time.

- Flow of labeled cells into an unlabeled, nondividing compartment

  By determining the labeling index of a nondividing cell compartment the transit

characteristic can be calculated. The basic assumption for calculation is the presence of a labeled inflow into an unlabeled compartment.

The listed techniques were reviewed by Bond [4] and Feinendegen [25].

2.1.4.4 Chemical Cytoplasm and Surface Labeling

With cytoplasm and surface labeling techniques cells are marked by certain chemical substances. For instance bone marrow and blood cells can be classified into different groups (eosinophiles, basophiles, ...) by such methods. For the megakaryocytic line acetylcholinesterase (AChE) is used which can be detected by chemical reactions. Cells that show acetylcholinesterase positive reactions are often called AChE+ cells and appear in the later development states of megakaryocyte precursors [63] [66].

Chemical labeling can be used for detecting certain types of cells. Cell kinetics can not directly be measured. Applications relevant for modeling cell systems are for instance determinations of concentrations of certain cell types such as megakaryocytic transitional cells [66].

2.1.4.5 Antibody Labeling

In the last years new labeling methods with antibodies were developed. Antibodies bind to certain surface antigens and can be used for specifying certain cell types. Well known example is the CD34+ reaction, which characterizes the early stem cells and disappears with maturation of the cells. Immune marker technology can be regarded as the current state-of-the-art method for separation of morphologically not differentiable cells. CD means "Cluster of Differentiation" and a CDx cluster describes a group of antibodies, which react in a certain manner on different tissue or cells types [51]. Similar to chemical markers, immune markers are used for the detection of certain cell types and cell concentrations.. Direct measurement of cell kinetics are not possible.

2.1.4.6 Highly Specific Radioactive DNA Precursor Suicide Techniques

Some highly specific radioactive DNA nucleotides like special ^{3}H-thymidin types, which are very intensively enriched by tritium, are able to kill cells by radiation after incorporation into the nuclei. This process is comparable to single cell autoradiography by

radiation from within the cells but with the difference that here the activity of radiation is strong enough to destroy the cell. For this reason the term "suicide techniques" is used. Since again a flash labeling is assumed one can estimate the number of cells in S phase by counting the fraction of killed cells [32].

2.1.4.7 Cytostatic Agents

Cytostatic agents are commonly used to destroy or damage cells, which are actively proliferating. Fast proliferating cells are destroyed to a greater extent than slowly dividing populations. Further, some cytostatic agents show their effects only in certain phases of the cell cycle. In this way dividing cell populations can sometimes be synchronized in their cell cycles. In hematological research cytostatic agents such as 5-fluorouracyl (5-FU) and hydroxyurea are used to destroy fast dividing progenitor and precursor cells for observing the reactions of the hematopoietic system to this kind of cell loss, for getting information about the proliferative activity, or to receive a higher concentration of early stem cells in cell preparations. Further information is provided by Chabner [16], Metcalf [70], and Calabresi [13] [12].

2.1.4.8 Cell Colony Experiments

Cell colony experiments are typical in vitro experiments, in which selected or unselected bone marrow cells are grown to colonies and observed. They serve to get information on proliferative potential, cell cycle times and differentiation potential of the cultivated cells. From these techniques derive the terms CFU (Colony Forming Unit) or BFU (Burst Forming Unit) which describe the patterns in which the colonies grow [70].

2.1.4.9 Ex-Colonization Technique

One technique that delivered a lot of the basic knowledge in hematological research is the ex-colonization technique for stem cells in mice. It was developed by Till and McCulloch. In these experiments, cells harvested from the bone marrow of one mouse are injected into another (lethally irradiated) mouse. After a certain time special cell colonies that grow in the spleen are investigated. The cells of interest in these experiments are called CFU-S (Colony Forming Unit - Spleen) according to their

occurence in the spleen and were the first direct experimental evidence for the existence of pluripotent stem cells in the hematopoietic system of the mouse. The technique is not applicable to other species.

The different applications of the CFU-S techniques were reviewed by Quesenberry [80] and Nothdurft [74].

2.2 Data on Irradiation

2.2.1 Data of Irradiated Humans

Data from radiation accidents were used for the estimation of remaining stem cell numbers of irradiated humans. These data have been collected in a database in our institute since 1990 [29]. The collection of data was performed in two steps:

- Collection of data from individual patient files into standardized questionnaires.
- Transfer of the data from the questionaires to a computer database.

The data are currently stored in an ORACLE 8® database management system (DBMS) which runs under the operating system SOLARIS 7 ® on a SUN SPARC ULTRA 10® workstation. Patient data can be retrieved by software applications like graphical user interfaces (GUIs), statistical and numerical software systems like SAS® and MATLAB® , and by special application programmer interfaces (APIs) via standard query language (SQL).

2.2.2 Data of Chronically Irradiated Dogs

The data used in the chapters on chronic irradiation were taken from a long time irradiation experiment on beagle-dogs performed at the Argonne National Laboratory, USA. In this experiment, groups of dogs were livelong exposed to different levels of gamma-irradiation from a sealed ^{60}Co radiation source. The animals were exposed about 23 h per day, the remaining one hour was necessary for the daily care for the dogs. The data sets were obtained directly from Dr. Fritz and Dr. Seed from Argonne

Laboratory in form of an ORACLE® database dump file and imported into our local database system which is described above in 2.2.1.

2.3 Mathematical Techniques and Methods

2.3.1 Selection of the Modeling Technique

One of the first basic decisions to be made for building a model of a system is to identify the appropriate kind of modeling perspective. If hematopoiesis is analyzed on the level of single cells, the model is a so called "microscopic" model. The term "microscopic" here is not used in an "optical" meaning. The other perspective is the macro level of cell populations. A model which deals with entire cell populations as basic elements would be a "macroscopic" model. Macroscopic models consist in general of several state variables which pool large sets of single objects or characteristics of these together into one or several model variables. In opposite, microscopic models concentrate on the single objects. In the case of thrombocytopoiesis one has to model cell populations with numbers of 10^5 to 10^{12}, in which the fate of single cells is not of interest. The appropriate technique in this case is a macroscopic one.

Examples for both modeling perspectives are simulations of traffic. For modeling large amounts of vehicles on highways macroscopic techniques based on theoretical fluid mechanics are used, whereas for simulating the traffic on small crossroads microscopic approaches with stochastic models for single cars are in use. Another example is the treatment of gases in physics. In the microscopic perspective a gas consists of particles which move in a stochastic manner. In the macroscopic perspective which is used in most technical tasks, gases are described by variables, which do not characterize single molecules but all together, like pressure, volume and temperature.

2.3.2 Important Aspects of Biomathematical Modeling

For the building of biomathematical models mathematical and biomedical aspects have to be considered:

- The variables of the model should be biologically interpretable. Disregarding this aspect would lead to models that are not capable to help explaining the "real" system.

- This condition of interpretability is essential for verification and validation of models.
- For the work in interdisciplinary projects in which mathematics, biology, medicine and informatics interact, a certain amount of flexibility of the modeling technique should be guaranteed.
- The "computerized" model should be able to perform the simulations in a suitable time. This is essential for using the model in connection with iterative optimization algorithms. For this it is necessary to perform up to several hundred single simulations. The difference between 10 and 100 seconds simulation time, which does not matter very much in single simulations then becomes a very important factor. An "economic" cost efficiency analysis in the case of including more complexity into the model should always be done.
- As a condition for most optimization routines the model should behave in a mathematical "friendly" way. This means that the model outputs should be at least continous. This problem appears for example when delay times have to be modeled.
- A perhaps trivial but nonetheless essential point to consider is the availability of suitable software. This implies numerical stability, financial aspects, flexibility and others.

For modeling cell proliferation systems compartment models based on ordinary differential equations (ODEs) have been established as an approved methodology. Other modeling approaches (in different scientific or industrial areas) work with stochastic and partial differential equations, but are difficult to apply because no established software solutions exist. For models built with ODEs a set of often applied and flexible software packages like MATLAB® , MAPLE® , and MATHEMATICA® are available.

2.3.3 Compartment Models

The term compartment in this context denotes a functional unity. In a compartment model for cell proliferation systems the cell groups, which are regarded to be homogeneous in a macroscopic view, are pooled together into compartments. More generally

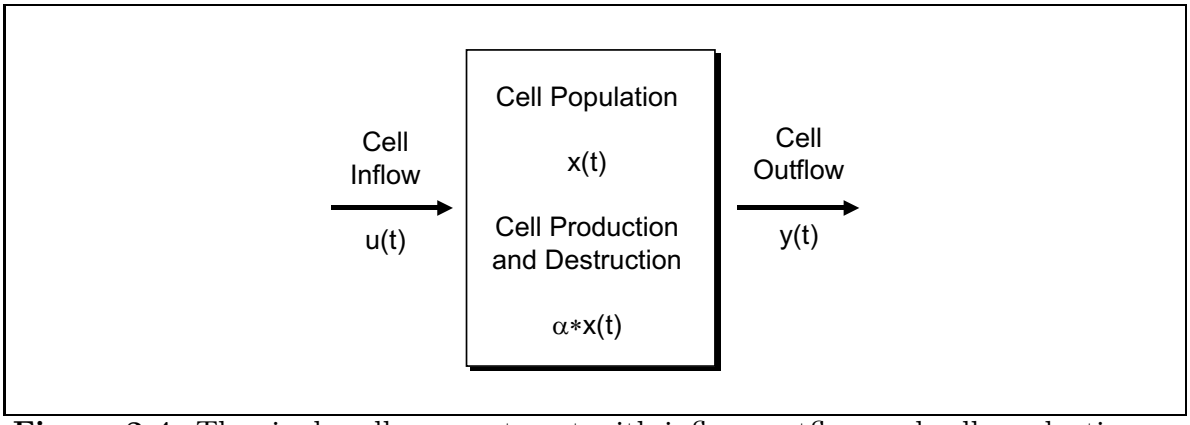

Figure 2.4: The single cell compartment with inflow, outflow and cell production as the basic element for modeling cell proliferation.

defined a compartment model is a model of cells ("compartments") which interact via exchange of material or information [45], [68]. The basic unit of such a model shows figure 2.4.

In general cell compartments can be separated in two classes:

- Functional compartments

  Cells are pooled by functionality, such as stem cells or platelets.

- Anatomical compartments

  Cells are pooled by locations in the body (organs or organ systems), such as bone marrow, spleen, or lung.

In the proposed model only functional compartments are used.

2.3.4 Mathematical Description of Compartment Models

This subsection explains the mathematics used in the theory of compartments models.

2.3.4.1 Mass Balance Equations

The variation of the content of a compartment per time unit can be calculated by the inflow into the compartment per time unit less the outflow per time unit. This can be formalized using a first order differential equation, the so called mass balance equation

$$\dot{x} = u(t) - y(t), \quad x(0) = x^0 \tag{2.2}$$

with the following denotations:

$$x(t) = \text{content of the compartment at time t} \tag{2.3}$$

$$\dot{x}(t) = \text{temporal derivative } \frac{dx(t)}{dt} \text{ at time t} \tag{2.4}$$

$$u(t) = \text{inflow per time unit at time t} \tag{2.5}$$

$$y(t) = \text{outflow per time unit at time t} \tag{2.6}$$

$$x(0) = \text{content of the compartment at time 0 .} \tag{2.7}$$

Biologically, an inflow into a compartment is caused by differentiation from other functional compartments or inflow from anatomical compartments. Outflows are caused by differentiation into other functional compartments or outflows into other anatomical compartments. When applied to cell proliferation systems, another part, $\alpha(t)$, has to be added to the cell balance equation 2.2, to reflect the normal physiological production of cells (cellular division) and cell death in the formalism:

$$\dot{x}(t) = u(t) + \alpha(t) - y(t), \quad x(0) = x^0 \tag{2.8}$$

where

$$\alpha(t) = \frac{\text{cell production at time t}}{\text{time unit}} - \frac{\text{cell destruction at time t}}{\text{time unit}}$$

2.3.4.2 State Space Equations

In the general notation of state space models the following formalisms are used: If i, j are compartments then the $\lambda_{i,j}$ is called the flow rate from compartment i to compartment j. The index 0 denotes external outflows into the environment. External inflows are abbreviated with u_i and production rates with α_i. The flow rates and the production rates in general depend on the model state variables $x_i, i = 1...n$, time,

and other parameters. This is written using

$$\lambda_{i,j} = \lambda_{i,j}(\vec{x}, t, \vec{\theta})$$
$$\alpha_i = \alpha_i(\vec{x}, t, \vec{\theta})$$

with the following definitions:

$\vec{x}$ denotes the vector of state variables.

t denotes the time.

$\vec{\theta}$ denotes the vector of other influencing parameters.

For the differential equations of the n state variables $x_i, i = 1...n$ one gets the general linear mass balance equation:

$$\dot{x}_i(t) = u_i(t) + \alpha_i(t) \cdot x_i(t) + \sum_{\substack{j=0 \\ j \neq i}}^{n} \lambda_{j,i}(\vec{x}, t, \vec{\theta}) \cdot x_j(t) - \sum_{\substack{i=0 \\ i \neq j}}^{n} \lambda_{i,j}(\vec{x}, t, \vec{\theta}) \cdot x_i(t) \tag{2.9}$$

In vector-matrix notation this can be written as:

$$\dot{\vec{x}}(t) = A \cdot \vec{x}(t) + B \cdot \vec{u}(t) \tag{2.10}$$
$$\vec{y}(t) = C \cdot \vec{x}(t) + D \cdot \vec{u}(t)$$
$$\vec{x}(0) = \vec{x}^0$$

with

$$A = (a_{i,j})_{nXn}, \quad B = I_{nXn} \tag{2.11}$$
$$C = (c_{i,j})_{nXn}, \quad D = 0_{nXn}$$

and

$$
\begin{aligned}
a_{i,j} = a_{i,i} = \alpha_i(\vec{x}, t, \vec{\theta}) - \sum_{\substack{j=i \\ j \neq i}}^{n} \lambda_{j,i}(\vec{x}, t, \vec{\theta}), & \qquad i = j \qquad (2.12)\\
a_{i,j} = \lambda_{i,j}(\vec{x}, t, \vec{\theta}), & \qquad i \neq j \\
c_{i,j} = 0, & \qquad i = j \\
c_{i,j} = \lambda_{i,j}(\vec{x}, t, \vec{\theta}), & \qquad i \neq j
\end{aligned}
$$

In practice, many of the $\lambda_{i,j}$ equal 0 and the equations become less complicated.

2.3.5 Linking Biological and Mathematical System Characteristics

Now that the biological and mathematical basics are introduced the question arises how to connect these disciplines.

2.3.5.1 Probabilistic Derivation of the Linear Mass Balance Equations

If one defines

n as the number of cells in a compartment at a certain time

and

p_i as the probability of cell i to leave the compartment (differentiate) within one time unit Δt

then the expectation value $E(n_{out})$ of the number n_{out} of cells leaving the compartment in one time unit Δt can be calculated as:

$$E(n_{out}) = \sum_{i=1}^{n} 1 \cdot p_i \tag{2.13}$$

Thus, the expectation value of the fraction of leaving cells per time unit $E(\frac{n_{out}}{n})$ satisfies the equation

$$E\left(\frac{n_{out}}{n}\right) = \frac{E(n_{out})}{n} = \frac{\sum_{i=1}^{n} 1 \cdot p_i}{n} = \frac{1}{n}\sum_{i=1}^{n} 1 \cdot p_i \ . \tag{2.14}$$

If λ is defined as

$$\lambda = \lim_{n\to\infty} \frac{1}{n} \sum_{i}^{n} p_i \tag{2.15}$$

one gets for rising cell numbers

$$\lim_{n\to\infty} E\left(\frac{n_{out}}{n}\right) = \lim_{n\to\infty} \frac{1}{n} \sum_{i=1}^{n} 1 \cdot p_i = \lambda \ . \tag{2.16}$$

For large cell numbers this means, that the number of cells leaving a compartment n_{out} in one time unit Δt is directly proportional to the total number of cells n in the compartment. If it is assumed that no inflow and no cell production exists, then the change in the number of cells Δn in the compartment during the time unit Δt is equal to n_{out} and one can write:

$$\frac{\Delta n}{\Delta t} = -n_{out}. \tag{2.17}$$

For the expectation values one gets

$$\begin{aligned} E\left(\frac{\Delta n}{\Delta t}\right) &= -E\left(\frac{n_{out}}{n} \cdot n\right) \\ &= -\lambda \cdot n \ . \end{aligned} \tag{2.18}$$

Translated to a continous formalism (which represents the macroscopic view) the result is:

$$\frac{dx(t)}{dt} = -\lambda \cdot x$$

or

$$\dot{x}(t) = -\lambda \cdot x \tag{2.19}$$

The cell production rate α can be derived analogously. Thus, one gets

$$\dot{x}(t) = \alpha \cdot x(t) - \lambda \cdot x(t). \tag{2.20}$$

In the common form with the inflow function $u(t)$ on gets

$$\dot{x}(t) = u(t) + \alpha \cdot x(t) - \lambda \cdot x(t) \tag{2.21}$$

This is an ordinary differential equation (ODE) of the type of equation 2.2.

With the help of the shown linearizations one gets a so called linear model of a compartment, which is a special form of the mass balance equation 2.2 . This is in general written in the notation

$$\begin{aligned} \dot{x}(t) &= u(t) + \alpha \cdot x(t) - \lambda \cdot x(t), \quad x(0) = x^0 \\ y(t) &= \lambda \cdot x(t) \ . \end{aligned} \tag{2.22}$$

The linear model equation 2.22 is solved by

$$x(t) = e^{-(\lambda-\alpha)\cdot t} \cdot x(t^0) + \int_{t^0}^{t} e^{-(\lambda-\alpha)\cdot(t-\tau)} \cdot u(\tau)\, d\tau \ . \tag{2.23}$$

2.3.5.2 Transit Times and Amplification Factors

The term "transit time" mathematically means the expectation value of the time for passing a compartment. "Amplification factor" means the factor by which the "cell stream" through a compartment is multiplied. Both parameters can be derived under steady state and dynamic conditions.

2.3.5.2.1 Compartment Without Amplification, Steady State Situation

Let us first consider a compartment without amplification under steady state conditions. Without amplification means, that the cell production α equals 0

$$\alpha = 0 \tag{2.24}$$

and the system equations

$$\begin{aligned} &\dot{x}(t) = u(t) + \alpha \cdot x(t) - \lambda \cdot \ x(t), && x(0) = x^0 \\ &y(t) = \lambda \cdot x(t) \end{aligned} \tag{2.25}$$

become

$$\begin{aligned} &\dot{x}(t) = u(t) - \lambda \cdot \ x(t), && x(0) = x^0 \\ &y(t) = \lambda \cdot x(t) \ . \end{aligned} \tag{2.26}$$

The steady state is defined by a non-dynamic state. In other words, all model variables stay at a (temporarily) constant level. Thus, the content, the inflow, and the outflow of a compartment are constant in time, and can be characterized by temporal derivatives that equal zero. Written in mathematical formalism, one gets:

$$\dot{x}(t) = 0 \Rightarrow x(t) = x^{steady\ state} = const. \tag{2.27}$$

$$\dot{u}(t) = 0 \Rightarrow u(t) = u^{steady\ state} = const. \ . \tag{2.28}$$

Inserted into equation 2.26 one gets

$$0 = u^{steady\ state} - \lambda \cdot x^{steady\ state} \tag{2.29}$$

or written in another form

$$x^{steady\ state} = \frac{u^{steady\ state}}{\lambda} \tag{2.30}$$

and thus

$$y^{steady\ state} = \lambda \cdot x^{steady\ state} = \lambda \cdot \frac{u^{steady\ state}}{\lambda} = u^{steady\ state} \ . \tag{2.31}$$

Therefore, it is easy to see that under steady state conditions without amplification

- the inflow equals the outflow
- with given inflow the content of the compartment is determined by the flow rates.

2.3.5.2.2 Compartment Without Amplification, Dynamic Situation

Here the model variables not necessarily have to be constant. Therefore, an examination of the dynamics has to be done in another way than in the upper case. One elegant method for examining the dynamics of a compartment uses the delta function $\delta(t - t^0)$, which is often used in theoretical physics. It is indirectly defined and characterized by the following features:

$$\delta(t - t^0) = 0 \qquad if \quad t \neq t^0 \tag{2.32}$$

$$\delta(t - t^0) = \infty \qquad if \quad t = t^0 \tag{2.33}$$

$$\int_{-\infty}^{+\infty} \delta(t - \tau) d\tau = 1 \tag{2.34}$$

$$\int_{-\infty}^{+\infty} f(t - \tau) \cdot \delta(\tau) d\tau = f(t) \ . \tag{2.35}$$

Assuming that a "virtual" cell cohort enters an empty compartment instantaneously at $t^0 = 0$ and fills the compartment to a "virtual" content of 1, this cell cohort can be formalized by the δ-function. Written in mathematical formalism, this becomes:

$$t^0 = 0 \tag{2.36}$$

$$x(t) = 0 \qquad \forall x < 0 \tag{2.37}$$

$$u(t) = \delta(t - t^0) \tag{2.38}$$

Inserting this into equation 2.26 the result is:

$$x(t) = e^{-\lambda \cdot t} \cdot x(0^-) + \int_0^t e^{-\lambda \cdot (t-\tau)} \cdot u(\tau)\, d\tau \tag{2.39}$$

$$= \int_0^t e^{-\lambda\cdot(t-\tau)} \cdot \delta(\tau)\, d\tau \tag{2.40}$$

$$= e^{-\lambda t} \qquad \forall t \geq 0 \tag{2.41}$$

$$= 0 \qquad \forall t < 0 \tag{2.42}$$

and thus

$$y(t) = \lambda \cdot x(t) = \lambda \cdot e^{-\lambda t} \qquad \forall t \geq 0 \tag{2.43}$$

$$y(t) = 0 \qquad \forall t < 0\ . \tag{2.44}$$

As easily can be seen, this dynamic response to the instantaenous entry of a virtual cell cohort at time $t = 0$ has the same solution as a depletion without inflow to the compartment with content $x(0) = 1$ and starting time $t = 0$.

Further the outflow function $y(t)$ fulfills the following criteria

$$y(t) >= 0 \qquad \forall t \in [-\infty; +\infty] \tag{2.45}$$

$$\int_{-\infty}^{+\infty} y(t)\, dt = \int_{-\infty}^{+\infty} \lambda \cdot e^{-\lambda\cdot t}\, dt = ... = 1\ . \tag{2.46}$$

These criteria are characteristic for a probability density function. Therefore, $y(t)$ can be interpreted as a probability density function for the exit of cells from the compartment. The expectation value of the time spent passing through one compartment is called transit time T, and since the entry time is defined to be 0, T is calculated by:

$$T = E(t) = \int_0^{\infty} t \cdot \lambda \cdot e^{-\lambda\cdot t}\, dt = \frac{1}{\lambda}\ . \tag{2.47}$$

2.3.5.2.3 Compartment With Amplification, Steady State Situation

Starting again with the assumptions of steady state

$$\dot{x}(t) = 0 \quad \Rightarrow x(t) = x^{steady\ state} = const. \tag{2.48}$$

$$\dot{u}(t) = 0 \quad \Rightarrow u(t) = u^{steady\ state} = const. \tag{2.49}$$

one gets by insertion of these into the basic equation 2.22

$$\dot{x}(t) = u(t) + \alpha \cdot x(t) - \lambda \cdot x(t), \quad x(0) = x^0 \tag{2.50}$$

$$y(t) = \lambda \cdot x(t) \tag{2.51}$$

this time with

$$\alpha > 0 \tag{2.52}$$

the condition

$$0 = u^{steady\ state} + \alpha \cdot x^{steady\ state} - \lambda \cdot x^{steady\ state} \tag{2.53}$$

which can be resolved to

$$x^{steady\ state} = \frac{u^{steady\ state}}{\lambda - \alpha} \tag{2.54}$$

and

$$y^{steady\ state} = \lambda \cdot x^{steady\ state} \tag{2.55}$$

$$= \lambda \cdot \frac{u^{steady\ state}}{\lambda - \alpha} \tag{2.56}$$

$$= \frac{\lambda}{\lambda - \alpha} \cdot u^{steady\ state} \ . \tag{2.57}$$

If one defines the steady state amplification $A^{steady\ state}$ of the compartment as:

$$A^{steady\ state} = \frac{\text{outflow}^{steady\ state}}{\text{inflow}^{steady\ state}} \tag{2.58}$$

one gets

$$A^{steady\ state} = \frac{y^{steady\ state}}{u^{steady\ state}} \tag{2.59}$$

$$= \frac{\frac{\lambda}{\lambda - \alpha} \cdot u^{steady\ state}}{u^{steady\ state}} \tag{2.60}$$

and thus

$$A^{steady\ state} = \frac{\lambda}{\lambda - \alpha} \ . \tag{2.61}$$

2.3.5.2.4 Compartment With Amplification, Dynamic Situation

The question arises if (and how) the amplification of a compartment in dynamic situations can be defined in a similar way like in the steady state and if the definitions match if the steady state is regarded as a special case of the dynamic state. The basic equation 2.22

$$\dot{x}(t) = u(t) + \alpha \cdot x(t) - \lambda \cdot x(t), \quad x(0) = x^0 \tag{2.62}$$

$$y(t) = \lambda \cdot x(t) \tag{2.63}$$

$$\alpha > 0 \tag{2.64}$$

is solved by equation 2.23:

$$x(t) = e^{-(\lambda-\alpha)\cdot t} \cdot x(t^0) + \int_{t^0}^{t} e^{-(\lambda-\alpha)\cdot(t-\tau)} \cdot u(\tau)\, d\tau \ . \tag{2.65}$$

If again the assumptions

$$t^0 = 0 \tag{2.66}$$

$$x(t) = 0 \qquad \forall x < 0 \tag{2.67}$$

$$u(t) = \delta(t - t^0) \tag{2.68}$$

are used, the solution is:

$$x(t) = e^{-(\lambda-\alpha)\cdot t} \qquad \forall t \geq 0 \tag{2.69}$$

$$= 0 \qquad \forall t < 0 \tag{2.70}$$

and

$$y(t) = \lambda \cdot x(t) = \lambda \cdot e^{-(\lambda-\alpha)\cdot t} \qquad \forall t \geq 0 \tag{2.71}$$

$$y(t) = 0 \qquad \forall t < 0 \tag{2.72}$$

The amplification $A^{dynamic}$ can be defined as the total amount of outflow related to the total amount of inflow:

$$A^{dynamic} = \frac{\text{total amount of outflow}}{\text{total amount of inflow}} \tag{2.73}$$

$$= \frac{\int_{-\infty}^{\infty} y(t)\,dt}{\int_{-\infty}^{\infty} u(t)\,dt} \tag{2.74}$$

$$= \frac{\int_{0}^{\infty} \lambda \cdot e^{-(\lambda-\alpha)t}\,dt}{\int_{-\infty}^{\infty} \delta(t)\,dt} \tag{2.75}$$

$$= \frac{\frac{\lambda}{\lambda-\alpha}}{1} \tag{2.76}$$

$$= \frac{\lambda}{\lambda-\alpha} \tag{2.77}$$

Thus, the result for the teady state is:

$$A^{dynamic} = A^{steady\,state} \tag{2.78}$$

2.3.5.3 Remarks on the Transit Time in Compartments with and without Amplification

In equation 2.47 the transit time for compartments without amplification was defined as

$$T = E(t) = \int_{0}^{\infty} t \cdot \lambda \cdot e^{-\lambda \cdot t}\,dt = \frac{1}{\lambda}\,. \tag{2.79}$$

In a compartment with amplification the analogously calculated value would be

$$\widetilde{T} = E(t) = \int_{0}^{\infty} t \cdot (\lambda-\alpha) \cdot e^{(-\lambda+\alpha)\cdot t}\,dt = \frac{1}{\lambda-\alpha} \tag{2.80}$$

but this value is related to the complete amount of inflown and "new born" cells. It is not easy to decide, if the definition for transit time should imply only the fraction corresponding to the inflown or the total amount of outflowing cells. On the one hand, one could argue, that the process of "flowing" through the compartment can be (formally) seen as independent from the process of birth, on the other hand, the

mathematically more consistent definition would be the upper calculation for $\widetilde{T}$, which includes also the birth process. In this thesis, the term transit time is used generally in the definition of 2.79, since mathematical treatment of the extended form results in different problems of modeling, like constant experimental biological transit time under changing cell production rates α. This would imply much more complicated approaches for the variable compartment parameters.

2.3.5.4 Cell Division and Compartment Parameters

If k denotes the number of cell divisions in the regarded compartment, and the biological amplification $A^{biological}$ denotes the number of produced cells per mother cell, one gets:

$$A^{biological} = \frac{\text{number of daughter cells}}{\text{mother cell}} \tag{2.81}$$

$$= \frac{\text{number of cells generated by k divisions}}{\text{mother cell}} \tag{2.82}$$

$$= \frac{2^k}{1} \tag{2.83}$$

$$= 2^k \tag{2.84}$$

where

$$k = \text{number of cell divisions in the compartment.} \tag{2.85}$$

Assuming that every cell leaves the compartment at some time, the following equation can be set up:

$$A^{biological} = A^{dynamic} \tag{2.86}$$

$$\Leftrightarrow$$

$$2^k = \frac{\lambda}{\lambda - \alpha} \tag{2.87}$$

and after resolving:

$$\alpha = \lambda \cdot (1 - 2^k) \ . \tag{2.88}$$

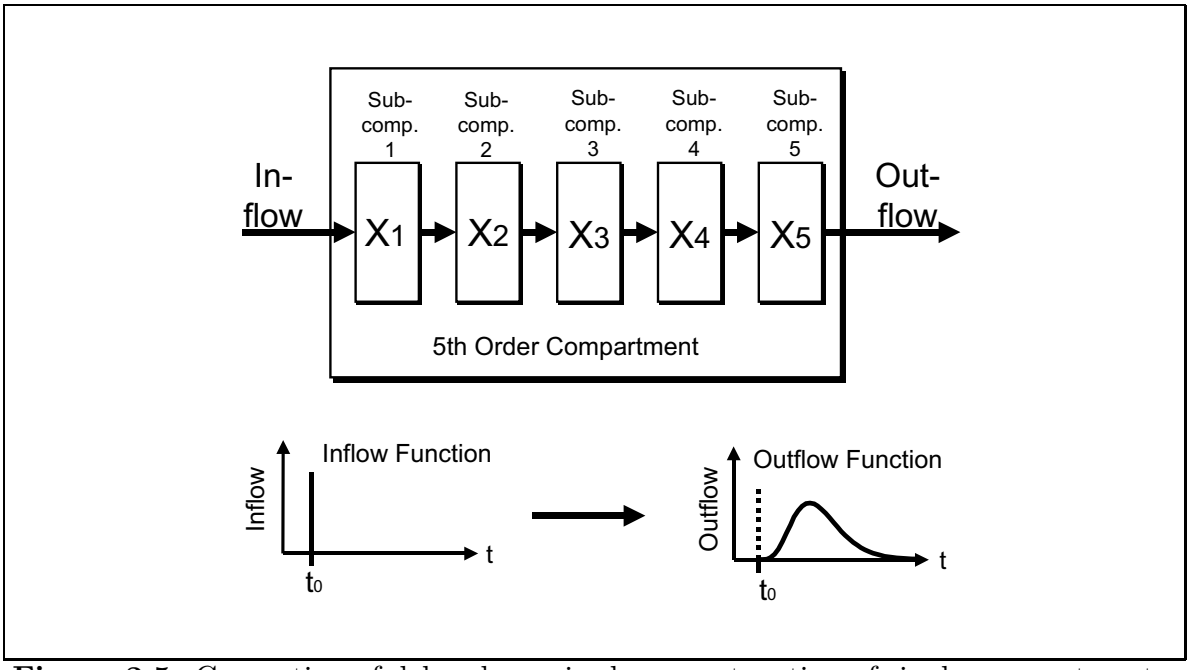

Figure 2.5: Generation of delay dynamics by concatenation of single compartments.

2.3.6 Modeling Delay Times

In experiments on the transit dynamics of cell populations these dynamics in general do not show the first order characteristics of single compartments, which would generate an exponential decrease of cell numbers or labeling substances immediately after entry time. This is caused physiologically by a minimal differentiation or maturation time, which is necessary to pass a development stage. On the stage of modeling this means that the regarded cells are not homogenous enough to justify the assumption of equal differentiation probability for all cells. Thus, it is not an appropriate solution to use a single compartment. A good approximation for the natural transit dynamics are gamma probability density functions. They can be generated by concatenating compartments represented by first order differential equations with identical kinetic parameters, like shown in figure 2.5.

Another method for modeling delay times uses dead time models which are described by differential equations of the form

$$\dot{x}(t) = a \cdot x(t - t_{delay}) + b \cdot u(t - t_{delay}) \ . \tag{2.89}$$

They appear to be a suitable solution to this problem [34]. The advantage of this equation is the lower order, which could be of interest in connection with simulation

times. Its disadvantages are:

- Delayed differential equations can produce non-differentiable solutions. They are difficult to use in connection with optimization routines.
- Numerical standard software packages in general do not contain solution algorithms for these problems.
- Delayed differential equations can not reproduce the variances of the probability variable transit time.
- Delayed differential equations can produce uncontinous solutions which are not compatible with fast optimization algorithms.

2.3.6.1 Gamma Distributed Delay Times: Generation and Application

For modeling time delays only concatenated ODEs are used. Most important in the decision for the concatenated ODE method was the fact, that solutions of these systems excellently can be fitted against data from tracer or cell counting experiments and thus approximate the "real world" distributions of transit times very closely. The differential equation system of such a structure (figure 2.5, n=5) looks like:

$$\begin{aligned}
\dot{x}_1(t) &= u(t) \qquad +\alpha \cdot x_1(t) - \lambda \cdot x_1(t) \\
\dot{x}_2(t) &= \lambda \cdot x_1(t) \quad +\alpha \cdot x_2(t) - \lambda \cdot x_2(t) \\
&\ldots \\
\dot{x}_n(t) &= \lambda \cdot x_{n-1}(t) + \alpha \cdot x_n(t) - \lambda \cdot x_n(t)
\end{aligned} \tag{2.90}$$

$$x_i(0) = x_i^0 \qquad\qquad i = 1 \ldots n$$

$$y(t) = \lambda \cdot x_n(t)\ . \tag{2.91}$$

For solving this concatenated differential equation system it is assumed that a cell cohort of the virtual measurement size 1 enters the first compartment $i = 1$ at $t = 0$. Like shown before this is equivalent to initializing the first compartment with $x_1(0) = 1$

and the others with zero. The problem to solve is the ODE system

$$\begin{aligned}
\dot{x}_1(t) &= u(t) \qquad +\alpha \cdot x_1(t) - \lambda \cdot x_1(t) \\
\dot{x}_2(t) &= \lambda \cdot x_1(t) \quad +\alpha \cdot x_2(t) - \lambda \cdot x_2(t) \\
&\ldots \\
\dot{x}_n(t) &= \lambda \cdot x_{n-1}(t) + \alpha \cdot x_n(t) - \lambda \cdot x_n(t)
\end{aligned} \tag{2.92}$$

with the initial conditions:

$$\begin{aligned}
x_1(0) &= 1 \\
x_i(0) &= 0 \qquad\qquad i = 2...n \ .
\end{aligned} \tag{2.93}$$

The equation system is solved with the help of Laplace transformation [11]. The transformed system results in

$$\begin{aligned}
sX_1(s) - 1 &= (\alpha - \lambda) \cdot X_1(s) \\
sX_2(s) &= (\alpha - \lambda) \cdot X_2(s) + \lambda \cdot X_1(s) \\
&\ldots \\
sX_n(s) &= (\alpha - \lambda) \cdot sX_n(s) + \lambda \cdot X_{n-1}(s) \ .
\end{aligned} \tag{2.94}$$

Resolving the system delivers:

$$\begin{aligned}
X_1(s) &= \frac{1}{(s - \alpha - \lambda)} \\
X_2(s) &= \frac{\lambda}{(s - \alpha - \lambda)^2} \\
&\ldots \\
X_n(s) &= \frac{\lambda^{n-1}}{(s - \alpha - \lambda)^n}
\end{aligned} \tag{2.95}$$

and back-transformation results in

$$x_i(t) = \frac{\lambda^{i-1}}{(i-1)!} \cdot t^{i-1} \cdot e^{-(\lambda - \alpha) \cdot t} \ . \tag{2.96}$$

Thus, the outflow function of the last compartment $y_n(t)$ can be calculated as

$$y_n(t) = \lambda \cdot x_n(t) \tag{2.97}$$

$$= \lambda \cdot \frac{\lambda^{i-1}}{(i-1)!} \cdot t^{i-1} \cdot e^{-(\lambda-\alpha)\cdot t} \ . \tag{2.98}$$

With

$$\tilde{\lambda} = (\lambda - \alpha) \tag{2.99}$$

one gets

$$y_n(t) = \frac{\lambda^n}{\tilde{\lambda}^n} \cdot \frac{\tilde{\lambda}^n}{(n-1)!} \cdot t^{n-1} \cdot e^{-\tilde{\lambda}\cdot t} \tag{2.100}$$

$$= \frac{\lambda^n}{\tilde{\lambda}^n} \cdot \frac{(\tilde{\lambda}\cdot t)^{n-1}}{(n-1)!} \cdot \tilde{\lambda} \cdot e^{-\tilde{\lambda}\cdot t} \ . \tag{2.101}$$

The term

$$\frac{(\tilde{\lambda}\cdot t)^{n-1}}{(n-1)!} \cdot \tilde{\lambda} \cdot e^{-\tilde{\lambda}\cdot t} \tag{2.102}$$

of the result is equivalent to a gamma probability density function of order n-1 and scale $\tilde{\lambda}$. Thus, the transit time through n concatenated compartments has a gamma shaped probability distribution. Figure 2.6 shows a series of gamma distributions of transit times with varying $\tilde{\lambda}$.

For the gamma distribution (equation 2.102) $E(t)$ and $Var(t)$ is calculated as:

$$E(t) = \frac{n}{\tilde{\lambda}} = \frac{n}{\lambda - \alpha} \tag{2.103}$$

and

$$Var(t) = \frac{n}{(\tilde{\lambda})^2} = \frac{n}{(\frac{n}{E(t)})^2} = \frac{E^2(t)}{n} \tag{2.104}$$

Again the problem of interpretation of the transit time appears, like mentioned before in section 2.3.5.3.

The term for the variance $Var(t)$ can be used to calculate the necessary number of

compartments for modeling delay times, if the variance of a transit time is known. In general, the variance is not known and calculation of n has to be done by other techniques.

2.3.6.2 Parameters of Serial Compartment Structures

Following the considerations on transit times in 2.3.5.3 the parameter λ is calculated for each single compartment of a serial structure from the transit time T by

$$\lambda = \frac{n}{T} \ . \tag{2.105}$$

The amplification can be calculated using the single compartment characteristic 2.77

$$A^{\text{one compartment}} = \frac{\lambda}{\lambda - \alpha} \ . \tag{2.106}$$

By reapplication of this n times (one time for each compartment of the serial structure) one gets

$$A^{\text{n compartments}} = \underbrace{\frac{\lambda}{\lambda - \alpha} \cdot \ldots \cdot \frac{\lambda}{\lambda - \alpha}}_{n \text{ times}} \tag{2.107}$$

$$= \left(\frac{\lambda}{\lambda - \alpha} \right)^n \ . \tag{2.108}$$

Resolved for α the result is

$$\alpha = \lambda \cdot \left(1 - A^{-\frac{1}{n}} \right) \ . \tag{2.109}$$

2.3.6.3 Transit Dynamics of Serial Compartment Structures

Figure 2.6 illustrates the change in the transit dynamics of a series of $n = 10$ compartments. The figure shows the outflow function $y_n(t)$ $(n = 10)$ from the last compartment caused by an instantaneous virtual $\delta(t)$ inflow of cells into the first compartment. Again this could be interpreted as a probability density function of the outflow time. It is easy to recognize how the modal outflow time (and the expectation value of the outflow time) shortens with increasing outflow rate λ. Figure 2.7 shows the outflow function $y_n(t)$ from the last compartment caused by an $\delta(t)$ inflow of a virtual cohort

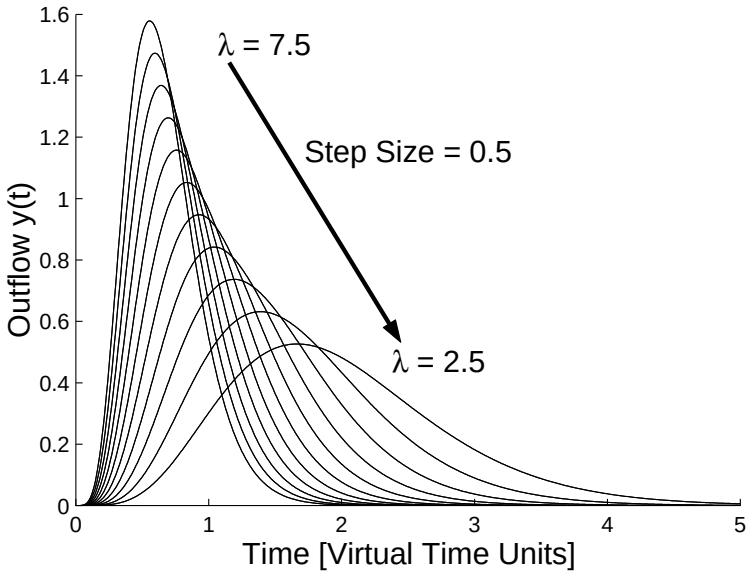

Figure 2.6: Changes in gamma distributions of transit times by variation of λ.

of 100 cells, this time with varying compartment number n. The flow rate λ of each simulation curve is adapted to a common transit time T following equation 2.105 by setting $\lambda_n = n \cdot \lambda$ to get comparable flow rates. The flattening of the initial part and the sharpening around the modal value of $y_n(t)$ with rising n is characteristic. In the interpretation of $y_n(t)$ as a probability density function this means a reduction of variance. Figure 2.8 shows again the dynamics of serial structures, but this time not the outflow function $y_n(t)$ but the total content $x_{all}(t)$ of all compartments together. This is defined as:

$$x_{all}(t) = \sum_{i=1}^{n} x_i(t) \ . \tag{2.110}$$

Figure 2.8 shows the filling dynamics under the assumption of a constant inflow and the depletion dynamics under the assumption of $x_{all}(0)$ distributed equally into all n compartments as initial contents

$$x_i(0) = \frac{x_{all}(0)}{n} \quad \forall\, i = 1...n \ .$$

The parameters are again adapted to the changing order n of the structure by setting $\lambda_n = n \cdot \lambda$. Characteristic for an increase in the order n of the structure is the appro-

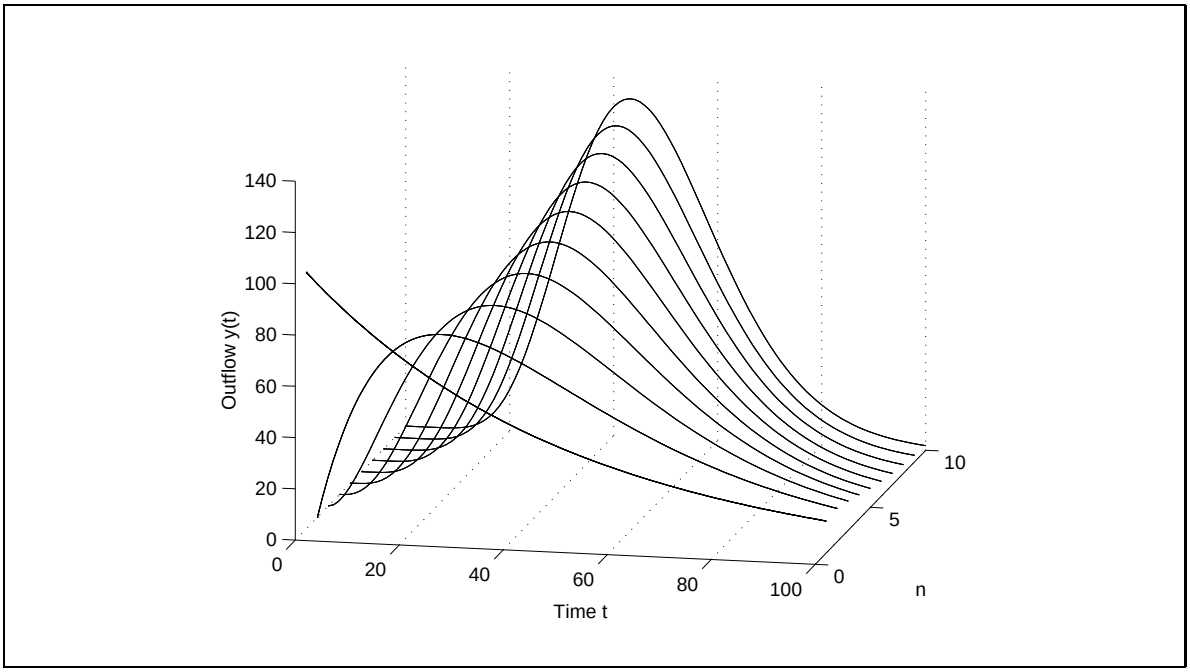

Figure 2.7: Gamma distributions of transit times with varying n and corresponding λ_n adapted by setting $\lambda_n = n \cdot \lambda$.

ximation of the initial slope of $x_{all}(t)$ to a more linear behaviour and the sharpening of the following curvature. This characteristic is later used for fitting (sub)models against experimental data from labeling experiments.

2.3.6.4 Regulation and the Origin of Nonlinearity in the Model

Since the megakaryocyte/platelet renewal system is very dynamic and reacts very strong on excess loss of platelets or other disturbances, the up to now introduced mathematical background of comparment models has to be extended with dynamical components, which serve as elements that actively operate to maintain or (in the case of disturbances) to reconstitute the steady state of the system. This means for the model equations, that some parameters are not constants, but functions of state variables. These functions are called regulators. In the organism regulation is done for example by changing cell population characteristics by hormones, which control most physiological processes. Since hormones have certain production and clearing times in the body, it can be necessary to build hormone like regulators with own clearing dynamics and compartments. For the model as a whole this means that it loses linearity and becomes a nonlinear system.

For the selection of the regulation functions biological and mathematical criteria have

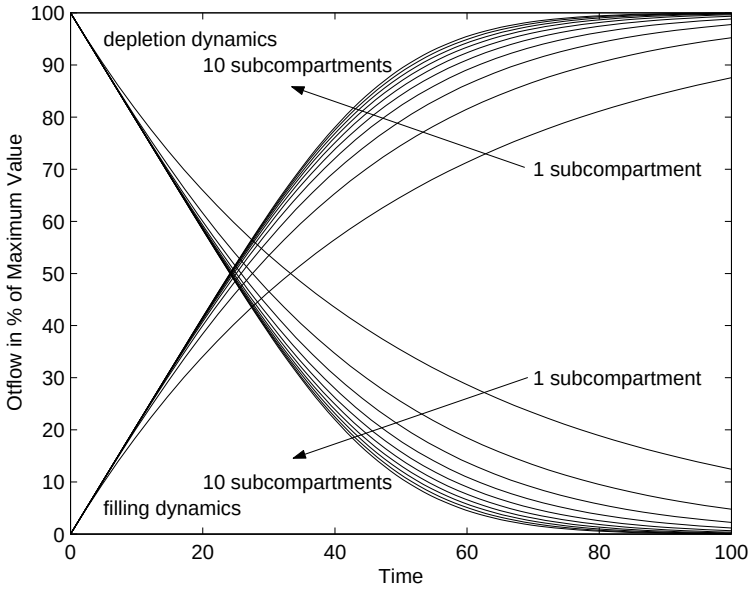

Figure 2.8: Filling and depletion dynamics of concatenated compartments with varying n, $\lambda_n = n \cdot \lambda$.

to be considered. On the biological side a regulation function should give a good approximation of the physiological reality, on the mathematical side the regulation function must not disturb the stability of the model.

Suitable functions for this approach are for example:

- A biased hyperbolic function:

$$R_1(N) = a + \frac{b}{c + N} \tag{2.113}$$

- A pure exponential function with negative argument:

$$R_2(N) = a + b \cdot e^{-c \cdot N} \tag{2.114}$$

- An exponential function with additional polynomial:

$$R_3(N) = a + b \cdot e^{-c \cdot S} \cdot (1 + c \cdot N) \tag{2.115}$$

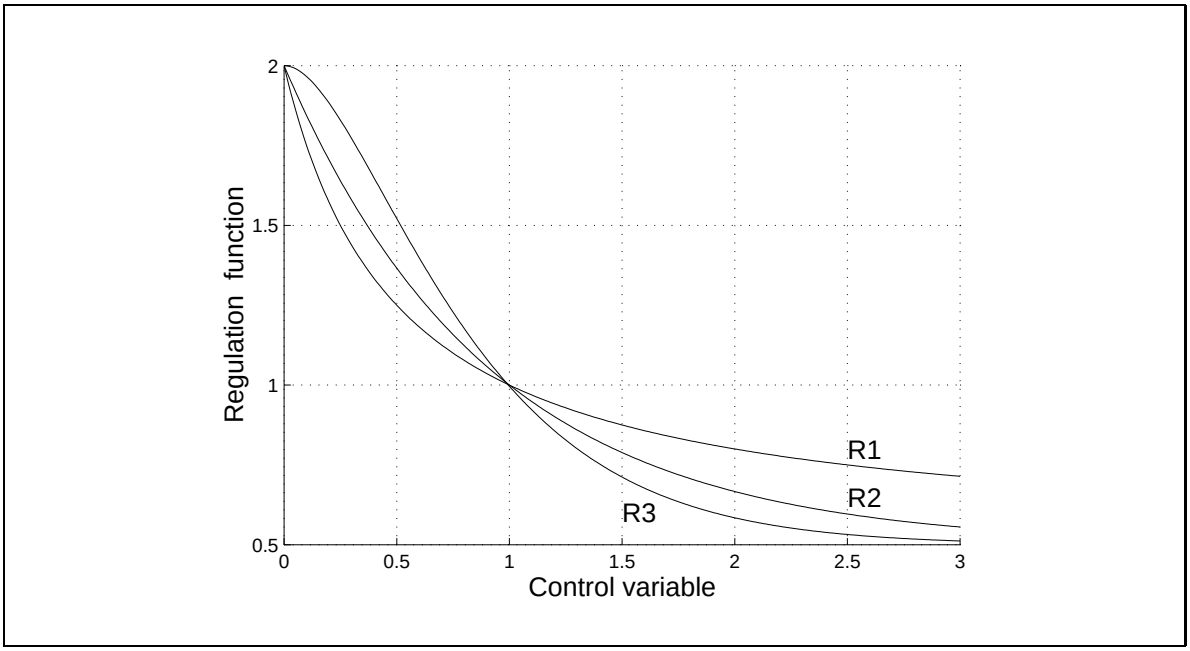

Figure 2.9: Examples for different types of regulation functions.

where

$$R_1, R_2, R_3 \text{ are the regulation function values} \tag{2.116}$$

and

$$N \text{ denotes the observer variable.} \tag{2.117}$$

Figure 2.9 shows the functions $R_1(N), R_2(N), R_3(N)$ as functions of the observer variable N. Often the regulation functions depend not only on one variable, but on two or more. Figure 2.10 shows a regulation function of the type R_3 (exponential function with additional polynomial) plotted over the two observer variables.

2.3.7 Evaluation of Experiments

The submodels for the several cell pools are all modeled with the basic structures of single or concatenated compartments. The number of necessary compartments and the kinetic parameters of these have to be calculated or estimated from experimental data.

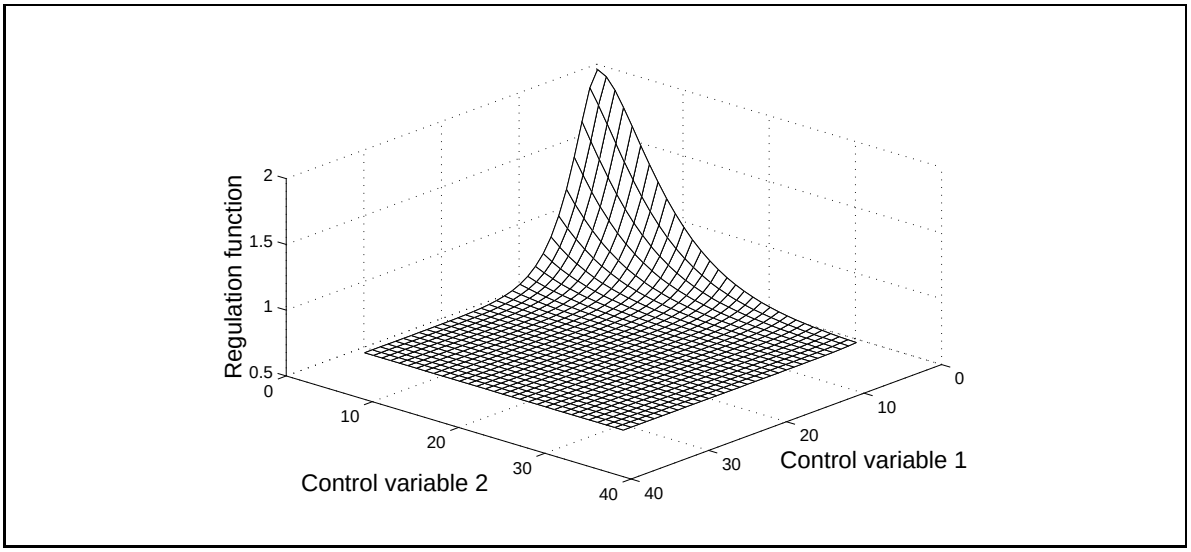

Figure 2.10: Example of a multivariate regulation function with two variables.

2.3.7.1 Evaluation of labeling experiments

Following equation 2.104 the estimation of the number of compartments sometimes is possible if one knows the variance of the distribution of the transit time. In most labeling experiments this is not applicable. For this reason, a different technique was developed to fit a serial structure of compartments against labeling data of different experimental methods by varying compartment number, transit time and initial conditions of the labeling simulation. A sum of least squares was used as deviation measurement. The estimators were implemented with MATLAB®.

The algorithm was designed to fit filling or depletion curves of submodels into experimental data by solving a set of minimization problems in the parameter λ and the initial values $\vec{x}(0)$ for different orders. The algorithm works in two steps:

- Step 1: Solve the fitting problem for a set of given orders of the compartment structure.
- Step 2: Select the order which delivered the smallest deviation function result.

Step 1 can be mathematically formalized as optimization problem:

$$(P_i) = \begin{cases} SLSQ_i(\lambda_i, \vec{x}_i(0)) = \sum_{j=1}^{r} \left(z_{i,j}(\lambda_i, \vec{x}_i(0)) - z_j^{exp} \right)^2 \rightarrow \min \\ \lambda_i^{min} \leq \lambda_i \leq \lambda_i^{max} \end{cases} \tag{2.118}$$

where

$$i = \text{number of concatenated compartments} \tag{2.119}$$

$$i = 1...n \text{ for a given n} \tag{2.120}$$

$$z_j^{exp} = \text{experimental value at time point } t_j \tag{2.121}$$

$$z_j^i(\lambda_i, \vec{x}_i(0)) = \text{corresponding model value at time point } t_j \tag{2.122}$$

$$\lambda_i = \text{adapted flow rate for } i \text{ compartments} \tag{2.123}$$

$$\lambda_i^{min}, \lambda_i^{max} = \text{adapted given limit values} \tag{2.124}$$

$$\vec{x}_i(0) = \text{adapted initial values of model ODEs .} \tag{2.125}$$

Step 2 works simplier. Let

$$(\lambda_i^*, \vec{x}_i^*(0)) \text{ denote the solutions of problem } P_i \tag{2.126}$$

and

$$SLSQ_i^* = SLSQ_i(\lambda_i^*, \vec{x}_i^*(0)) \tag{2.127}$$

Then the overall minimum $SLSQ_{i^*}^*$ can be defined as

$$SLSQ_{i^*}^* = \min_{i=1...n} SLSQ_i^* \tag{2.128}$$

and the solution for modeling a cell pool with a concatenated compartment structure is characterized by the optimum compartment number i^* and the corresponding flow rate $\lambda_{i^*}^*$.

Since only experiments on nondividing cell pools were evaluated this way, the cell production parameter α is set to 0 and vanishes from the system equations.

Identification of a reasonable number of compartments should take into account, that the results of the upper optimizations do not necessarily give solutions that are optimal for application. From a number of about 5 compartments onward a rapidly increasing number of compartments is necessary to produce a more differentiated dynamic behaviour. Since the number of differential equations is one of the most important

factors determining the simulation times, a good compromise between accuracy of model dynamics and simulation performance has to be found. Especially, if results of fitting procedures corresponding to different experiments are compared, the accuracy of approximating the biological reality has to be relativated. The common result of all fitting procedures shows, that structures of concatenated compartments show very clearly to be the better model for maturation processes of cells compared to single compartments. Overall, a number of 5 compartments showed good agreement with most data sets used.

The original aim of using this estimation technique was to avoid arbitrary choices in the compartment numbers n. This goal could not be accomplished completely, but it is possible to determine areas of compartment numbers by performing estimations based on different experimental results. If subsequent a certain value is selected, the estimation of the corresponding value for the flow rate can excellently be done by this method.

2.3.7.2 Evaluation of Cell Colony Experiments

Cell culture experiments can deliver information on proliferative potential, doubling, and differentiation times of cell populations, with respect to the danger of producing artefacts.

Under the assumption, that a culture of n cells is derived from one single mother cell by continous cell doubling, the number of divisions can be calculated from the number of cells of the colony. With additional information on the corresponding durations, cell doubling times can be calculated. Maturation times can be estimated by measuring the time until certain identifiable markers appear.

The following example shows a simple calculation on cell colonies: Lets assume that a clone of n cells from a single cell grows within the duration t. Then the number k of performed cell doublings can be calculated by

$$k = \log_2(n) \ . \tag{2.129}$$

Division of the colony development time t by the number of doublings k results in the

average cell generation time T_G:

$$T_G = \frac{t}{k} . \tag{2.130}$$

For calculations of the proliferative potential of a cell type, the cell colonies should have been given enough time to develop into differentiated cells. Similar considerations of course are important for all development times.

2.3.8 Modular Modeling of Cell Pools

Not absolute but relative numbers are used for modeling the several development stages or cell pools. There are two reasons for this approach:

- Experimental data of different rodents are used together under the assumption that the kinetic characteristics are similar or identical. Of course, this is not true for the cell numbers in the different organisms (the body weight of the rat is about ten times that of the mouse). Therefore, transformations of cell numbers are necessary. To avoid false interpretations and for simplifying connections of submodels derived from different rodent species, cell numbers are not directly adapted between species.
- For optimizing the possibilities of modification and expansion and for simplifying the handling of the model a modular approach of modeling the cell pools is used.

This modular approach uses the following basic ideas:

- For every cell pool a set of compartments is built. This set only tries to model the dynamics of the cell pool.
- Corresponding cell numbers are calculated with conversion factors from the compartment contents.
- Every cell compartment is calculated with a steady state inflow of 1. This is achieved by normalization factors of the corresponding in and outflows.
- For the regulation loops a normalized steady state value of each cell pool of 1 is used.

This approach makes the model independent of absolute cell numbers and therefore easier to modify parts of the model or to adapt it to other species.

2.4 Computer Science and Data Processing

For primary model constructions the simulation system SIMULINK® (Version 2) was used [94]. SIMULINK® is a software package based on MATLAB® which is designed for modeling, simulating, and analyzing dynamical systems. SIMULINK® provides a graphical user interface (GUI) for constructing models as block diagrams based on modeling objects. Using the GUI of SIMULINK® models can be built on the screen by mouse operations. A set of basic objects is provided in the software package by a library containing blocks for sinks, sources, linear and nonlinear components, monitors and connectors. New user defined objects can be created by combining the given basic objects or by programing objects. Self programed objects can be implemented in the languages MATLAB® , C or C++ and be linked into the SIMULINK® models by special application program interfaces (APIs). For simulation a set of differential equation solvers is provided.

After construction, the models were reimplemented to be used by optimization algorithms in the well established numerical software programming language MATLAB® (Release 11) [92]. MATLAB® is a language for scientific numerical computing. It provides packages for scientific computation and visualization. MATLAB® is used as a programming language with a syntax which is similar to familiar mathematical notation. This problem oriented syntax allows to implement computing problems within very short time. Like for SIMULINK® it is possible to include other modules based on C or C++ in MATLAB® applications. The basic MATLAB® package can be extended for application-specific solutions by several toolboxes. Thus, MATLAB® provides an ideal developing environment for modeling projects.

The performance of MATLAB® compared to C or C++ is rather slow. Pure C or C++ implementations run about 10-20 times faster than pure MATLAB® applications.

The numerical differential equation solver ode23 of the MATLAB® package was used for the simulation runs [81].

Optimization algorithms for the estimation procedures were taken from the MATLAB OPTIMIZATION TOOLBOX® (Version 2) [17].

For online database access the MATLAB DATABASE TOOLBOX® (Version 1) was used. For some special tasks interfaces were implemented in the programming language Java® [58].

Data visualization was performed using the MATLAB® (Release 11) plotting functions and utilities [92].

MATLAB® was used both on a Windows NT® driven 450 MHz Pentium II® PC and on a SOLARIS 7 ® driven 300 MHz SUN SPARC ULTRA 10® workstation.

Chapter 3

Results

Contents

3.1 Modeling Thrombocytopoiesis in Rodents

As there are lot of reliable data on the hematopoietic system of rodents gained in clearly defined experimental settings, in a first step a mathematical model of thrombocytopoiesis based on rodent data will be developed. Most experiments on the thrombocytopoietic system are available for rats. Important experiments on the stem cell system were done with mice by the spleen colony techniques of Till and McCulloch. These techniques were reviewed by Quesenberry [80]. For building a model, which is planned to reproduce the dynamics of the megakaryocyte/platelet system in rodents, it is assumed that the differences between rats and mice regarding the dynamics of the hematopoietic system are small enough to be used mutually. Sometimes additional experimental data from other species are used (of course not for kinetic data) when these can be assumed to be relevant and are based on better experimental techniques.

The first version of a mathematical model including the complete development of thrombocytes starting at the stage of the pluripotent stem cell [35] will be revised in the following sections. Important changes were done in the following areas:

- Simplification and unification of functionally similar or equal cell compartments.
- Simplification of the regulation structure and its functions.
- The ploidy distribution function was set up with a completely different approach, which is less explanatory but gives the same results and helps saving simulation time.
- New approaches for validation of the model.

3.1.1 Structure of the Developed Model

For a better understanding of the following calculations of the single compartments the general structure of the model will be shortly introduced. Figure 3.1 gives an overview of the model. The first compartment PS represents the pluripotent stem cells. This feeds the compartment NC of the noncommitted stem cells. The cells develop further into megakaryocyte lineage committed early and late stem cells which are set up with the compartments C1 and C2. The compartments NC, C1, and C2 represent

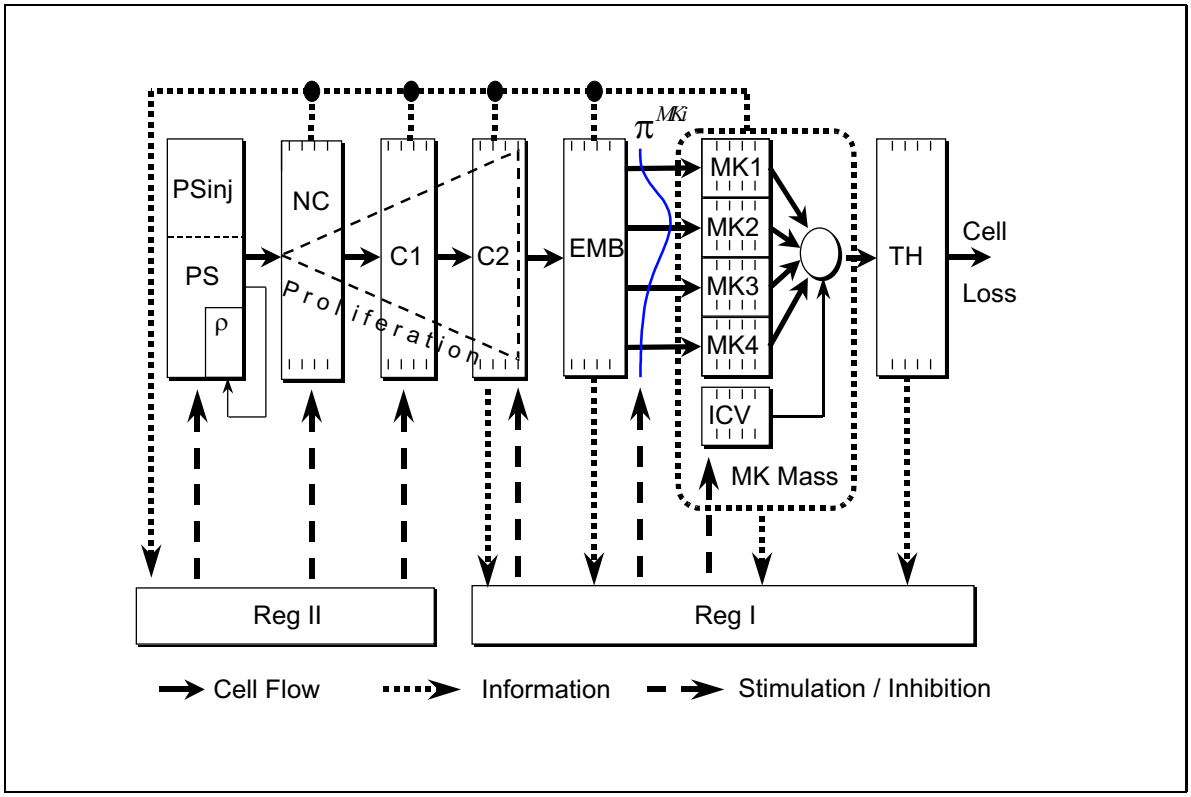

Figure 3.1: The structure of the basic biomathematical model of thrombocytopoiesis. PS = pluripotent stem cells. PSinj = injured stem cells. NC = noncommitted progenitor cells. C1 = early committed progenitor cells. C2 = late committed progenitor cells. EMB = endoreduplicating precursor cells and megakaryoblasts. MK1...MK4 = maturing megakaryocytes. TH = thrombocytes. ICV = intra ploidy class volume. RegI, RegII = regulators. MkMass = megakaryocyte mass. ρ = self replication probability. π^{MKi} = probability for differentiation into the megakaryocyte compartment MKi.

the proliferation part of the megakaryocytopoietic cell line. The compartment EMB summarizes the cell development stages, which perform endoreduplication. These are in general megakaryoblast precursors, megakaryoblasts, and young megakaryocytes. The endoreduplications stop after different numbers of chromosome doublings. Thus, this compartment produces different ploidy groups of megakaryocytes. Ploidy is an essential characteristic in megakaryocytopoiesis, since it determines the megakaryocyte volume which again is proportional to the platelet productivity. The model reflects the four ploidy groups 8N, 16N, 32N, and 64N in the MK1, MK2, MK3, and MK4 compartments. The ploidy distribution can change in case of a disturbance of the system. This is also true for the average megakaryocyte volume within ploidy groups. Thus, an additional compartment ICV is set up for this volume. The fragmenting megakaryocytes produce the platelets which are represented by the TH compartment. The compartments themselves are all but the PS compartment structured into 5 sub-

compartments to represent time delays resulting from differentiation times of the cells. The regulation is subdivided into two areas: One area which reacts on disturbances of the later part of thrombocytopoiesis, especially in the thrombocyte compartment, represented by RegI. Another regulatory system called RegII reacts on disturbances in the early and middle part of the thrombocytopoietic system. The self replication probability ρ^{PS} of the pluripotent stem cells is regulated by the number of pluripotent stem cells. The compartment and regulation structure is based on experimental observations, which are mentioned in detail in the following description of the modeling process.

3.1.2 Calculation of the Compartments

With the worked out biological and mathematical techniques the compartments of the model are calculated.

3.1.2.1 Pluripotent Stem Cells (PS)

The dual process of pluripotent stem cell proliferation has to fulfill the tasks of maintaining the pluripotent stem cell pool and supplying the hematopoietic system with inflow of cells. The "biological model" of this process is based on the following assumptions:

- In the steady state on average 50% of the cells which are "born" by cell division of pluripotent stem cells differentiate to cells of the peripheral blood through different development stages.
- The other 50% are identical clones of the mother cell and remain in the population of the PS.

This kind of cell doubling is called asymmetric division. Of course this asymmetry is not for each single cell division exactly given by 50%/50%. The value of 50% is an average value of an entire cell population. On the cellular level this macroscopic value has to be interpreted again as a probability. The probability of a stem cell to reproduce a new identical cell is called self replication probability ρ^{PS}. The self replication probability can be influenced by the hematopoietic system, for example,

in the case of repopulation of a damaged cell pool. Another characteristic of the pluripotent stem cells is their relative inactivity in the undisturbed bone marrow.

The mathematical model, that is derived from this assumptions can be described by differential equations in the following way:

If the cell generation time of an actively proliferating cell averages T_G, then the flow rate λ_{active} of produced cells relative to the active cells is calculated as

$$\lambda_{active}^{PS} = \frac{1}{T_G} \ . \tag{3.1}$$

In the undisturbed bone marrow only a fraction γ^{PS} of pluripotent stem cells is active in cell generation. Relative to all pluripotent stem cells this means, that the flow rate for all cells λ^{PS} is given by

$$\lambda^{PS} = \lambda_{active}^{PS} \cdot \gamma^{PS} \ . \tag{3.2}$$

Let $x^{PS}(t)$ denote the number of pluripotent stem cells. Then per time unit $\lambda^{PS} \cdot x^{PS}$ cells go into division. Via cell division arise $2 \cdot \lambda^{PS} \cdot x^{PS}$ cells. From these cells on average the fraction ρ^{PS} returns into the pool of pluripotent stem cells, the other fraction $(1 - \rho)$ differentiates into another compartment. This process, illustrated by figure 3.2, can be formalized be the equations:

$$\dot{x}^{PS} = -\gamma^{PS} \cdot \lambda_{active}^{PS} \cdot x^{S} + 2 \cdot \rho^{PS} \cdot \gamma^{PS} \cdot \lambda_{active}^{PS} \cdot x^{PS} \tag{3.3}$$

$$y^{PS} = 2 \cdot (1 - \rho^{PS}) \cdot \gamma^{PS} \cdot \lambda_{active}^{PS} \cdot x^{PS} \tag{3.4}$$

In the steady state bone marrow, which is mathematically characterized by

$$\rho_{\text{steady state}}^{PS} = 0.5 \tag{3.5}$$

one gets

$$\dot{x}^{PS} = -\gamma^{PS} \cdot \lambda_{active}^{PS} \cdot x^{PS} + 2 \cdot \rho^{PS} \cdot \gamma^{PS} \cdot \lambda_{active}^{PS} \cdot x^{PS} \tag{3.6}$$

$$\dot{x}^{PS} = -\gamma^{PS} \cdot \lambda_{active}^{PS} \cdot x^{PS} + 2 \cdot 0.5 \cdot \gamma^{PS} \cdot \lambda_{active}^{PS} \cdot x^{PS} \tag{3.7}$$

$$\dot{x}^{PS} = 0 \ . \tag{3.8}$$

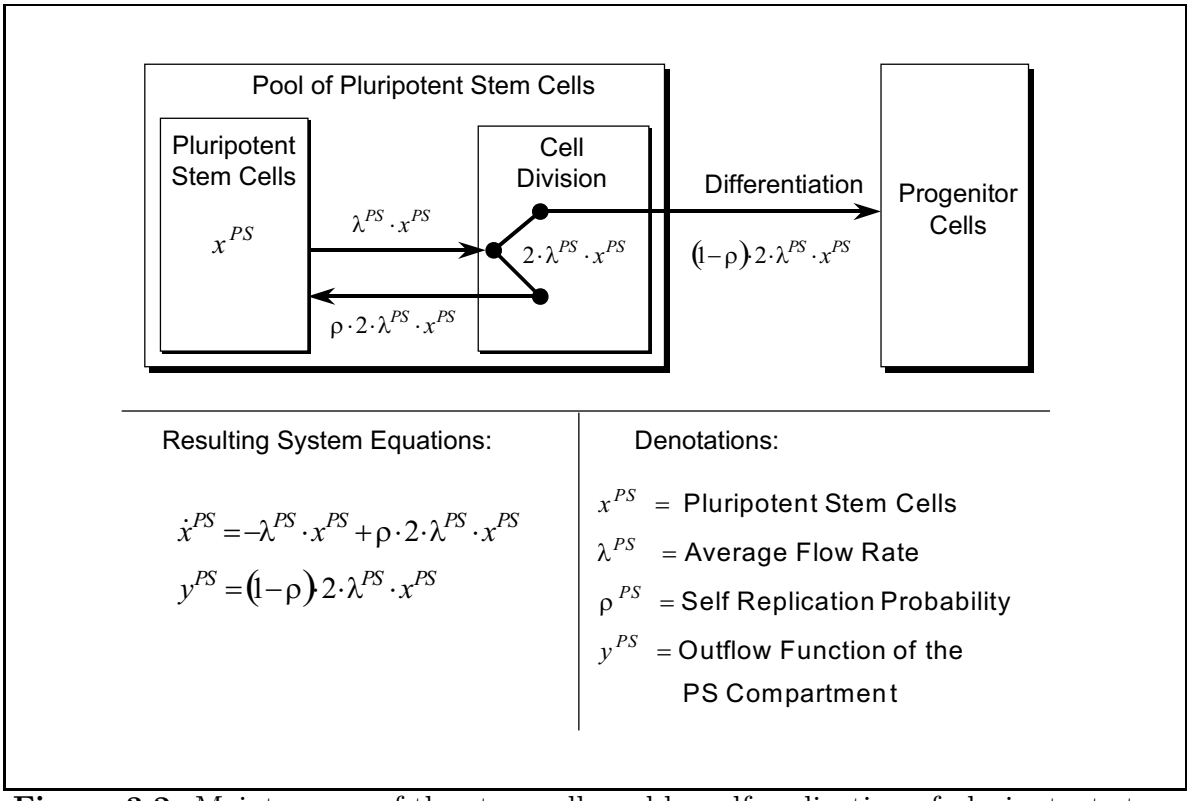

Figure 3.2: Maintenance of the stem cell pool by self replication of pluripotent stem cells.

This means, that the number of pluripotent stem cells x^{PS} remains constant.

3.1.2.1.1 Parameters

The underlying cell population that is used for calculation in this model are the CFU-S (Colony Forming Unit - Spleen) cells. The cell cycle time T_G^{CFU-S} of CFU-S was estimated to be about 10h [41] [96] [77]. In steady state bone marrow only a fraction of cells of about 10% is active, the other 90% remain in a resting phase (G_0 phase), until they are triggered into activity if a higher demand for cells is signalized. In regenerating bone marrow their self replication probability can increase to higher values than 0.5. A value for a higher self replication probability of 0.63 was estimated by statistical methods applied to experiments on CFU-S [97] [70]. The parameters have to be interpreted as average values, since the stem cell pool is considered to be a heterogeneous cell population.

3.1.2.2 Noncommitted Progenitor Cells (NC)

The NC (noncommitted progenitor cells) compartment represents cells, which have the potential to develop into different hematopoietic cell lines, but are not capable of unlimited self replication and depend on a continous inflow from another cell population. In-vitro candidates for such cells are CFU-GEMM, CFU-GM, CFU-EM and others. Experiments on CFU-GEMM [90] show, that about 20% of the grown colonies show megakaryocytic activity. Therefore, it can be assumed that about 20% of the cell-flow through this compartment differentiates into megakaryocyte committed precursor cells. Comparison of this value with the cell production of the PS compartment leads to an average amplification factor of about 2 or one cell division for the megakaryocyte determined outflows of this compartment. With the assumption, that the proliferative activity of noncommited stem cells is at about 20%, which is between the activity of PS cells and the C1 cells, and the cell generation time is about 10h, a transit time of 50h is calculated. Since no labeling data for the exact calculation of the transit dynamics are available, but differentiation processes and therefore delay effects are assumed, five concatenated single compartments are used as default value.

3.1.2.2.1 System Equations

$$u^{NC} = \nu^{PS,NC} \cdot y^{PS} \tag{3.9}$$

$$\begin{aligned}
\dot{x}_1^{NC} &= u^{NC} \qquad +\alpha^{NC} \cdot x_1^{NC} - \lambda^{NC} \cdot x_1^{NC} \\
\dot{x}_2^{NC} &= \lambda^{NC} \cdot x_1^{NC} + \alpha^{NC} \cdot x_2^{NC} - \lambda^{NC} \cdot x_2^{NC} \\
\dot{x}_3^{NC} &= \lambda^{NC} \cdot x_2^{NC} + \alpha^{NC} \cdot x_3^{NC} - \lambda^{NC} \cdot x_3^{NC} \\
\dot{x}_4^{NC} &= \lambda^{NC} \cdot x_3^{NC} + \alpha^{NC} \cdot x_4^{NC} - \lambda^{NC} \cdot x_4^{NC} \\
\dot{x}_5^{NC} &= \lambda^{NC} \cdot x_4^{NC} + \alpha^{NC} \cdot x_5^{NC} - \lambda^{NC} \cdot x_5^{NC}
\end{aligned} \tag{3.10}$$

$$y^{NC} = \lambda^{NC} \cdot x_5^{NC} \tag{3.11}$$

3.1.2.3 Early Committed Progenitor Cells (C1)

One early type of (in-vitro) committed stem cells developing into pure megakaryocytic colonies are the BFU-Mk [65]. It can be assumed that these cells represent early megakaryocytic lineage committed progenitor cells. In cell colony experiments BFU-Mk produce on average 121 megakaryocytes per colony [65]. This corresponds to $log_2(121) = 6,9189 \approx 7$ cell divisions. With the assumption that the BFU-Mk derived cells develop to megakaryocytes over the stage of CFU-Mk (described in the next section) an average number of cell divisions of 3 remains for the development time from BFU-Mk to CFU-Mk. Since there are no data on transit behaviour a default compartment number of 5 is used.

3.1.2.3.1 System Equations

$$u^{C1} = \nu^{NC,C1} \cdot y^{NC} \tag{3.12}$$

$$\begin{aligned}
\dot{x}_1^{C1} &= u^{C1} \quad +\alpha^{C1} \cdot x_1^{C1} - \lambda^{C1} \cdot x_1^{C1} \\
\dot{x}_2^{C1} &= \lambda^{C1} \cdot x_1^{C1} + \alpha^{C1} \cdot x_2^{C1} - \lambda^{C1} \cdot x_2^{C1} \\
\dot{x}_3^{C1} &= \lambda^{C1} \cdot x_2^{C1} + \alpha^{C1} \cdot x_3^{C1} - \lambda^{C1} \cdot x_3^{C1} \\
\dot{x}_4^{C1} &= \lambda^{C1} \cdot x_3^{C1} + \alpha^{C1} \cdot x_4^{C1} - \lambda^{C1} \cdot x_4^{C1} \\
\dot{x}_5^{C1} &= \lambda^{C1} \cdot x_4^{C1} + \alpha^{C1} \cdot x_5^{C1} - \lambda^{C1} \cdot x_5^{C1}
\end{aligned} \tag{3.13}$$

$$y^{C1} = \lambda^{C1} \cdot x_5^{C1} \tag{3.14}$$

3.1.2.4 Late Committed Progenitor Cells (C2)

The next assumed development stage of megakaryocyte lineage commited stem cells are the CFU-Mk. In cell colony experiments [65] cultivated CFU-Mk generate about 16.5 megakaryocytes per colony within five days. In the following days no further megakaryocytes are observed. Thus, the proliferative potential of the CFU-Mk is estimated to be about $log_2(16.5) = 4.0444 \approx 4$. The growth rate of the colonies

described in [65] has its highest value between the days 3 and 5. Between these days a multiplication of the colony cell numbers by a factor of about 15 is observed. This value corresponds to a number of $log_2(15) = 3.9069 \approx 4$ cell divisions. With 4 cell divisions between day 3 and 5 a cell generation time of $\frac{48h}{4} = 12h$ is calculated.

Single cell autoradiography experiments with ^{3}H-thymidine in [20] lead to an average division time of about 16h. This value fits well with the upper calculations if one assumes, that the in vivo candidates of the CFU-Mk in the steady state organism are not proliferating with maximum speed. According to this it can be assumed that the 4 in-vitro cell divisions done with 12h generation time within 48h correspond to a number of 3 in-vivo cell divisions done with 16h generation time within 48h. Thus, a transit time of 48h and 3 cell divisions or an amplification factor of 8 for this compartment is calculated. Again a number of 5 single compartments is used.

3.1.2.4.1 System Equations

$$u^{C2} = \nu^{C1,C2} \cdot y^{C1} \tag{3.15}$$

$$\begin{aligned}
\dot{x}_1^{C2} &= u^{C2} \qquad +\alpha^{C2} \cdot x_1^{C2} - \lambda^{C2} \cdot x_1^{C2} \\
\dot{x}_2^{C2} &= \lambda^{C2} \cdot x_1^{C2} + \alpha^{C2} \cdot x_2^{C2} - \lambda^{C2} \cdot x_2^{C2} \\
\dot{x}_3^{C2} &= \lambda^{C2} \cdot x_2^{C2} + \alpha^{C2} \cdot x_3^{C2} - \lambda^{C2} \cdot x_3^{C2} \\
\dot{x}_4^{C2} &= \lambda^{C2} \cdot x_3^{C2} + \alpha^{C2} \cdot x_4^{C2} - \lambda^{C2} \cdot x_4^{C2} \\
\dot{x}_5^{C2} &= \lambda^{C2} \cdot x_4^{C2} + \alpha^{C2} \cdot x_5^{C2} - \lambda^{C2} \cdot x_5^{C2}
\end{aligned} \tag{3.16}$$

$$y^{C2} = \lambda^{C2} \cdot x_5^{C2} \tag{3.17}$$

3.1.2.5 Endoreduplicating Megakaryoblasts and Precursor Cells (EMB)

3.1.2.5.1 Polyploidy

During their development to mature megakaryocytes the young megakaryocytes and megakaryocyte precursors like megakaryoblasts and perhaps earlier stages usually dou-

ble their DNA content one or more times without dividing the cytoplasm of the cell. This process is called endomitosis or endoreduplication. The number of chromosome sets in a cell is called ploidy, like known from common haploid or diploid chromosome sets. The reason of the organism to produce this kind of cells is assumed to be an increased capacity for protein synthesis [46] and as a consequence of this an increased platelet productivity of the megakaryocytes.

It is not possible to assign the endoreduplications to one clearly defined differentiation stage of megakaryocytopoiesis, but it is known from ^{3}H-thymidine single cell autoradiography experiments that endoreduplication takes place only in early development stages of the megakaryocytes like megakaryoblasts, megakaryoblast precursors and megakaryocytes of type I. This can be seen in autoradiography experiments, in which only these early phases show DNA synthesis activity recognizable by an initial labeling immediatly after administration of ^{3}H-thymidine [76]. Since this is a prerequisite for chromosome doubling it can be assumed that the later stages are not endoreduplicating. It is assumed that 2N megakaryocyte precursors start endoreduplication and become morphologically recognizable as megakaryoblasts between the 4N and the 8N stage. The more mature development stages of the megakaryocytes consist mostly of cells with ploidy 8N, 16N, 32N, and 64N. The biological model of the process of endoreduplication is shown in figure 3.3.

3.1.2.5.2 Modeling the Genesis of Megakaryocyte Ploidy

An exact model of the biological process of endoreduplication would require a complicated implementation regarding the regulation of the ploidy distribution. For this reason this process is approximated in the proposed model with the assumption that endoreduplication is done mainly in the beginning of the megakaryocyte/megakaryoblast development. The biologically exact compartment structure shown in figure 3.3 is simplified to a structure shown in figure 3.4 where one compartment represents all endoreduplicating cells. The cell outflow is subdivided by the fractions $f^{MK1}...f^{MK4}$ into the maturation trees of the different ploidy groups represented by the megakaryocyte compartments $MK1...MK4$. Thus, the flow parameter λ subdivides into four partial flows $\lambda 1...\lambda 4$. The exact calculation of the distribution function is done in section 3.1.3. Calculations performed with an approximation method described in [35] lead

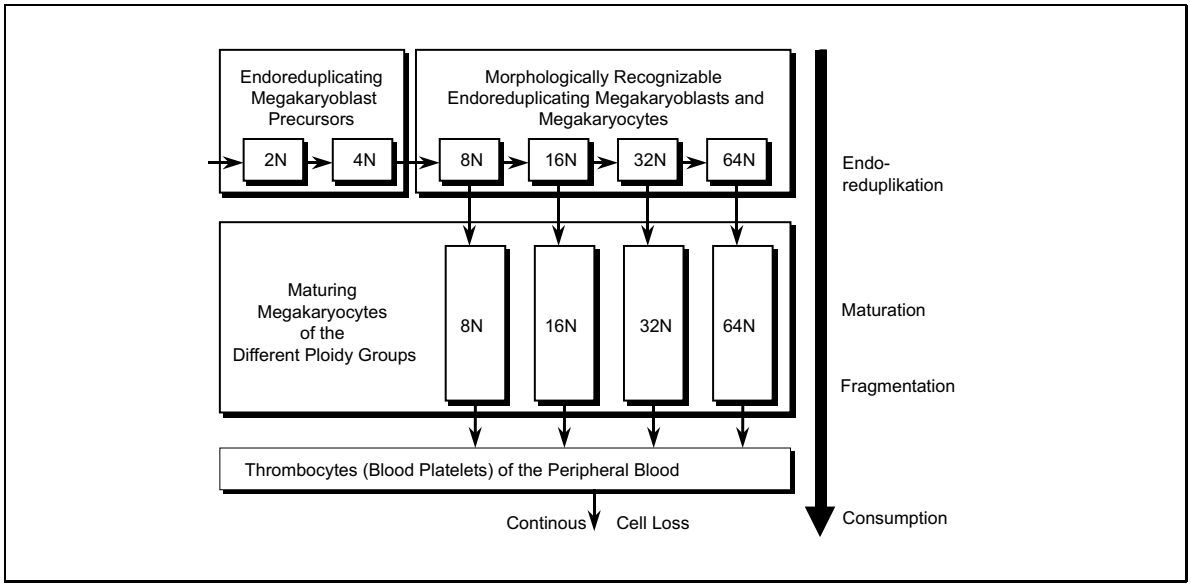

Figure 3.3: The development of polyploid megakaryocytes by multiple endoreduplications.

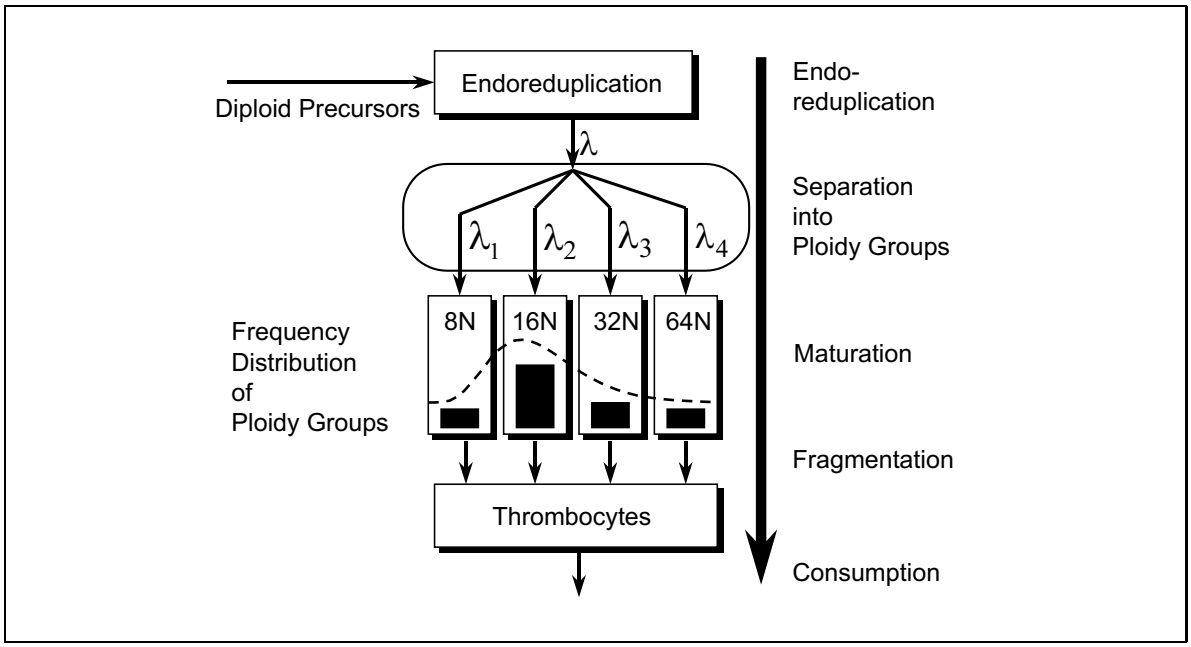

Figure 3.4: Model approximation for the endoreduplication process. λ and λ_i denote the flow rates into the several compartments.

to an average transit time of the endoreduplicating cells of about 35h.

3.1.2.5.3 System Equations

$$u^{EMB} = \nu^{C2,EMB} \cdot y^{C2} \tag{3.18}$$

$$\begin{aligned}
\dot{x}_1^{EMB} &= u^{EMB} &&- \lambda^{EMB} \cdot x_1^{EMB} \\
\dot{x}_2^{EMB} &= \lambda^{EMB} \cdot x_1^{EMB} &&- \lambda^{EMB} \cdot x_2^{EMB} \\
&\dots \\
\dot{x}_5^{EMB} &= \lambda^{EMB} \cdot x_4^{EMB} &&- \lambda^{EMB} \cdot x_5^{EMB}
\end{aligned} \tag{3.19}$$

$$\begin{aligned}
y_1^{EMB} &= f^{MK1}(TH) \cdot \lambda^{EMB} \cdot x_5^{EMB} \\
&\dots \\
y_4^{EMB} &= f^{MK4}(TH) \cdot \lambda^{EMB} \cdot x_5^{EMB}
\end{aligned} \tag{3.20}$$

$f^{MKi}(TH)$ see section 3.1.3

3.1.2.6 Maturing Megakaryocytes (MK1...MK4)

The submodel of the maturing megakaryocytes describes the development stages which follow endoreduplication. The ploidy groups 8N, 16N, 32N, and 64N, which contain mostly all maturing megakaryocytes are set up in the model. The ploidy groups are separated in four series of compartments MK1...MK4. It is assumed, that all ploidy groups have the same maturation time. The parameters are estimated from single cell autoradiography experiments described in [20]. A number of 5 compartments is used and a transit time of 35h is estimated. As megakaryocytes are not observed to divide, the number of cell divisions in this submodel is set to 0. This corresponds to an amplification of 1.

Evaluation Rat 1			
Ploidy	8N	16N	32N
Section area in help units	1.57	2.92	5.37
Calculated increase factor per endoreduplication	-	1.8599	1.8390
Corresponding increase factor of volume ($x^{1.5}$)	-	2.5346	2.4939

Table 3.1: Evaluation of experimental data of the megakaryocyte volume in rats [75], Rat 1.

Evaluation Rat 1			
Ploidy	8N	16N	32N
Section area in help units	1.57	2.74	4.7
Calculated increase factor per endoreduplication	-	1.7452	1.7153
Corresponding increase factor of volume ($x^{1.5}$)	-	2.3055	2.2466

Table 3.2: Evaluation of experimental data of the megakaryocyte volume in rats [75], Rat 2.

3.1.2.7 Ploidy Specific Platelet Productivity

Megakaryocytes of different ploidy groups differ much in the volume of their cytoplasm. Since platelets are produced by fragmentation of cellular cytoplasm of megakaryocytes it is assumed that platelet productivity is proportional to the volume of megakaryocytes and that the megakaryocyte volume is proportional to the ploidy. The volume of the nucleus is neglected.

Experimental results from Mazur [67] describe an increase of the average megakaryocyte diameter from about 12μm to 25μm between 4N to 64N. This is an increase in the diameter by the factor $\frac{25}{12} = 2.0833$ or in volume by the factor 9.0418 during 4 endoreduplications. This corresponds to a factor of $\sqrt[4]{9.0418} = 1.7341$ per endomitosis. Calculations on experimental data of Odell [75] come to a similar result. The cross-section areas of megakaryocytes of the ploidy groups 8N, 16N and 32N of rats were measured. These averaged 1.57, 2.92, and 5.37 helping units for rat 1 and 1.57, 2.74, and 4.70 for rat 2. Tables 3.1 and 3.2 show the calculated increase of volume for the endoreduplication steps. From these an average increase of megakaryocytic volume of 2.3952 per endoreduplication is calculated. Experimental values of Harker [37] result in a volume increase of exact 2.0 per endoreduplication. Taking all the

described experiments together, an average value of $2.0431 \approx 2$ per endoreduplication can be seen as an adequate increase factor.

The ploidy-specific platelet productivity p^{MKi} of megakaryocytes is assumed to be proportional to the megakaryocyte volume and p^{MKi} increases with each doubling of ploidy by the same factor. The productivities are given in relation to that of the 8N ploidy class.

$$\begin{aligned} p^{MK1} &= p^{8N} = 1 \\ p^{MK2} &= p^{16N} = 2 \\ p^{MK3} &= p^{32N} = 4 \\ p^{MK4} &= p^{64N} = 8 \end{aligned} \tag{3.21}$$

3.1.2.7.1 System Equations

$u^{MK\,i}$ see section 3.1.3

$$\begin{aligned} \dot{x}_1^{MK\,i} &= u^{MK\,i} && -\lambda^{MK\,i} \cdot x_1^{MK\,i} \\ \dot{x}_2^{MK\,i} &= \lambda^{MK} \cdot x_1^{MK\,i} && -\lambda^{MK} \cdot x_2^{MK\,i} \\ \dot{x}_3^{MK\,i} &= \lambda^{MK} \cdot x_2^{MK\,i} && -\lambda^{MK} \cdot x_3^{MK\,i} \\ \dot{x}_4^{MK\,i} &= \lambda^{MK} \cdot x_3^{MK\,i} && -\lambda^{MK} \cdot x_4^{MK\,i} \\ \dot{x}_5^{MK\,i} &= \lambda^{MK} \cdot x_4^{MK\,i} && -\lambda^{MK} \cdot x_5^{MK\,i} \end{aligned} \tag{3.22}$$

$$y^{MK\,i} = \lambda^{MK} \cdot x_5^{MK\,i} \tag{3.23}$$

The index

$i = 1...4$

denotes the four ploidy groups 8N, 16N, 32N, and 64N.

3.1.2.8 Average Megakaryocyte Volume within Ploidy Groups (ICV)

Experiments on rats [22] show that under thrombocytopenic conditions not only an increase in the overall average volume of megakaryocytes caused by the ploidy shift appears, but additionally an increase of the average megakaryocyte volume within the ploidy classes. In the experiment a chronic thrombocytopenia with platelet counts below 10% of the normal value was induced by injections of APS (Anti Platelet Serum) and the average volume within ploidy classes was determined. At the 10% level an average increase of the intra-ploidy-group size, which was measured in area units, of about 40% was observed. This means an increase of the average volume of ≈ 1.7.

Since the intra ploidy class volume results from the amount of cytoplasm of the cell which is synthesized during the maturation of the megakaryocytes, the submodel for this volume development is built with identical parameters like the megakaryocyte maturation compartments. The intra class volume is expressed relative to the normal value with a steady state value of 1. Since the platelet productivity of a megakaryocyte is assumed to be proportional to the megakaryocyte volume, the platelet productivity of the different ploidy classes is multiplied with the output of the last compartment of the intra class volume submodel. Thus, an additional factor influencing platelet productivity is set up.

3.1.2.8.1 System Equations

u^{ICV} see section 3.1.3

$$
\begin{aligned}
\dot{x}_1^{ICV} &= u^{ICV} &&- \lambda^{ICV} \cdot x_1^{ICV} \\
\dot{x}_2^{ICV} &= \lambda^{ICV} \cdot x_1^{ICV} &&- \lambda^{ICV} \cdot x_2^{ICV} \\
\dot{x}_3^{ICV} &= \lambda^{ICV} \cdot x_2^{ICV} &&- \lambda^{ICV} \cdot x_3^{ICV} \\
\dot{x}_4^{ICV} &= \lambda^{ICV} \cdot x_3^{ICV} &&- \lambda^{ICV} \cdot x_4^{ICV} \\
\dot{x}_5^{ICV} &= \lambda^{ICV} \cdot x_4^{ICV} &&- \lambda^{ICV} \cdot x_5^{ICV}
\end{aligned}
\tag{3.24}
$$

$$
y^{ICV} = \lambda^{ICV} \cdot x_5^{ICV} \tag{3.25}
$$

$$\lambda^{ICV} = \lambda^{MK} \tag{3.26}$$

3.1.2.9 Thrombocytes (TH)

The basic compartment model for the platelets is a set of concatenated subcompartments without amplification ($\alpha = 0$), since platelets are no complete cells but cell fragments without a nucleus that are not able to divide. For further calculation information about the transit time and their distribution is necessary. Since these information can not be observed directly other methods based on curve fitting procedures together with filling and depletion experiments have to be used.

A first approach for measuring the transit behaviour is radioactive ex-vivo labeling with ^{3}HDFP (tritium labeled diisopropylfluorophosphate) of a fraction of platelets and retransfusion into the body. One would expect that the dynamics of radioactivity in the blood reflect the transit dynamics of platelets [64] [40]. However, in hypertransfusion experiments with labeled platelets it can be shown that this is not true. The trend of the platelet count in the beginning is nearly linear and an exponential pattern appears later. This is in contrast to the early exponential dynamics of radioactivity in the blood [21]. It seems that the radioactive labeling is influenced by strong diffusion or reutilization processes [21]. For this reason, the parameters of the thrombocyte compartment were estimated by a different approach from hypertransfusion experiments with platelet enriched blood and total body irradiation experiments.

From labeling experiments it can be assumed that the platelet productivity is not reduced very much after hypertransfusion [21]. Therefore, kinetics of the platelet count after hypertransfusion should be nearly the same like in the undisturbed system. Estimations were done data taken from Ebbe [21] using least-square fitting (see section 2.3.7.1) of submodels [35].

Another estimation was done using data of platelet counts after total body irradiation (TBI) experiments with rats [87] under the assumption, that after passing the typical (see 3.2.7) shoulder in the platelet counts (that means that the megakaryocyte pool is depleted) no more platelets are delivered into the peripheral blood.

The experimental data of Ebbe [21] (hypertransfusion experiments) delivered a transit time of 104.7 h for a given compartment number of 5, the experimental data of Stein

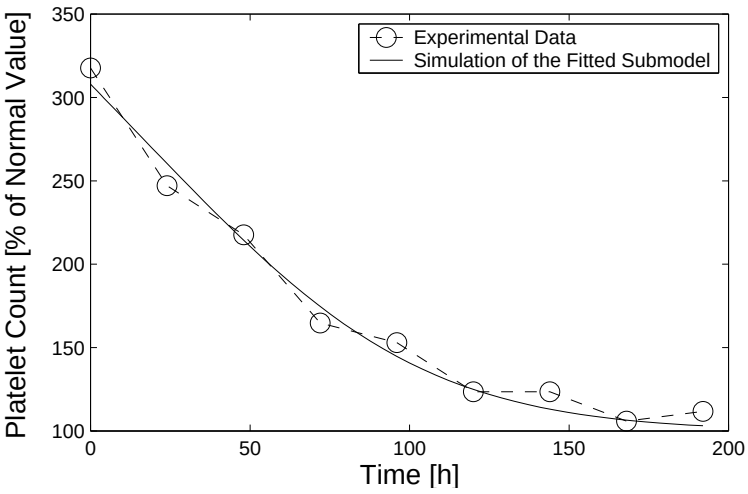

Figure 3.5: Fitting result of the estimation of transit time from data of a hypertransfusion experiment. Fitting performed with least square optimization. Data from Ebbe [21]. Underlying assumptions are given in the text.

[87] (TBI) resulted in 70.7 h. Figure 3.5 shows the result of fitting for the data of Ebbe with 5 compartments, figure 3.6 for those of Stein. As a compromise between these values, 96 h are taken as the transit time. As a rule of thumb, this value is often used for the platelet survival time in Sprague-Dawley rats in literature [82].

3.1.2.9.1 System Equations

$$u^{TH} = \nu^{MK,TH} \cdot \sum_{i=1}^{4} p^{MKi} \cdot y^{ICV} \cdot y^{MKi} \tag{3.27}$$

$$\begin{aligned}
\dot{x}_1^{TH} &= u^{TH} \qquad -\lambda^{TH} \cdot x_1^{TH} \\
\dot{x}_2^{TH} &= \lambda^{TH} \cdot x_1^{TH} - \lambda^{TH} \cdot x_2^{TH} \\
\dot{x}_3^{TH} &= \lambda^{TH} \cdot x_2^{TH} - \lambda^{TH} \cdot x_3^{TH} \\
\dot{x}_4^{TH} &= \lambda^{TH} \cdot x_3^{TH} - \lambda^{TH} \cdot x_4^{TH} \\
\dot{x}_5^{TH} &= \lambda^{TH} \cdot x_4^{TH} - \lambda^{TH} \cdot x_5^{TH}
\end{aligned} \tag{3.28}$$

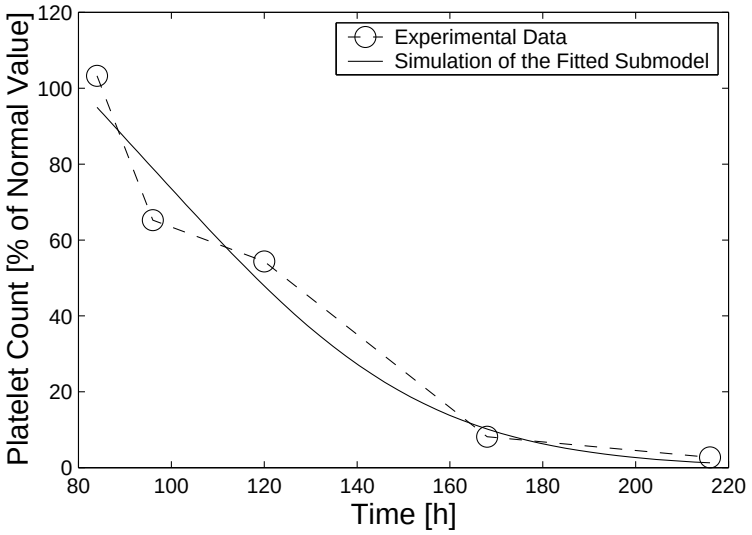

Figure 3.6: Fitting result of the estimation of transit time from data of TBI experiments with least square optimization. Data from Stein [87]. Underlying assumptions are given in the text.

3.1.3 Regulation

In thes section the regulation functions of the model are constructed. The experimental results which are the background for the structure of the regulation are explained and the mathematical regulation functions are derived.

3.1.3.1 Dynamics of the Megakaryocyte/Platelet Renewal System

Results of different experiments like exchange transfusion, administration of APS (Anti Platelet Serum), administration of cytostatic agents and irradiation give reasons for the assumption, that there exist at least two different regulation loops of the thrombocytopoietic system [67]. If one disturbes only the platelet numbers in the peripheral blood in experimental animals, a strong reaction to compensate the disturbances with overshooting thrombocyte numbers [77] results. These reaction mechanisms have effects on the

- number [76],
- intra ploidy class volume [22],
- average volume [19],

- and ploidy [60]

of megakaryocytes. An increasing number of megakaryocytes indicates that the megakaryocyte producing progenitor pools must become more active in proliferation. Experiments on CFU-Mk under thrombocytopenic circumstances result in an increased fraction of cells in S-phase. This means increased proliferative activity of CFU-Mk but no relevant increase in numbers of CFU-Mk [99] [50] [67]. This could be explained by fast differentiation of CFU-Mk during or after cell doubling and loss of proliferative potential, and therefore, of the characteristics of CFU-Mk.

3.1.3.2 Calculation of the Model Regulation Functions

The regulation structure of the model follows the basic ideas described in section 3.1.3.1. The calculation of the several regulation functions is based in general on three values regarding the parameter that has to be influenced by the regulation function:

- The value of the parameter in the steady state.
- The value of the parameter at minimum stimulation.
- The value of the parameter at maximum stimulation.

The values of the parameters are derived by the following methods:

- Experimentally observed cell kinetic parameters in regulation activity.
- Estimations based on physiologically reasonable assumptions.
- Adaption of model regulation dynamics to reproduce experimentally observed regulation dynamics.

The regulator functions were mostly set up with the approach of exponential functions of equation 2.114

$$R = R^{steady\,state} \cdot \left(a + b \cdot e^{-c \cdot N}\right) \tag{3.29}$$

which was described in 2.3.6.4.

3.1.3.2.1 Regulation of Proliferative Activity

The self replication probability ρ^{PS} is assumed to be a function of the compartment content of the pluripotent stem cells (TH). The regulatory function for the proliferative activity γ^{PS} is assumed to depend on the weighted sum of compartment contents Z corresponding to the numbers of bone marrow cells (see 3.1.4).

The megakaryocyte numbers, ploidy, and volume within ploidy group are summarized in the variable MkMass (see 3.1.4), which describes the megakaryocyte mass.

The cell production rate of the C2 compartment is assumed to be a function of the thrombocyte number, megakaryocyte mass, and number of endoreduplicating precursors. Various simulations showed, that an approach using a compartment R for a hormone-like regulator yielded results closer to reality and better stability of the model.

The equations for the regulated parameters are:

$$\rho^{PS} = \xi_1^{PS} + \xi_2^{PS} \cdot e^{-\xi_3^{PS} \cdot PS} \tag{3.30}$$

$$\gamma^{PS} = \xi_4^{PS} + \xi_5^{PS} \cdot e^{-\xi_6^{PS} \cdot Z} \tag{3.31}$$

$$\alpha^{NC} = \xi_1^{NC} + \xi_2^{NC} \cdot e^{-\xi_3^{NC} \cdot Z} \tag{3.32}$$

$$\alpha^{C1} = \xi_1^{C1} + \xi_2^{C1} \cdot e^{-\xi_3^{C1} \cdot (C1+C2+EMB+MkMass)/4} \tag{3.33}$$

$$\alpha^{C2} = \xi_1^{C2} - \xi_2^{C2} \cdot e^{-\xi_3^{C2} \cdot R} \tag{3.34}$$

$$\dot{x}^R = u^R - \lambda^R \cdot x^R \tag{3.35}$$

$$u_1^R = \xi_1^R + \xi_2^R \cdot e^{-\xi_3^R \cdot TH} \tag{3.36}$$

$$u_2^R = \xi_4^R + \xi_5^R \cdot e^{-\xi_6^R \cdot (C2+EMB+MkMass)/3} \tag{3.37}$$

$$u^R = u_1^R + u_2^R \ . \tag{3.38}$$

The average volume of megakaryocytes within ploidy groups is also assumed to be controlled by R. This is achieved by regulating the inflow function u^{ICV} of the ICV submodel. Of course, in reality there is no inflow of volume, but if u^{ICV} is interpreted, for example, as cytoplasma production, the "inflow" model makes sense.

$$u^{ICV} = \xi_1^{ICV} - \xi_2^{ICV} \cdot e^{-\xi_3^{ICV} \cdot R} \tag{3.39}$$

Parameter	steady state	max	min
ρ^{PS}	0.5	0.63	0.49
γ^{PS}	0.1	1	0.098
A^{NC}	2	1	1
A^{C1}	8	32	4
A^{C2}	8	20	4

Table 3.3: Summarized characteristic values of regulated model parameters.

Table 3.3 summarizes characteristic values of regulated model parameters. For better understanding the amplifications of the compartments instead of the parameters of the regulation functions are given.

3.1.3.2.2 Regulation of Ploidy Distribution

The regulation of the frequency of the megakaryocyte ploidy distributions requires a different approach. The fractions of the cell streams into the maturation compartments are calculated based on experiments of [60]. In these experiments the frequencies of the main four ploidy classes 8N, 16N, 32N, and 64N were counted in dependency of an imposed variation of the platelet count in the peripheral blood. The resulting frequency distributions were approximated by least square fitting of four second order polynomials against the experimental data.

The polynomials

$$q^{MKi}(TH) = \xi_0^{MKi} + \xi_1^{MKi} \cdot TH + \xi_2^{MKi} \cdot (TH)^2 \tag{3.40}$$

where

$$TH = \frac{\sum_{i=1}^{5} x_i^{TH}}{\sum_{i=1}^{n_{TH}} x_i^{Th\ \text{steady state}}} \tag{3.41}$$

are calculated by solving the following optimization problem in the variables ξ_0^{Mk1}, ξ_1^{MK1}, and ξ_2^{MK1}:

$$(P^{MKi}) = \begin{cases} \sum_{j=1}^{r} \left(y_j^{MKi} - q_j^{MKi}\left(\xi_0^{MKi}, \xi_1^{MKi}, \xi_2^{MKi}\right)\right)^2 \rightarrow \min \\ \xi_0^{MKi}, \xi_1^{MKi}, \xi_2^{MKi} \epsilon\, \mathbb{R} \end{cases} \tag{3.42}$$

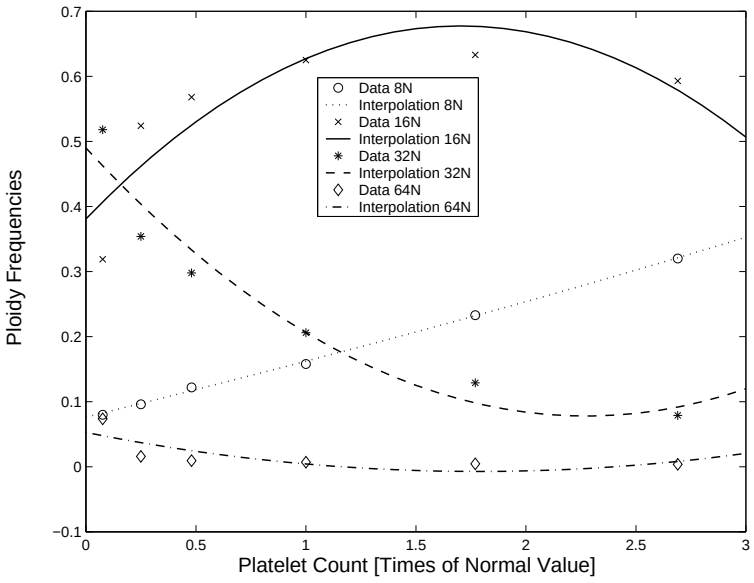

Figure 3.7: Approximation of the regulation of ploidy distribution by second order polynomials. Fitted polynomials and experimental data. Data taken from Kuter [60].

where

$$q_j^{MKi}\left(\xi_0^{MKi},\xi_1^{MKi},\xi_2^{MKi}\right) = q^{MKi}\left(\xi_0^{MKi},\xi_1^{MKi},\xi_2^{MKi},TH_j\right)$$

and

$$y_j^{MKi} = \text{experimentally found frequency of ploidy group i}$$
$$\text{at a normalized thrombocyte count } TH\ .$$

Figure 3.7 shows the approximated polynomials $q^{MKi}(TH)$ which regulate the ploidy distribution in the model.

The fractions $f^{MK1}...f^{MK4}$ of the cell outflow of the EMB compartment into the megakaryocyte compartments are calculated by normalization of the sum of the polynomials q^{MKi} to 1:

$$f^{MK1}(TH) = \frac{q^{MK1}(TH)}{q^{MK1}(TH)+q^{MK2}(TH)+q^{MK3}(TH)+q^{MK4}(TH)} \tag{3.43}$$
$$f^{MK2}(TH) = \frac{q^{MK2}(TH)}{q^{MK1}(TH)+q^{MK2}(TH)+q^{MK3}(TH)+q^{MK4}(TH)}$$

$$f^{MK3}(TH) = \frac{q^{MK3}(TH)}{q^{MK1}(TH) + q^{MK2}(TH) + q^{MK3}(TH) + q^{MK4}(TH)}$$
$$f^{MK4}(TH) = \frac{q^{MK4}(TH)}{q^{MK1}(TH) + q^{MK2}(TH) + q^{MK3}(TH) + q^{MK4}(TH)}$$

Thus, one gets

$$f^{MK1}(TH) + f^{MK2}(TH) + f^{MK3}(TH) + f^{MK4}(TH) = 1 \ . \tag{3.44}$$

This means that the cell stream leaving the endoreduplication compartment is distributed completely into the four megakaryocyte maturation compartments MK1...MK4.

3.1.4 Summarized System Equations of the Rat Model

$$\dot{x}^{PS} = -\lambda^{PS}_{active} \cdot \gamma^{PS} \cdot x^{PS} + 2 \cdot \rho^{PS} \cdot \gamma^{PS} \cdot \lambda^{PS}_{active} \cdot x^{PS} \tag{3.45}$$

$$y^{PS} = 2 \cdot (1-\rho) \cdot \gamma^{PS} \cdot \lambda^{PS}_{active} \cdot x^{PS} \tag{3.46}$$

$$\dot{x}^{C}_1 = u^C + \alpha^C \cdot x^C_1 - \lambda^C \cdot x^C_1 \tag{3.47}$$

$$\dot{x}^{C}_2 = \lambda^C \cdot x^C_1 + \alpha^C \cdot x^C_2 - \lambda^C \cdot x^C_2$$

...

$$\dot{x}^{C}_5 = \lambda^C \cdot x^C_4 + \alpha^C \cdot x^C_5 - \lambda^C \cdot x^C_5$$

$$y^C = \lambda^C \cdot x^C_5 \tag{3.48}$$

where

C = NC, C1, C2, EMB, MK1, MK2, MK3, MK4, ICV, TH

with

$$\alpha^{EMB},\ \alpha^{MK1},\ \alpha^{MK2},\ \alpha^{MK3},\ \alpha^{MK4},\ \alpha^{TH} = 0 \tag{3.49}$$

$$\dot{x}^R = u^R - \lambda^R \cdot x^R \tag{3.50}$$

$$u^{NC} = \nu^{PS,NC} \cdot y^{PS} \tag{3.51}$$

$$u^{C1} = \nu^{NC,C1} \cdot y^{NC} \tag{3.52}$$

$$u^{C2} = \nu^{C1,C2} \cdot y^{C1} \tag{3.53}$$

$$u^{EMB} = \nu^{C2,EMB} \cdot y^{C2} \tag{3.54}$$

$$u^{MKi} = f^{MKi} \cdot \nu^{EMB,MK} \cdot y^{EMB} \tag{3.55}$$

$$u^{TH} = \nu^{MK,TH} \cdot \sum_{i=1}^{4} p^{MKi} \cdot y^{ICV} \cdot y^{MKi} \tag{3.56}$$

$$f^{MKi}(TH) = \frac{q^{MKi}(TH)}{\sum_{j=1}^{4} q^{MKj}(TH)}, \qquad i = 1...4 \tag{3.57}$$

$$q^{MKi}(TH) = \xi^{MKi}_0 + \xi^{MKi}_1 \cdot TH + \xi^{MKi}_2 \cdot (TH)^2, \quad i = 1...4 \tag{3.58}$$

$$\rho^{PS} = \xi^{PS}_1 + \xi^{PS}_2 \cdot e^{-\xi^{PS}_3 \cdot PS} \tag{3.59}$$

$$\gamma^{PS} = \xi^{PS}_4 + \xi^{PS}_5 \cdot e^{-\xi^{PS}_6 \cdot Z} \tag{3.60}$$

$$\alpha^{NC} = \xi_1^{NC} + \xi_2^{NC} \cdot e^{-\xi_3^{NC} \cdot Z} \tag{3.61}$$

$$\alpha^{C1} = \xi_1^{C1} + \xi_2^{C1} \cdot e^{-\xi_3^{C1} \cdot (C1+C2+EMB+MkMass)/4} \tag{3.62}$$

$$\alpha^{C2} = \xi_1^{C2} - \xi_2^{C2} \cdot e^{-\xi_3^{C2} \cdot R} \tag{3.63}$$

$$u_1^R = \xi_1^R + \xi_2^R \cdot e^{-\xi_3^R \cdot TH} \tag{3.64}$$

$$u_2^R = \xi_4^R + \xi_5^R \cdot e^{-\xi_6^R \cdot (C2+EMB+MkMass)/3} \tag{3.65}$$

$$u^R = \frac{1}{2} \cdot u_1^R + \frac{1}{2} \cdot u_2^R \tag{3.66}$$

$$u^{ICV} = \xi_1^{ICV} - \xi_2^{ICV} \cdot e^{-\xi_3^{ICV} \cdot R} \tag{3.67}$$

$$PS = \frac{x^{PS}}{x^{\text{PS steady state}}} \tag{3.68}$$

$$PSinj = \frac{x^{PSinj}}{x^{\text{PS steady state}}} \tag{3.69}$$

$$C = \frac{\sum_{i=1}^{5} x_i^C}{\sum_{i=1}^{5} x_i^{C\text{ steady state}}} \tag{3.70}$$

where

$$C = \text{NC, C1, C2, EMB, MK1, MK2, MK3, MK4, ICV, TH} \tag{3.71}$$

$$MK = \frac{\sum_{i=1}^{4} \sum_{j=1}^{5} x_j^{MKi}}{\sum_{i=1}^{4} \sum_{j=1}^{5} x_j^{\text{MKi steady state}}} \tag{3.72}$$

$$R = \frac{x^R}{x^{\text{R steady state}}} \tag{3.73}$$

$$MkMass = MK \cdot ICV \tag{3.74}$$

$$\begin{aligned} Z = \big(&w^{PS} \cdot (PS + PSinj) + w^{NC} \cdot NC + w^{C1} \cdot C1 \\ &+ w^{C2} \cdot C2 + w^{EMB} \cdot EMB + w^{Mk} \cdot Mk\big) \\ &\cdot \left(w^{PS} + w^{NC} + w^{C1} + w^{C2} + w^{EMB} + w^{Mk}\right)^{-1} \end{aligned} \tag{3.75}$$

Denotations

x_i^C = state variables

u_i^C = inflow functions

y_i^C = outflow functions

λ^C = flow rates or cell differentiation rates

α^C = cell production rates

ξ_i^C = regulation coefficients

p^{MKi} = specific platelet productivity of ploidy groups

$\nu^{A,B}$ = flow normalization factor for flow from A to B

w^C = weighting factors according to cell frequency in bone marrow

q^{MKi} = values of interpolation polynomials for ploidy frequencies

f^{MKi} = normalized interpolated ploidy frequencies

Constants

$\lambda^{PS} = 1/10$	$\lambda^{NC} = 5/50$	$\lambda^{C1} = 5/96$
$\lambda^{C2} = 5/48$	$\lambda^{EMB} = 5/35$	$\lambda^{MKi} = 5/35$
$\lambda^{ICV} = \lambda^{MKi}$	$\lambda^{TH} = 5/96$	$\lambda^{R} = 1/10$

$\xi_1^{PS} = 0.49$	$\xi_2^{PS} = 0.14$	$\xi_3^{PS} = 2.639$
$\xi_4^{PS} = 0.098$	$\xi_5^{PS} = 0.902$	$\xi_6^{PS} = 6.115$
$\xi_1^{NC} = 0$	$\xi_2^{NC} = 0.0426$	$\xi_3^{NC} = 1.1903$
$\xi_1^{C1} = 0.0126$	$\xi_2^{C1} = 0.0134$	$\xi_3^{C1} = 0.9664$
$\xi_1^{C2} = 0.0469$	$\xi_2^{C2} = 0.0217$	$\xi_3^{C2} = 0.6355$
$\xi_1^{R} = 0$	$\xi_2^{R} = 1000$	$\xi_3^{R} = 6.9078$
$\xi_4^{R} = 0$	$\xi_5^{R} = 10$	$\xi_6^{R} = 2.3026$
$\xi_4^{ICV} = 0.0469$	$\xi_5^{ICV} = 0.0217$	$\xi_6^{ICV} = 0.6335$
$\xi_0^{MK1} = 0.0755$	$\xi_1^{MK1} = 0.0838$	$\xi_2^{MK1} = 0.0026$
$\xi_0^{MK2} = 0.3770$	$\xi_1^{MK2} = 0.3522$	$\xi_2^{MK2} = -0.1034$
$\xi_0^{MK3} = 0.4848$	$\xi_1^{MK3} = -0.3577$	$\xi_2^{MK3} = 0.0786$
$\xi_0^{MK4} = 0.0523$	$\xi_1^{MK4} = -0.0667$	$\xi_2^{MK4} = 0.0187$

$w^{PS} = 4.4759 \cdot 10^5$	$w^{NC} = 3.4577 \cdot 10^5$	$w^{C1} = 3.5360 \cdot 10^5$
$w^{C2} = 1.4144 \cdot 10^6$	$w^{EMB} = 2.0052 \cdot 10^6$	$w^{MK} = 2.0052 \cdot 10^6$

$\nu^{PS,NC} = 1/0.01$	$\nu^{NC,C1} = 1/2$	$\nu^{C1,C2} = 1/8$
$\nu^{C2,EMB} = 1/8$	$\nu^{EMB,MK} = 1$	$\nu^{MK,TH} = 0.2197$

3.1.5 Approaches to Verification and Validation

Examination of the quality of such a model should take into account different methods to compare different model variables against reality. To examine the steady state characteristics the model and experimental cell numbers have to be compared. To examine the model dynamics different disturbances are simulated.

3.1.5.1 Verification of Steady State Model and "Real World" Cell Numbers

The following sections explain the methods of comparing model compartment contents to experimentally determined cell concentrations.

3.1.5.1.1 Principles of Calculation

As it was mentioned before, the "real world" cell numbers are not used in the mathematical model equations, so the cell numbers corresponding to the several compartments have to be calculated separately. Based on well known numbers of thrombocyte turnover in rats and the parameters of the model, the absolute cell numbers corresponding to the model compartments are derived.

The approaches for the calculations are based on the equation

$$OutFlow^{\text{steady state}} = \lambda^{\text{steady state}} \cdot CellNumber^{\text{steady state}} \tag{3.76}$$

which is transformed to

$$CellNumber^{\text{steady state}} = \frac{OutFlow^{\text{steady state}}}{\lambda^{\text{steady state}}} \tag{3.77}$$

and with

$$\lambda^{\text{steady state}} = \frac{1}{TransitTime^{\text{steady state}}} \tag{3.78}$$

finally results in

$$CellNumber^{\text{steady state}} = OutFlow^{\text{steady state}} \cdot TransitTime^{\text{steady state}} \ . \tag{3.79}$$

The basic size $OutFlow$ is successivly calculated throughout the model compartments by the compartment steady state amplifications $A^{\text{steady state}}$ of the cell streams:

$$OutFlow^{\text{steady state}} = A^{\text{steady state}} \cdot InFlow^{\text{steady state}} \tag{3.80}$$

where A in general denotes the amplification resulting from cell divisions.

3.1.5.1.2 Calculation and Verification

Schermer [82] assumes the thrombocyte count in rats to be about

$$ThCount = 800 \cdot 10^9/l(G/l), \tag{3.81}$$

the blood volume

$$BloodVolPerBodyWeight = 5.5\text{ml / 100g body weight}, \tag{3.82}$$

and the body weight

$$BodyWeight = 250g\ . \tag{3.83}$$

This gives a total thrombocyte number in the rat of

$$\begin{aligned} ThNum &= ThCount \cdot BloodVolPerBodyWeight \cdot BodyWeight \\ &= 1.1 \cdot 10^{10}. \end{aligned} \tag{3.84}$$

With the (model) turnover time for thrombocytes of

$$T_{Th} = 96\,h \tag{3.85}$$

which means that every 96 h the total amount of platelets is renewed, one gets a thrombocyte turnover of

$$\begin{aligned} ThTurnOver &= \frac{ThNumber}{T_{Th}} \\ &= 1.1458 \cdot 10^8/h \end{aligned} \tag{3.86}$$

in the rat. If the thrombocyte productivity of a megakaryocyte is assumed to be on average about

$$ThProdPerMk \approx 2000 \tag{3.87}$$

thrombocytes per megakaryocyte, this leads to a megakaryocyte turnover of

$$\begin{aligned} MkTurnOver &= \frac{ThTurnOver}{ThProdPerMk} \\ &= 5.73 \cdot 10^4/h \end{aligned} \tag{3.88}$$

in rats. With an estimated fraction of 15h of the transit time of 35h of the EMB compartment where the megakaryocytes become morphologically recognizable and 35h in the compartments of the maturing megakaryocytes MKi one gets a transit time of

$$\begin{aligned} T_{MkMorphRec} &= 15h + 35h \\ &= 50h \end{aligned} \tag{3.89}$$

for morphologically recognizable megakaryocytes. This corresponds to a total megakaryocyte number of

$$\begin{aligned} MkCorrCellNum &= MkTurnOver \cdot T_{MkMorphRec} \\ &= 2.86 \cdot 10^6 \end{aligned} \tag{3.90}$$

for one rat. Related to the value of

$$BmCellNumPerBodyWeight = 1200 \cdot 10^4/g \text{ body weight} \tag{3.91}$$

rat bone marrow cells per g body weight [63] and a resulting number of bone marrow cells of

$$\begin{aligned} BmCellNum &= BmCellNumPerBodyWeight \cdot BodyWeight \\ &= 3.0 \cdot 10^9 \end{aligned} \tag{3.92}$$

this gives a frequency of megakaryocytic cells in bone marrow of

$$\begin{aligned} MkCellFreq &= \frac{MkCellNumber}{BmCellNum} \\ &= 9.54 \cdot 10^{-4} \\ &\approx 0.1\% \end{aligned} \tag{3.93}$$

which corresponds very good to the experimental values of 0.2% reported by Boll [2]. The corresponding steady state cell number of the C2 compartment can be calculated as:

$$\begin{aligned} C2CorrCellNum &= \sum_{1}^{5} x_i^{C2Corr} \\ &= \sum_{1}^{5} C2OutFlow \cdot (A^{C2})^{\frac{i}{5}} \cdot \frac{TransTime^{C2}}{5} \\ &= \sum_{1}^{5} MkInflow \cdot (A^{C2})^{\frac{i}{5}} \cdot \frac{TransTime^{C2}}{5} \\ &= \sum_{1}^{5} MkTurnover \cdot (A^{C2})^{\frac{i}{5}} \cdot \frac{TransTime^{C2}}{5} \\ &= MkTurnover \cdot \frac{TransTime^{C2}}{5} \cdot \sum_{1}^{5} (A^{C2})^{\frac{i}{5}} \\ &= 1.4144 \cdot 10^{6} \text{ (cells)} \end{aligned} \tag{3.94}$$

The corresponding frequency is

$$\begin{aligned} C2CorrCellFreq &= \frac{C2CorrCellNum}{BmCellNum} \\ &= 4.7147 \cdot 10^{-4} \end{aligned} \tag{3.95}$$

in bone marrow cells. Assuming that the CFU-Mk are histogenetically located at the earlier part of the C2 compartment and thus colony formation is only possible for a fraction of the compartment, this result fits well to experimental values of 0.01% to 0.025% reported by Williams [99] and 0.0367% reported by Long [65].

The corresponding cell number for the C1 compartment is

$$\begin{aligned} C1CorrCellNum &= \sum_{1}^{5} x_i^{C1Corr} \\ &= \sum_{1}^{5} C1OutFlow \cdot (A^{C1})^{\frac{i}{5}} \cdot \frac{TransTime^{C1}}{5} \\ &= \sum_{1}^{5} C2Inflow \cdot (A^{C1})^{\frac{i}{5}} \cdot \frac{TransTime^{C1}}{5} \\ &= \sum_{1}^{5} \frac{C2Outflow}{A^{C2}} \cdot (A^{C1})^{\frac{i}{5}} \cdot \frac{TransTime^{C1}}{5} \\ &= \frac{C2Outflow}{A^{C2}} \cdot \frac{TransTime^{C1}}{5} \cdot \sum_{1}^{5} (A^{C1})^{\frac{i}{5}} \\ &= 3.5360 \cdot 10^5 \end{aligned} \tag{3.96}$$

cells. The frequency in bone marrow is

$$\begin{aligned} C1CorrCellFreq &= \frac{C1CorrCellNum}{BmCellNum} \\ &= 11.787 \cdot 10^{-5} \ . \end{aligned} \tag{3.97}$$

Experimental values for the BFU-Mk, which is again assigned to the early part of the C1 compartment are about $7.3 \cdot 10^{-5}$, reported by Long [65].

For calculation of the model derived corresponding cell number of the NC compartment it is assumed, that about 20% of the cells produced by the noncommitted progenitor cells develop into megakaryocytic committed progenitor cells. This assumption is derived from cell colony experiments with CFU-GEMM [90], in which a fraction of $\approx 20\%$ of colonies grow into megakaryocytic colonies. Like described for the C1 and C2 compartment, the corresponding cell number of compartment NC are calculated as

$$NCCorrCellNum = 1.73 \cdot 10^5 \tag{3.98}$$

cells. Thus, the frequency in bone marrow would be

$$NCCorrCellFreq = 5.77 \cdot 10^{-5} \ . \tag{3.99}$$

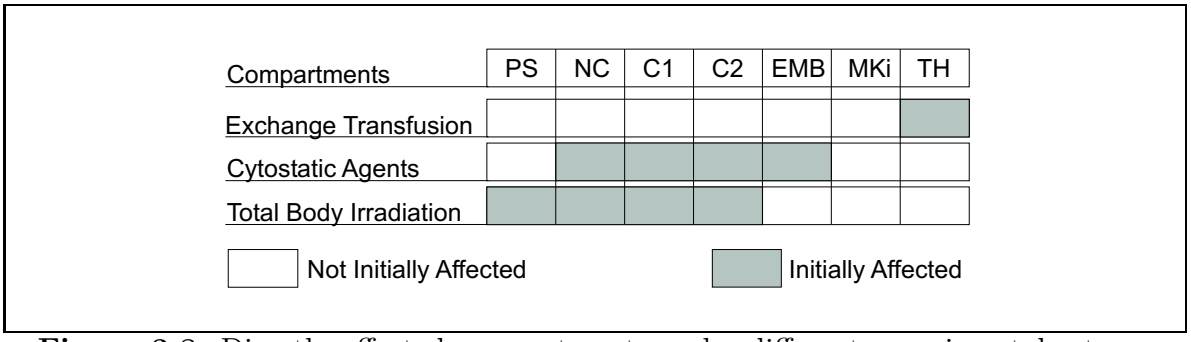

Figure 3.8: Directly affected compartments under different experimental setups.

Experimental values for the CFU-GEMM, which are in-vitro examples for noncommitted progenitor cells are about $4 \cdot 10^{-5}$ in bone marrow [69].

The content of the PS compartment corresponds to

$$PSCorrCellNumber = 2.24 \cdot 10^5 \tag{3.100}$$

cells or a frequency in bone marrow of

$$PSCorrCellFreq = 7.46 \cdot 10^{-4} \ . \tag{3.101}$$

Experimental frequencies of CFU-S which are known to be histogenetically close to the pluripotent stem cells are about $5 - 30 \cdot 10^{-5}$ [70].

In general, it is to say, that the quality of information about cell development decreases with decreasing differentiation. Another problem is the possibility of in-vitro experiments to produce artefacts. However, most calculations based on the model fit well to experimental values.

3.1.5.2 Verification of the Model Dynamics in the Disturbed System

Figure 3.8 shows the initially affected compartments of these disturbances simulated in the following sections. Of course other cell compartments are involved indirectly in the following reactions.

3.1.5.2.1 Disturbances of the Platelet Numbers in the Peripheral Blood

In experiments of Odell [77] rats were made thrombocytopenic (reduced platelet count) to levels of 10%, 40% and 70% by exchange transfusion with platelet-poor blood. In

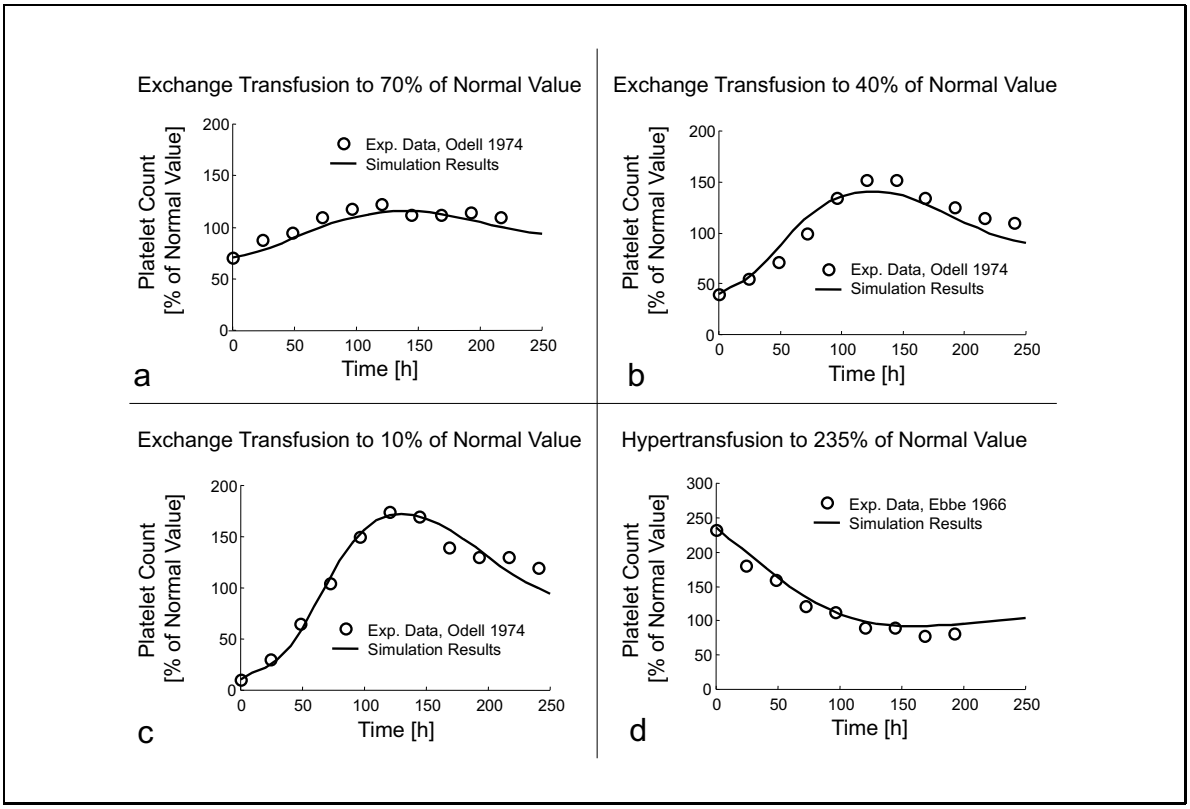

Figure 3.9: Simulations of exchange transfusion experiments. Experimental data and simulation results.

these experiments only the latest part of thrombocytopoiesis, the thrombocyte compartment is manipulated. Characteristic for the simulations of these experiments is, that in the resulting reaction only the part of the later development stages is involved. The earlier compartments and the pluripotent stem cells are not stimulated by this disturbance. Simulations were performed by setting the initial values of the TH compartment to the platelet levels achieved by the exchange transfusion. Figures 3.9a-c show the experimental data and the simulation results. In another experiment the reaction of the system to thrombocytosis (increased platelet count) induced by hypertransfusion is tested [21]. For the simulation the initial value for the TH compartment was set up corresponding to the experimental platelet count. The result is shown in figure 3.9d.

3.1.5.2.2 Administration of Cytostatic agents

The cytostatic drug 5-Fluorouracyl (5-FU) is known to damage mainly cells which are synthesizing DNA and to spare the early stem cells. Thus, in the presented model the strongly affected cell pools are C1, C2 and EMB compartments. The 5-FU experiment

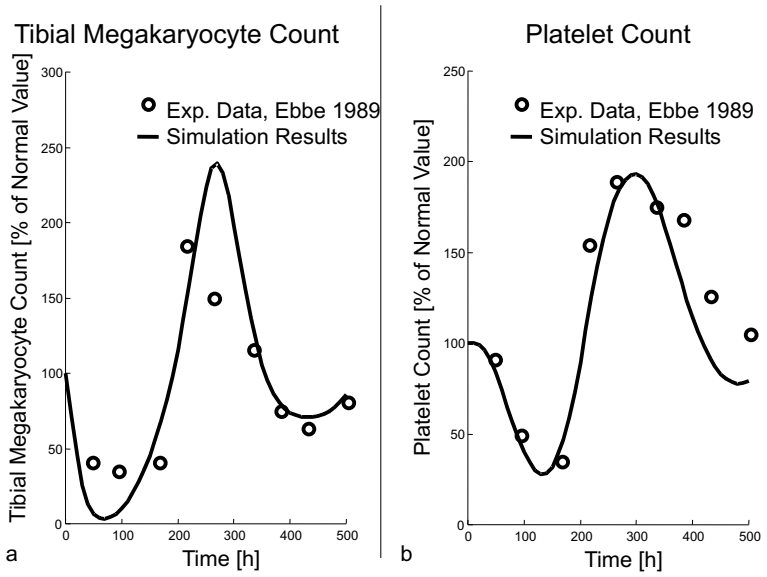

Figure 3.10: Single administration of 5-Fluorouracil at time 0. Experimental data and simulation results.

causes disturbances in the middle stages of the model and spares the PS, MK and TH compartment. In the following reaction, the PS compartment is strongly involved to repopulate the damaged cell pools. For simulation of the administration of 5-FU the initial value for the fraction of remaining cells in C2 was set to 1% according to experimental results [100]. The numbers for NC, C1 and EMB were estimated via least-square fitting of platelet counts against experimental data from Ebbe [23]. The estimated remaining cell numbers were 100% for NC, 23% for C1, and 0% for EMB. These values are compatible to known effects of cytostatic agents. The initial values for other cell pools were not changed and are 100% for the PS, MK1...MK4 and TH compartment. Figures 3.10a,b show a simulation of the mouse thrombocytopoetic system in reaction to 5-FU.

3.1.5.2.3 Repopulation of the Stem Cell Compartment

Calculations based on the repopulation dynamics of the stem cell compartment shown in figure 3.11 result in a doubling time of

$$T_{doubling} = \frac{t_1 - t_0}{log_2(\frac{x_1}{x_0})} \approx \frac{100\,h}{log_2(\frac{2 \cdot 10^{-3}}{2 \cdot 10^{-2}})} = 30\,h\ . \tag{3.102}$$

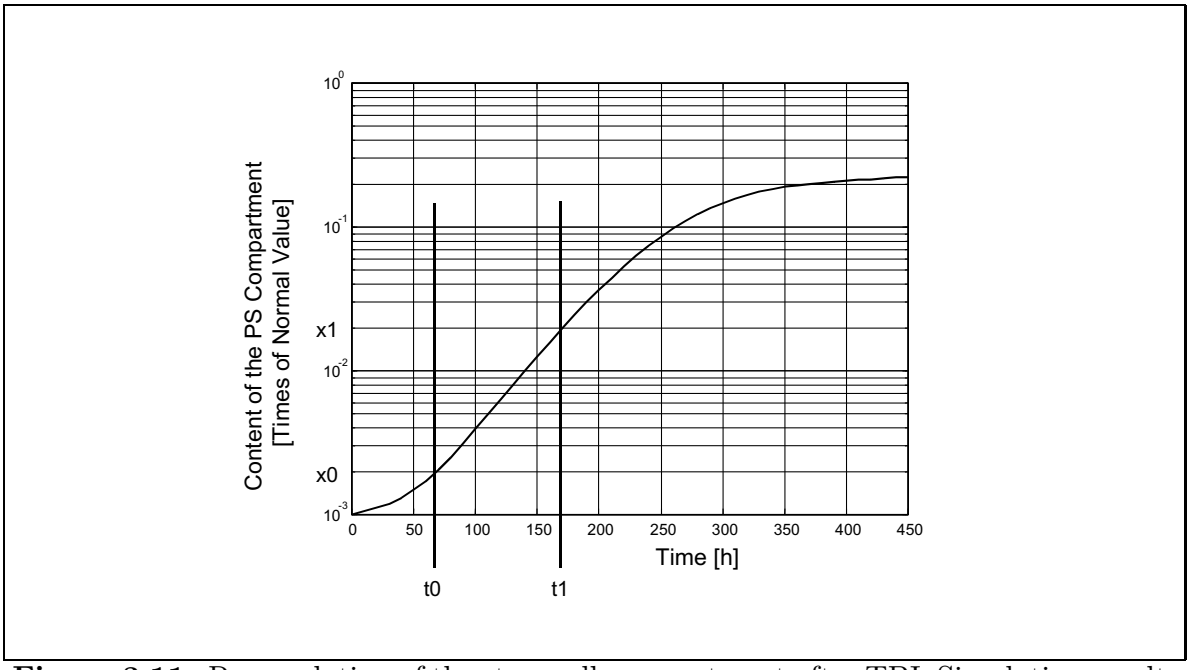

Figure 3.11: Repopulation of the stem cell compartment after TBI. Simulation result.

This is similar to the 27-30 h which were estimated in [32] from experiments of several authors.

3.1.6 Simulation and Estimation Times

A simulation of the system in MATLAB® takes about 10 seconds for a simulated "real life" time of 1000 hours. Estimation (optimization) times are in the area of about 5 to 10 minutes on a 500 MHz Pentium II® PC with a modified version of the model, in which simulation speed was increased by mathematically combining the parallel MK1...MK4 compartments into one serial compartment.

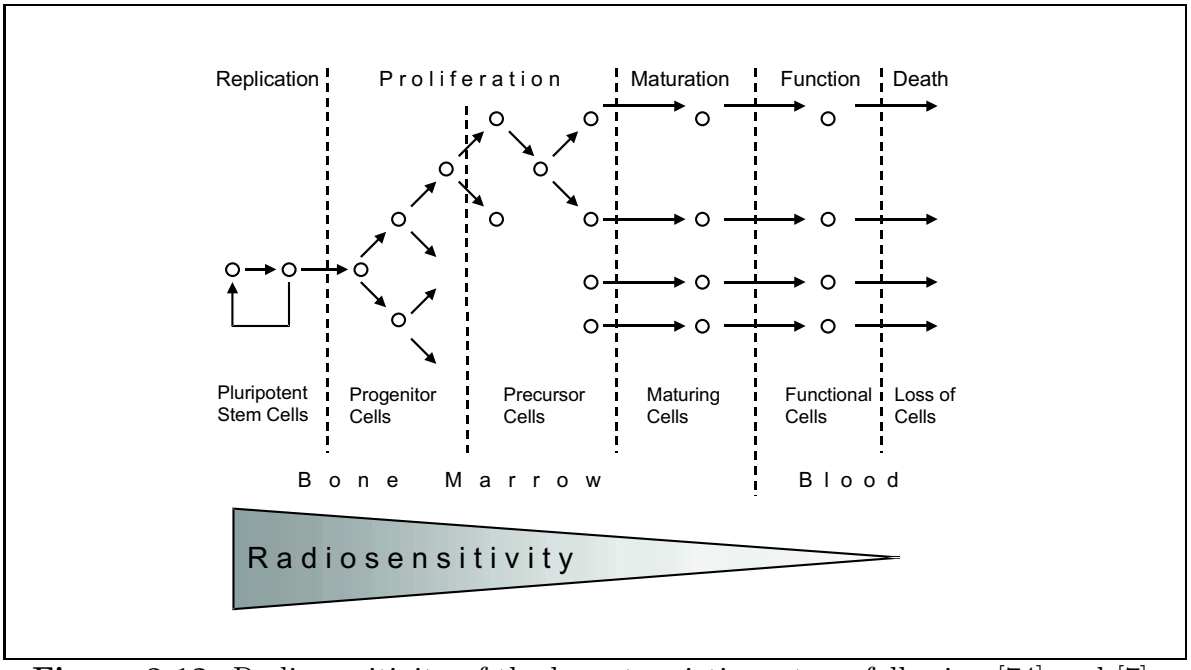

Figure 3.12: Radiosensitivity of the hematopoietic system, following [74] and [7].

3.2 Model Based Analysis of the Hematological Effects of Acute Irradiation

The following sections show the application of the developed model of thrombocytopoiesis for the analysis of hematological effects of acute irradiation. The necessary extensions of the model and the model based methods for estimation of surviving fractions of stem cells are explained. Data of rats and humans are evaluated.

3.2.1 Hematological Effects of Acute Irradiation

The effects of irradiation on hematopoiesis are a consequence of the physiology of the hematopoietic system with its fast cell turnover [6] Since the hematopoietic system has a part of very active cell proliferation it is very radiosensitive. Experiments show further, that the earlier development stages of hematopoieisis are in general more radiosensitive than the later ones. Peripheral blood cells are in general radioresistant and not affected in radiation experiments or accidents (with exception of the lymphocytes) [5] [74]. The general scheme of hematopoietic radiation sensitivity is summarized in figure 3.12. Cells can either be destroyed immediatly if hit by radiation or injured with the consequence that they can only perform a few divisions more [5]. The con-

sequence of the destruction of stem, progenitor, and precursor cells is a reversible or irreversible drop of cell numbers in the peripheral blood. The typical reaction pattern of the thrombocytes in humans shows a stable shoulder in a range of 2 to 10 days after irradiation with a subsequent drop of platelet counts. Granulocyte counts can show an initial overshoot over the individual normal values between the days 0 and 5 and a following decrease of cell numbers. Lymphocytes in general react very fast and counts decrease immediately after irradiation and reach minimum values already within 2 days. Erythrocytes in general stay at a normal level since their survival time is with about 120 days very much longer compared to the white blood cells and platelets.

Irradiation damages not only the hematopoietic system, but in general all cell systems with a fast cell turnover. Such are, for example, the gastrointestinal system with its fast cell renewal system of the mucous membranes and the skin [8].

As a result, several pathophysiological dysfunctions occur, such as the hematopoietic syndrome, the gastrointestinal syndrome, radiation skin burns, oligo and azoo spermia and some others. The full picture of these interacting syndromes and impairments is called the "acute radiation syndrome".

3.2.2 Model Extension: A Compartment for Injured Stem Cells

Experiments with cell cultures led to the conclusion that after irradiation there exists a fraction of "injured" stem cells, which show reduced self replication probability and a slower proliferation than normal cells [9]. Estimations based on experimental results described in [9] show for example a doubling in generation time of cells irradiated with 5 Gy. For this reason for the proposed model of acute radiation effects it is considered to be important to assume the presence of an "injured stem cell" compartment composed of cells "hit" by radiation and injured in their proliferative potential.

The general structure of this model is the same like in the "normal" pluripotent stem cells, but with another proliferative activity and self replication probability. The cell generation time is assumed to be twice as much as in normal cells, what means that $\lambda^{PSinj} = 0.5 \cdot \lambda^{PS}_{active}$, for the self replication probability a value of 0.05 is chosen, which was already used in [33].

The system equations are similar to that of the "healthy" pluripotent stem cell compartment:

$$\dot{x}^{PSinj} = -\lambda^{PSinj} \cdot x^{PSinj} + 2 \cdot \rho^{PSinj} \cdot \lambda^{PSinj} \cdot x^{PSinj} \tag{3.103}$$

$$y^{PSinj} = 2 \cdot \left(1 - \rho^{PSinj}\right) \cdot \lambda^{PSinj} \cdot x^{PSinj} \tag{3.104}$$

As a consequence of splitting the PS compartment into a PS and a PSinj compartment several model equations have to be adapted:

$$u^{NC} = \nu^{PS,NC} \cdot \left(y^{PS} + y^{PSinj}\right) \tag{3.105}$$

$$\rho^{PS} = \xi_1^{PS} + \xi_2^{PS} \cdot e^{\xi_3^{PS} \cdot (PS + PSinj)} \tag{3.106}$$

$$PSinj = \frac{x^{PSinj}}{x^{\text{PS steady state}}} \tag{3.107}$$

$$\begin{aligned} Z = \Big(&w^{PS} \cdot (PS + PSinj) + w^{NC} \cdot NC + w^{C1} \cdot C1 \\ &+ w^{C2} \cdot C2 + w^{EMB} \cdot EMB + w^{MK} \cdot MK\Big) \\ &\cdot \left(w^{PS} + w^{NC} + w^{C1} + w^{C2} + w^{EMB} + w^{MK}\right)^{-1} \end{aligned} \tag{3.108}$$

3.2.3 Least Square Estimation with a Nonlinear ODE Model

From the mathematical perspective estimating the contents of cell pools can be described as a curve fitting or optimization problem with the initial values of the differential equation system as optimization parameters. In general the solution of the differential equation system can not be given in an analytical way, and a numerical solution has to be calculated by suitable solution algorithms like the Runge-Kutta, Euler or other methods. In the proposed model only ordinary differential equations (ODEs), for which in general different kinds of solution algorithms exist, were used.

The calling sequence of such an optimization or curve fitting procedure is implemented in the following iterative way:

Find suitable initial values $\vec{v}$ for the ODE system.

Calculate numerical solution of the ODE system with $\vec{v}$.

Compare deviation data/model.

REPEAT

Modify solution $\vec{v}$ to $\vec{v}'$ according to search strategy / optimization routine.

Calculate numerical solution of the ODE system with $\vec{v}'$.

Calculate deviation data/model.

IF $\vec{v}'$ is better than $\vec{v}$ THEN

$\vec{v} := \vec{v}'$

END IF

UNTIL no better solution is found (for a longer time).

END REPEAT

Figure 3.13 visualizes the work of the estimation procedure. For a given set of data stored in a vector M the optimizing algorithm follows a special strategy for fitting the output Y_j of the simulations to the data set M. The deviation of the model output and the data set is given by

$$D_j = (M - Y_j)^T (M - Y_j) \ . \tag{3.109}$$

For each iteration step the optimizer has to perform one or more simulations of the complete model. After a sequence of iterations the optimizer stops. Stopping criteria are reached if no more improvement of the solution can be achieved or if the number of iterations becomes too large.

3.2.4 Implementation of the Estimation Method

An implementation of the estimation method described above has to take into account several tasks.

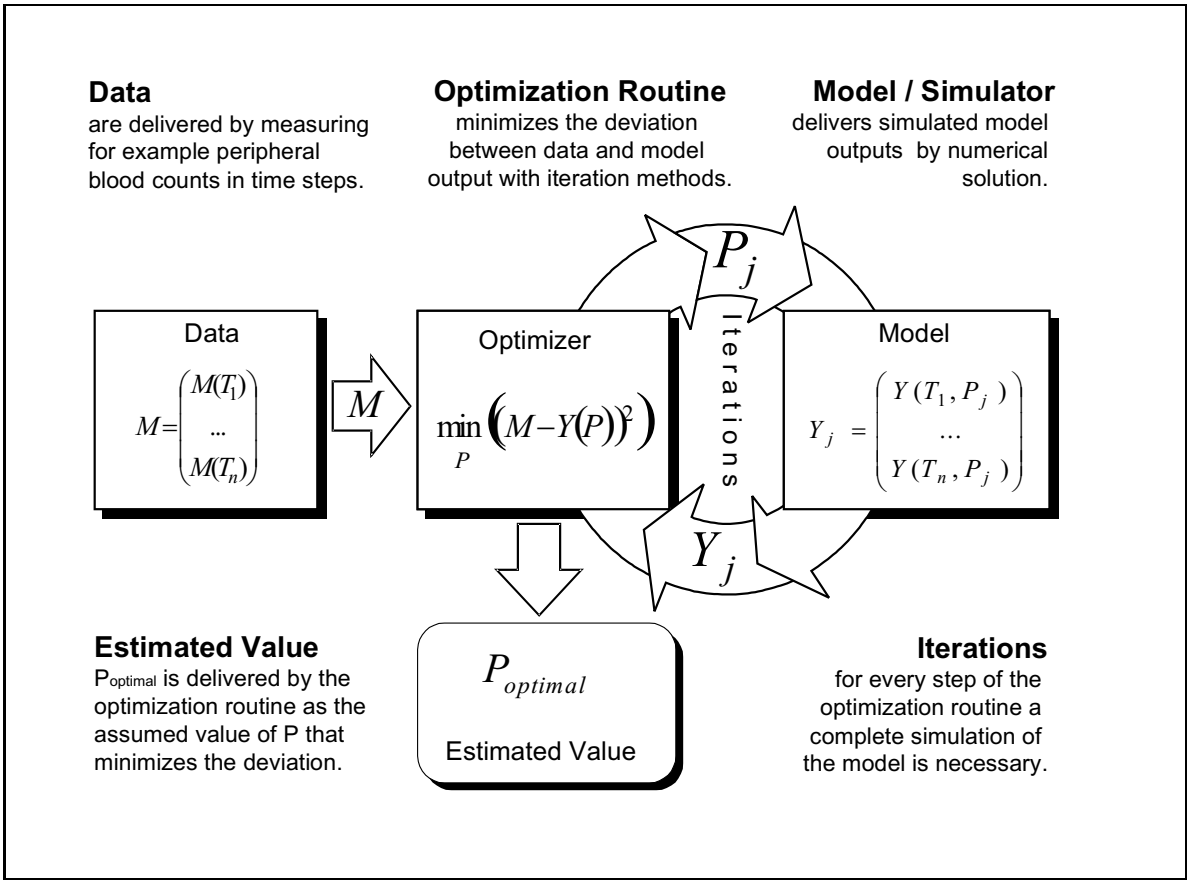

Figure 3.13: Process structure of a least square estimator based on nonlinear differential equations.

3.2.4.1 Characteristics of the Optimization Problem

In the case of the optimization problems, which have to be solved for the realization of the proposed estimation method, one has to deal with the following optimization problem characteristics:

- Nonlinearity caused by the model and the objective function.
- Type of objective function (sum of least squares).
- Variables of the objective function (multivariate, real numbers).
- Constraints (No negative solutions for cell pool contents, biological prerequisites).
- Incomplete convexity.

The identifyed characteristics are important prerequisites for the selection of suitable optimization algorithms.

3.2.4.2 Identification of Suitable Optimization Algorithms

There exist no secure standard solution methods for the described mathematical problem. For this reason it is necessary to identify heuristic mathematical optimization algorithms, which are suitable for the characteristics of the optimization problem. Possible algorithms are

- nonlinear optimization algorithms with constraints, like
  - Sequential Quadratic Programming Algorithms
  - Trust Region Algorithms
- nonlinear optimization algorithms without constraints and work-arounds for constraints by penalty functions like the Levenberg-Marquardt algorithm.

A review on the relevant optimization techniqes is found in the book of Neumann [73].

3.2.4.3 Identification of the Necessary Free Parameters

The mathematical model of thrombocytopoiesis for acute radiation effects consists of 53 ordinary differential equations (ODEs). Taking all 53 initial values of the model ODEs as separate optimization variables would result in a large optimization problem. In connection with characteristics of our problem like constraints and unsecure convexity it is reasonable to assume that in most fitting cases todays optimization algorithms could not produce a convergent optimal solution. Another reason is the calculation time, that would be enormous for a 53 variable optimization problem of that structure. Since every function evaluation in the optimization algorithm means a complete simulation of the model, calculation times in the area of one or more days could be the consequence. Thus, it is reasonable to make clear, which initial values have to be regarded as optimization variables and which can be used as non-variable initial values. An argument for a non-variable initial value is for example a neglectible radiation sensitivity. Moreover it is reasonable to bundle sets of initial values. The first obvious step is to merge the single ODEs of the compartments belonging to one cell pool to one variable. The next step is to find out, if initial values of two or more cell pools can be merged. For the estimation problem the following assumptions were made:

- PS and PSinj are set up with own optimization variables, since a correlating radiation sensitivity is not known.
- The NC, C1 and C2 compartment are set up with own optimization variables
- Cells of the EMB compartment are assumed to be radioresistant. This assumption is based on evulations of experimental results of Mueller [71] and Stein [88].
- Megakaryocytes of the compartments MK1...MK4 are assumed to be radioresistant [18] [10] [71] [88].

The following optimization variables were used:

$$\theta_1 = \text{ fraction of surviving cells of compartment PS} \tag{3.110}$$

$$\theta_2 = \text{ fraction of injured stem cells in compartment PSinj} \tag{3.111}$$

$$\theta_3 = \text{ fraction of surviving cells of compartment NC} \tag{3.112}$$

$$\theta_4 = \text{ fraction of surviving cells of compartment C1} \tag{3.113}$$

$$\theta_5 = \text{ fraction of surviving cells of compartment C2} \tag{3.114}$$

These variables are connected to the model ODEs in form of initial values, which are calculated by multiplication of the θ_i values with the steady state values of the corresponding state variables. If

${}^0x^C$ denotes the initial value of variable x^C

and

$*$ denotes the the steady state values

the initial values satisfy the equations:

$${}^0x^{PS} = \theta_1 \cdot {}^0x^{PS*} \tag{3.115}$$

$${}^0x^{PSinj} = \theta_2 \cdot {}^0x^{PS*} \tag{3.116}$$

$${}^0x_i^{NC} = \theta_3 \cdot {}^0x_i^{NC*} \qquad i = 1...n^{NC} \tag{3.117}$$

$$ {}^{0}x_i^{C1} = \theta_4 \cdot {}^{0}x_i^{C1*} \qquad i = 1...n^{C1} \tag{3.118} $$

$$ {}^{0}x_i^{C2} = \theta_5 \cdot {}^{0}x_i^{C2*} \qquad i = 1...n^{C2} \tag{3.119} $$

3.2.4.4 Identification of Suitable Software

Many different software systems exist for optimization problems. Since the model functions were implemented in MATLAB® programming language [92] it was decided to use this software system again for the optimization problems. For the MATLAB® system two algorithm collections are available, the MATLAB Optimization Toolbox® [93] and the well known NAG® numerical library of the NAG® Numerical Algorithms Group Ltd. [91] in form of the NAG® Foundation Toolbox For Use with MATLAB® .

3.2.4.5 Selection of the Optimization Algorithm for Application

Since there exist no standard methods for analytical solution of the model ODE system, solutions have to be calculated by numerical approximation methods, like discussed above. As a consequence, the fitting optimization problem can not easily be analyzed for nonlinearity, convexity and other typical characteristics used in operations research. The best algorithm(s) can only be found by comparison of the results of the different algorithm applications. Test runs have to be performed and evaluated for convergence, number of iterations, and influence of the optimization starting values.

Different optimization methods and algorithms implemented in the MATLAB Optimization Toolbox® were tested for the optimization problems:

- SQP-Algorithms (Sequential Quadratic Programming Algorithms) with constraints [93] [73] .
- Trust Region Algorithms with constraints [93], [73] .
- Levenberg-Marquardt algorithms with penalty functions for including constraints [93] [73] .

Taken all together, the Trust Region Algorithms delivered the most satisfying results.

3.2.5 Estimation of Remaining Stem Cell Numbers in Rat Experiments

Figure 3.14 shows simulations which are results of least square optimization processes. Data were taken from experimental works of Stein [87] (a-e) and Ebbe [19] (f).

Figure 3.15 summarizes the important results of the optimization runs on the data of the several irradiation experiments done by Stein [87]. The experimental animals were rats.

3.2.6 Adaption of the Model to the Human Thrombocytopoietic System

To apply the stem cell estimation methods developed in section 3.2.5 to humans, it is necessary to adapt the basic rat model to the human thrombocytopoietic system.

Since typical cell division times and differentiation times are in general longer than in the rat, the cell kinetic parameters of the model have to be calculated for the human system. Further, the regulation parametes have to be adapted in the case of changing ratios of compartment cell numbers. Then, new steady states for the cell pools have to be calculated.

Compared to the model of thrombocytopoiesis in rodents, there are less data available for calculating the parameters of the human system. For this reason, several parameters of the human model have to be extrapolated by known relations between cell development times in rodents and in men.

3.2.6.1 Adaption of Model Parameters to Human Cell Generation Times

The cell generation time in rodents was estimated to be about 10h (see chapter 3.1). In general, it is assumed that cell turnover times in humans are about twice as long compared to rodents. For the human hematopoietic system typical cell generation times of about 18-24 h are estimated [89], which supports this assumption. For this reason, it can be assumed that the average cell generation time for the mathematical model in humans is twice as long as in rodents. The same assumptions are made for the differentiation times.

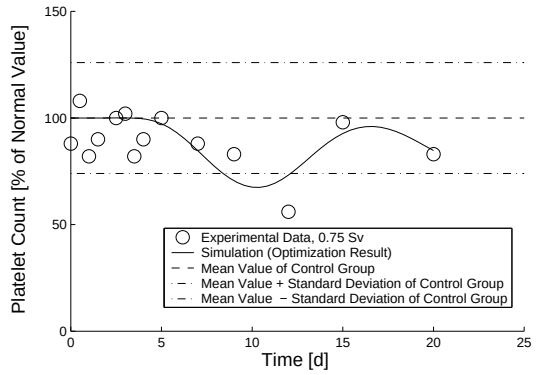

(a) 0.75 Sv, Stein

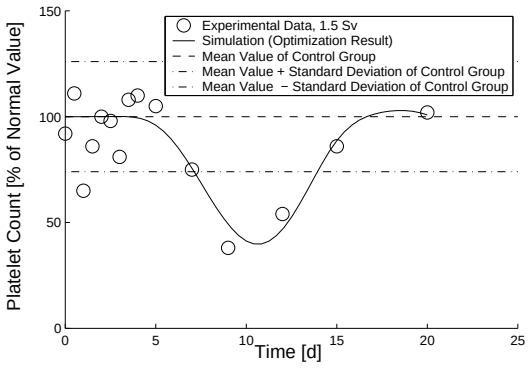

(b) 1.5 Sv, Stein

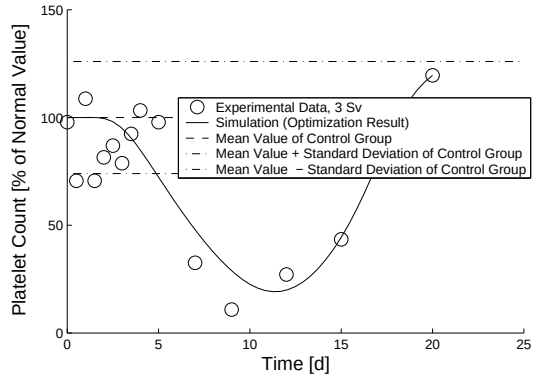

(c) 3.0 Sv, Stein

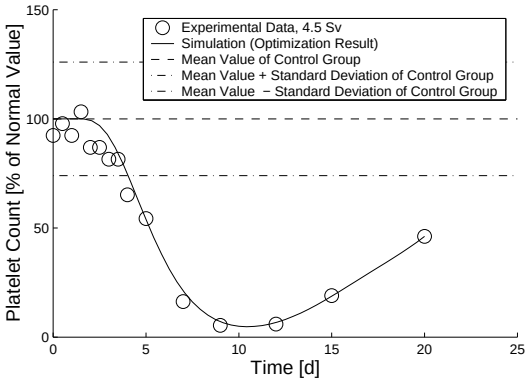

(d) 4.5 Sv, Stein

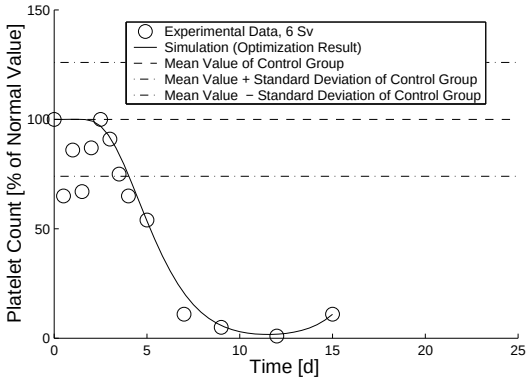

(e) 6.0 Sv, Stein

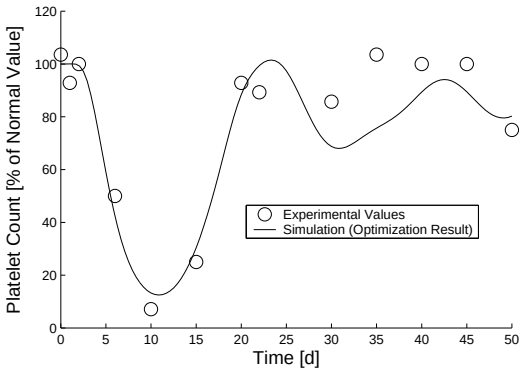

(f) 6.5 Sv, Ebbe

Figure 3.14: Fitting results for the estimation of stem cell numbers after total body irradiations of rats at different doses. Experimental data and simulation results. Data from Stein [87] and Ebbe [19].

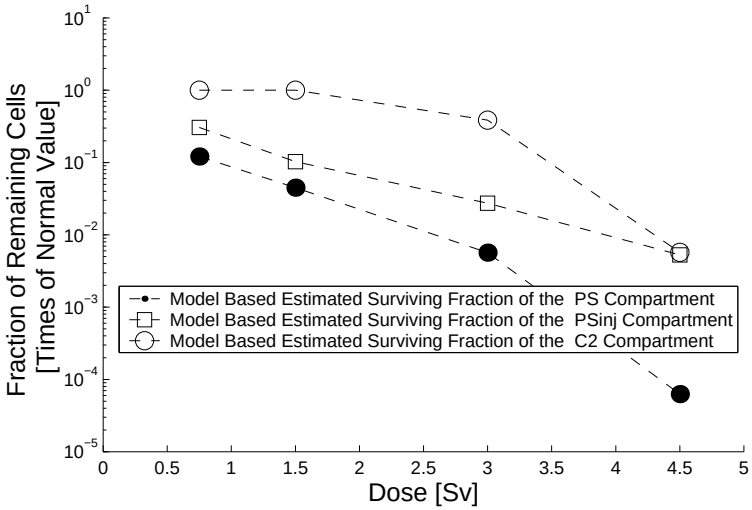

Figure 3.15: Estimated fractions of surviving and injured stem cells in rats after irradiation. Data from Stein [87].

3.2.6.2 Megakaryocyte Turnover Time

For the rodent model the transit time for megakaryocytes was estimated by least square fitting of gamma-delayed serial compartments against experimental data (see section 2.3.7.1) to be about 35h. For the human system no data of the quality which would be necessary for the same estimation process are available. However, there exist other estimations which give rise to the assumption, that the megakaryocyte transit time in humans is about 10 days [5].

3.2.7 Model Extension: A Damage Function for Human Megakaryocytes

The simulations of total body irradiation experiments with the rodent model were performed using the assumption that megakaryocytes are radioresistant. This means on the modeling level, that the complete megakaryocyte compartment was simulated to be not initially affected. This hypothesis is supported by the typical "shoulder" before the drop in thrombocyte counts after TBI. The length of this shoulder is about 48h and does not change recognizably by varying radiation doses. This behaviour is different from that found in data from accidentally irradiated humans. There, one can recognize that the length of this shoulder varies in correlation to the received radiation

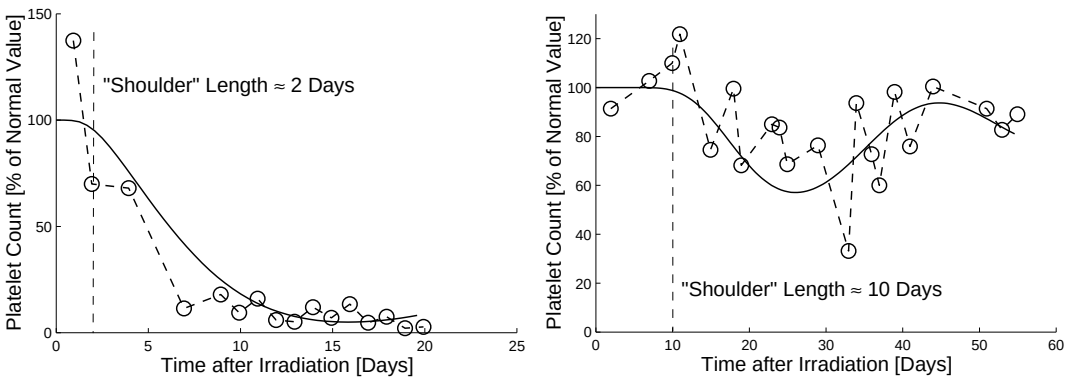

(a) Thrombocyte response pattern with a shoulder of about 2d.

(b) Thrombocyte response pattern with a shoulder of about 10d.

Figure 3.16: Thrombocyte response patterns with different drop delay "shoulder" lengths.

dose. In less severe affected cases typical shoulder lengths in the thrombocyte count of about 10 d are observed. These can shorten down to 2 d in severe cases (figure 3.16). This can be explained by the assumption, that megakaryocytes in humans show a more differentiated radiosensitivity which is negatively correlated to their degree of differentiation. Figure 3.17 visualizes the damage patterns of megakaryocytes and the corresponding response patterns of the thrombocytes. This megakaryocyte damage pattern can be simulated by adapting the initial values $x_1^{MKi}(0) \ldots x_5^{MKi}(0)$ of the single compartments of the megakaryocyte submodel. This has the disadvantage, that 5 new parameters have to be introduced to the model in case of stem cell estimations with optimization routines. The consequences would be a very much longer estimation time and impaired convergence behaviour of the optimization procedure. The task arising from this problem is to reduce the number of necessary parameters for the megakaryocyte submodel to a minimal set. In our model this was done by using the bundle of functions

$$ {}^0x_i^{MKj}(\xi) = q^{\omega_i \cdot \xi}, \quad j = 1...4, i = 1...5 \tag{3.120} $$

$$ \omega_i \geq 1 \tag{3.121} $$

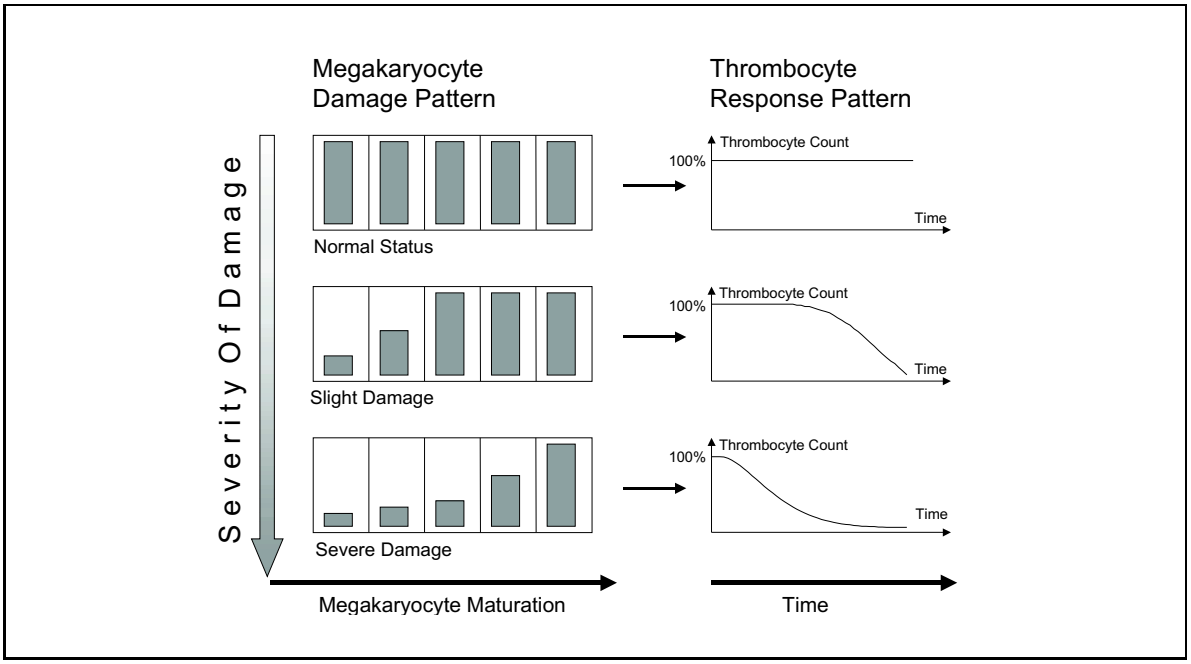

Figure 3.17: Megakaryocyte damage patterns and corresponding thrombocyte response patterns.

where

$^0x_i^{MKj}(\xi)$ denotes the initial value at time 0
of the compartment with index i
in the megakaryocyte submodel
for the ploidy group with index j

and

$i =$ index of the compartment i in submodel j

$n =$ number of compartments in the megakaryocyte submodel

$j =$ index of the megakaryocyte ploidy

$\omega_i =$ development/compartment specific damage parameters

$\xi =$ general parameter for the degree of damage

$q =$ parameter which describes the steepness of change
in the degree of damage between the compartments.

For the values of ω_j the functional approach

$$\omega_i = (n - i + \mu) \cdot \xi \tag{3.122}$$

was used, where

$$\mu > 0$$

describes the basic damage behaviour. One gets for the initial values of the compartments the bundle of functions:

$${}^0x_i^{MKj}(\xi) = q^{(n-i+\mu)\cdot\xi} \tag{3.123}$$

where

$i =$ index of the compartment

$n =$ number of compartments in the megakaryocyte submodel

$j =$ index of the megakaryocyte ploidy

$\mu =$ damage behaviour starting with the last compartment

$\xi =$ parameter which characterizes the degree of damage

$q =$ parameter which controls the effect of the damage parameter.

Different values for the parameters q and μ were testet in various simulations. The values 0.64 for q and 0 for μ gave good fittings to most cases. Quality of fitting regarding different aspects including flexibility of adaption to different damage patterns can not easily be measured by a mathematically defined size. Thus, assessment of fitting quality was done using visual comparisons of several simulation results. Thus, the finally used initial value functions ${}^0x_i^{MKj}(\xi)$ become:

$$\begin{aligned} {}^0x_1^{MKj}(\xi) &= q^{4\cdot\xi} \\ {}^0x_2^{MKj}(\xi) &= q^{3\cdot\xi} \\ {}^0x_3^{MKj}(\xi) &= q^{2\cdot\xi} \\ {}^0x_4^{MKj}(\xi) &= q^{1\cdot\xi} \end{aligned} \tag{3.124}$$

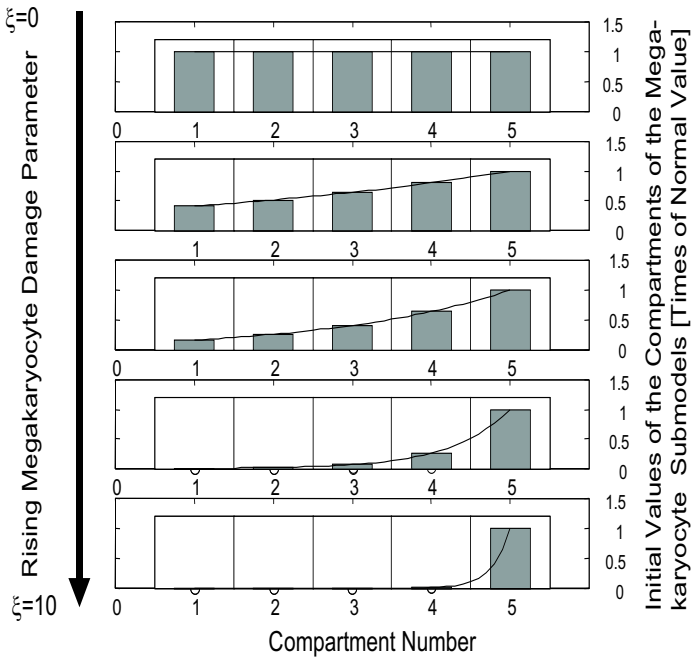

Figure 3.18: Initial values of compartments of the megakaryocyte submodels with rising damage parameter ξ.

$$
\begin{aligned}
{}^{0}x_5^{MKj}(\xi) &= q^{0\cdot\xi} \\
q &= 0.64 \ . \qquad (3.125)
\end{aligned}
$$

Figure 3.18 shows the changes in the initial values ${}^{0}x_j^{MKi}(\xi)$ of 5 serial compartments of the megakaryocyte submodel in dependency of the megakaryocyte damage parameter ξ. Finally, the initial values for the compartments are controlled by one parameter which replaces the former five independent values.

3.2.8 Model Extension: A Compartment for Fragmenting Megakaryocytes

Since it can be observed that the typical shoulder of the thrombocyte count after TBI in the peripheral blood does not shorten to values below $\approx$ 48h it can be concluded, that in this phase the production of platelets must be nearly completely radioresistant comparable to mature platelets. It can be assumed that this time is the phase between the termination of all normal cellular functions of the megakaryocytes and the

appearance of the platelets in the peripheral blood. It is likely, that in this time the megakaryocytes fragment to platelets. For this reason the human model was extended by an additional compartment for this fragmentation phase. A transit time of 48 h was assumed. The structure is a series of 5 concatenated differential equations. The system equations are

$$\begin{aligned} \dot{x}_1^{MKF} &= u^{MKF} &&- \lambda^{MKF} \cdot x_1^{MKF} \\ \dot{x}_2^{MKF} &= \lambda^{MKF} \cdot x_1^{MKF} &&- \lambda^{MKF} \cdot x_2^{MKF} \\ &\dots \\ \dot{x}_5^{MKF} &= \lambda^{C} \cdot x_4^{MKF} &&- \lambda^{MKF} \cdot x_5^{MKF} \end{aligned} \tag{3.126}$$

$$y^{MKF} = \lambda^{MKF} \cdot x_5^{MKF} \ . \tag{3.127}$$

The compartment series is supplied by the four megakaryocyte ploidy groups. The inflow function becomes

$$u^{MKF} = \nu^{MK,TH} \cdot \sum_{1}^{4} p^{MKi} \cdot y^{ICV} \cdot y^{MKi} \ . \tag{3.128}$$

The inflow function of the thrombocyte compartment changes to

$$u^{TH} = \nu^{MKF,TH} \cdot y^{MKF} \ . \tag{3.129}$$

3.2.9 Estimation of Remaining Stem Cell Numbers of Radiation Accident Patients

Now that the basic model of thrombocytopoiesis developed for rodents is transformed to the human system this model can be used for estimation of remaining stem cell numbers in humans. Data are taken from radiation accident patients of the Chernobyl accident and others.

3.2.9.1 Details of the Estimation Method, Optimization Parameters, Deviation Function

The basic approach for estimation of stem cell numbers is the same like developed for the rat experiments. An extension is made by an additional parameter for the simulation of the megakaryocyte damage pattern (see 3.2.7). For the human system again an appropriate selection of optimization variables has to be found. The following assumptions were used:

- PS and PSinj are represented by separate optimization variables.
- The NC initial value is set up by an separate optimization variable.
- The initial values for C1 and C2 are merged into one collective optimization variable.
- The EMB initiation is regarded to be a function of the megakaryocyte damage parameter ξ (see 3.2.7):

$$ {}^0x_i^{EMB}(\xi) = q^{5\cdot\xi} \tag{3.130}$$

- The MK1...MK4 compartments are initialized by the development specific damage functions ${}^0x_i^{MKj}(\xi)$ which were defined in section 3.2.7 .

3.2.9.2 Estimation Results

The resulting simulations of the estimation runs are shown in figures 3.19 and 3.20. The data used for estimation are taken from selected patient data sets of the radiation accident database of our institute [29]. These patients were assigned to so called response categories (RCs) reflecting the severity of injury by relevant clinical symptoms. The given response categories are derived from rules worked out by the METREPOL team. METREPOL is project of the European Comission (EU contract number FI4PCT970067) consisting of international radiation medicine experts. The aim of METREPOL is to elaborate treatment protocols for the clinical management of radiation accident patients.

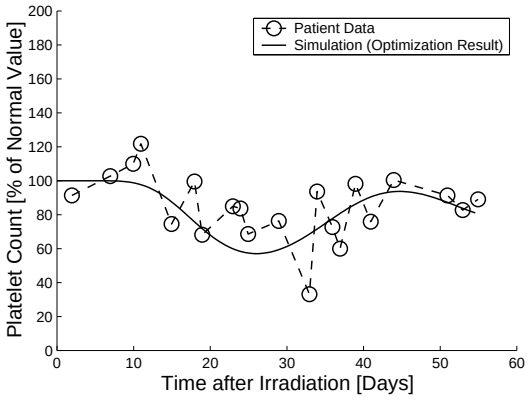

(a) RC1, Case 1078. Estimation results: PS = $6.4{\cdot}10^{-2}$, PSinj = $6.4{\cdot}10^{-2}$.

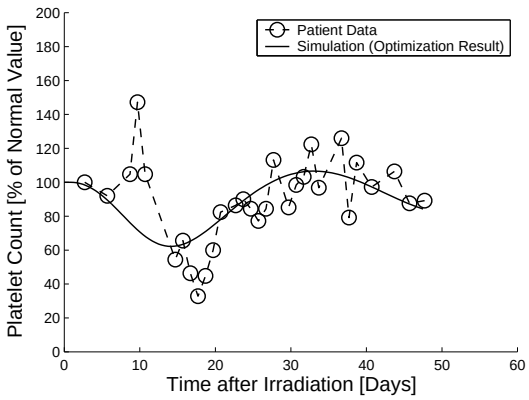

(b) RC1, Case 1115. Estimation results: PS = $3.9{\cdot}10^{-1}$, PSinj =$3.9{\cdot}10^{-1}$.

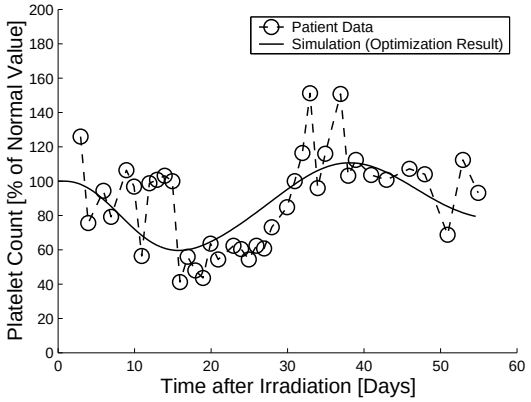

(c) RC1, Case 1121. Estimation results: PS = $3.8{\cdot}10^{-1}$, PSinj = $6.2{\cdot}10^{-1}$.

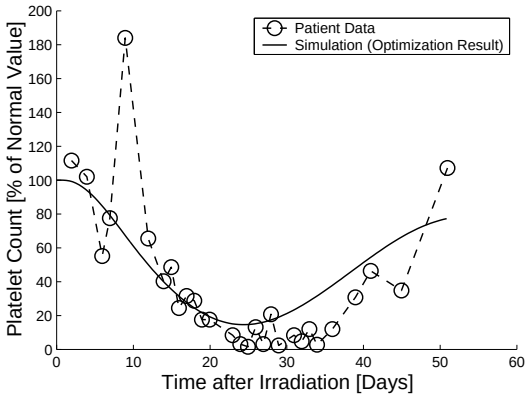

(d) RC2, Case 1035. Estimation results: PS = $2.8{\cdot}10^{-4}$, PSinj = $2.8{\cdot}10^{-4}$.

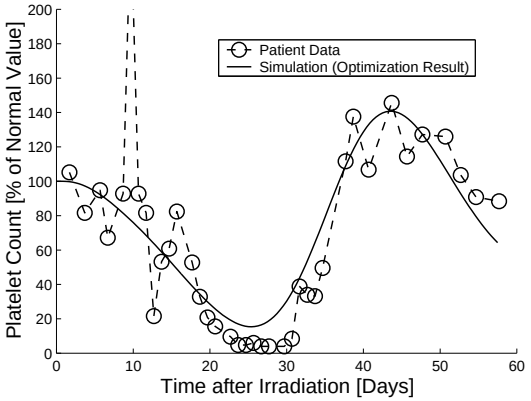

(e) RC2, Case 1106. Estimation results: PS = $3.4{\cdot}10^{-3}$, PSinj = $1.3{\cdot}10^{-2}$.

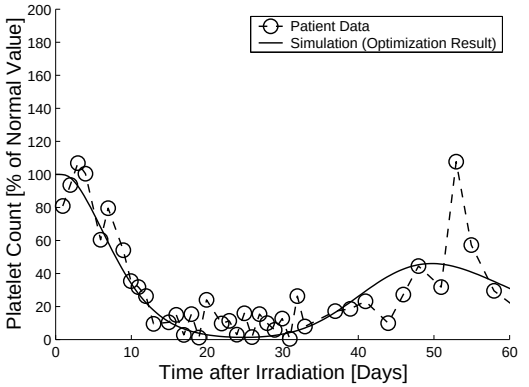

(f) RC3, Case 1013. Estimation results: PS = $8.0{\cdot}10^{-9}$, PSinj = $3.2{\cdot}10^{-4}$.

Figure 3.19: Patient data of different response categories (see text) and fitting results for the estimation of surviving fractions of stem cells. Surviving fractions for PS and PSinj are given in [Times of Normal Value].

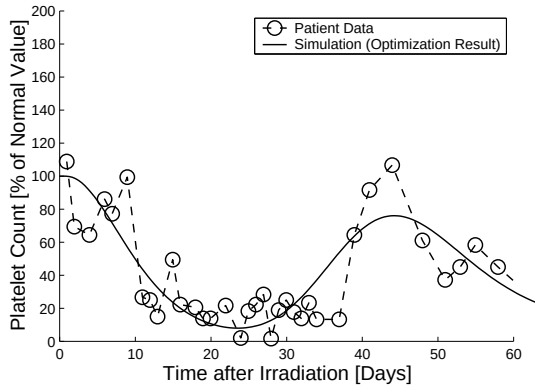

(a) RC3, Case 1033. Estimation results: PS = $1.3{\cdot}10^{-8}$, PSinj = $2.1{\cdot}10^{-3}$.

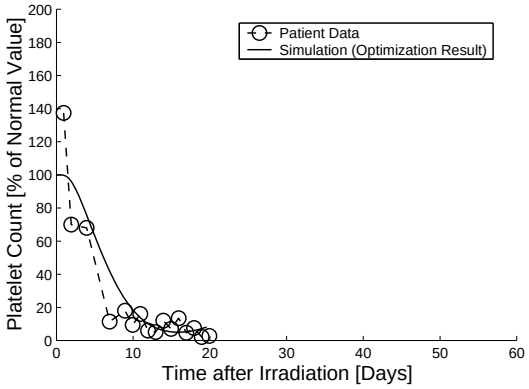

(b) RC4, Case 1026. Estimation results: PS = $5.2{\cdot}10^{-3}$, PSinj = $5.2{\cdot}10^{-3}$.

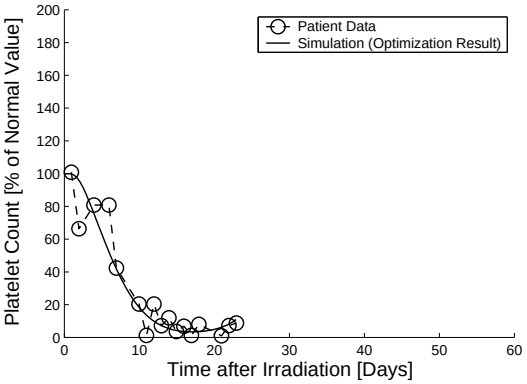

(c) RC4, Case 1012. Estimation results: PS = $2.5{\cdot}10^{-1}$, PSinj = $4.2{\cdot}10^{-1}$.

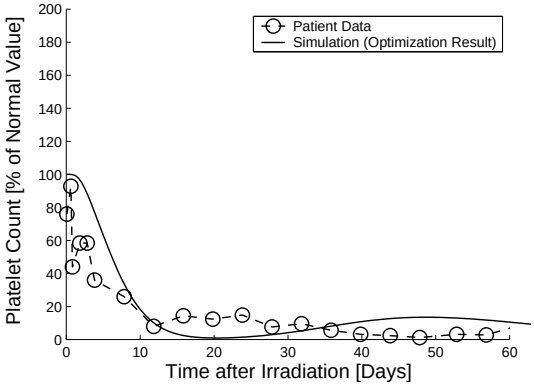

(d) RC4, Case 3088. Estimation results: PS = $9.9{\cdot}10^{-14}$, PSinj = $1.3{\cdot}10^{-5}$.

Figure 3.20: Patient data of different response categories RCx (see text) and fitting results for the estimation of surviving fractions of stem cells. Surviving fractions for PS and PSinj are given in [Times of Normal Value].

Figure 3.21 shows the relationship of the estimated remaining fractions of pluripotent and injured (model) stem cell numbers and the clinical response categories.

In response category 4 the estimations for two cases resulted in values which are of orders of magnitude like found in RC1. The reason for this is the short time span of the data. The very severly irradiated patients with the numbers 1012 and 1026 died within a short time after irradiation. As a consequence, the available time span of data is about 20 days. Since platelets and megakaryocytes have transit times of 8 - 10 days, this duration is too short for reasonable estimations of the PS and PSinj compartments. The patient 3088 lived longer and a better estimation of stem cell numbers was able, showing the very low surviving fraction of PS and PSinj, as would

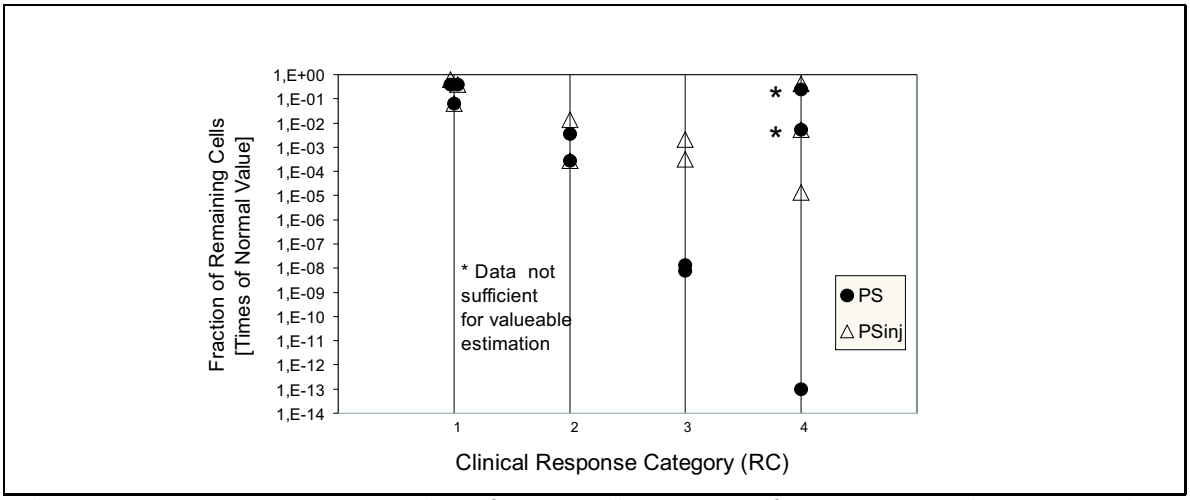

Figure 3.21: Estimation results of stem cell surviving fractions in radiation accident patients.

have been expected from the clinical picture.

3.3 Model Based Analysis of the Hematological Effects of Chronic Irradiation

Chronic radiation exposure experiments on animals show several interesting effects on the hematopoietic system. One of these effects is the temporary compensation of excess cell loss caused by radiation induced permanent cell damage. Of course, there are other phenomena caused by radiation exposure of the hematopoietic system as well. These can overlay the results of the compensatory mechanisms.

3.3.1 Hematological Effects of Chronic Radiation Exposure

The effects of chronic radiation exposure to hematopoiesis are again based on the damaging or destructing effects of radiation on the cellular level. So it has to be assumed that in chronic radiation fields cells are permanently destructed or damaged and affected in their proliferative and functional potential. Extensive experimental work on the effects of chronic radiation exposure to mammals was done by Lamerton on rats [62] and by the group around Fritz and Seed on dogs [85] [83] [14] [15]. Further experimental results can be found in [83] [39] [1] [62] [79]. An overview on the pathophysiology of hematopoiesis in radiation fields can be found in [30]. The results of these experiments can be summarized in the following effects of chronic irradiation:

- Suppression of blood cell numbers (figure 3.22) with temporary sufficient compensation.
- Fast breakdown of the hematopoietic system with resulting death (figure 3.23).
- Suppression and following repopulation of blood cell counts (figure 3.24).
- Reduction of bone marrow cell numbers [48] [47] [61].
- Clinical consequences of blood cell suppression (e.g. infections).
- Acquired radioresistance of hemopoietic progenitors [84].
- Genetic damages with late effects such as leukemia (figure 3.25).
- Life shortening (figure 3.26).

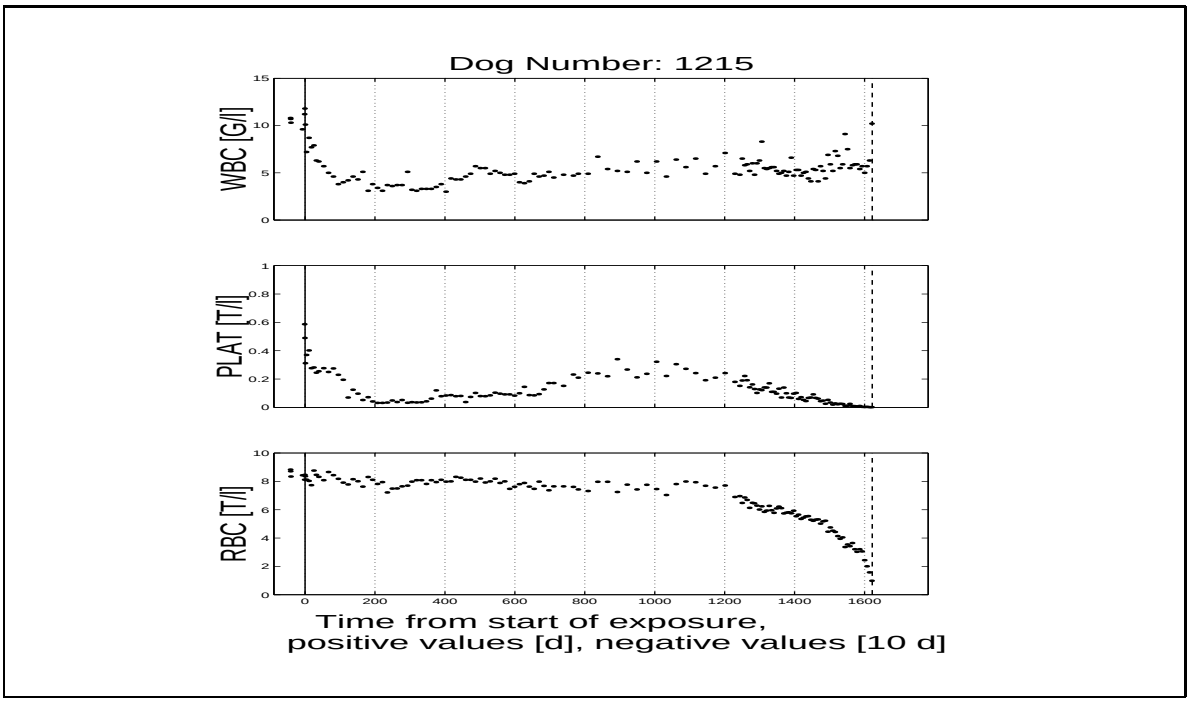

Figure 3.22: Bloodcount changes of a chronically irradiated dog with temporary new steady state values. Daily dose: 75mSv. WBC = white blood cell count. PLAT = platelet count. RBC = red blood cell count. - - - = termination of the experiment caused by death or removal from the radiation field. Data from Dr. Fritz and Dr. Seed, Argonne National Laboratory.

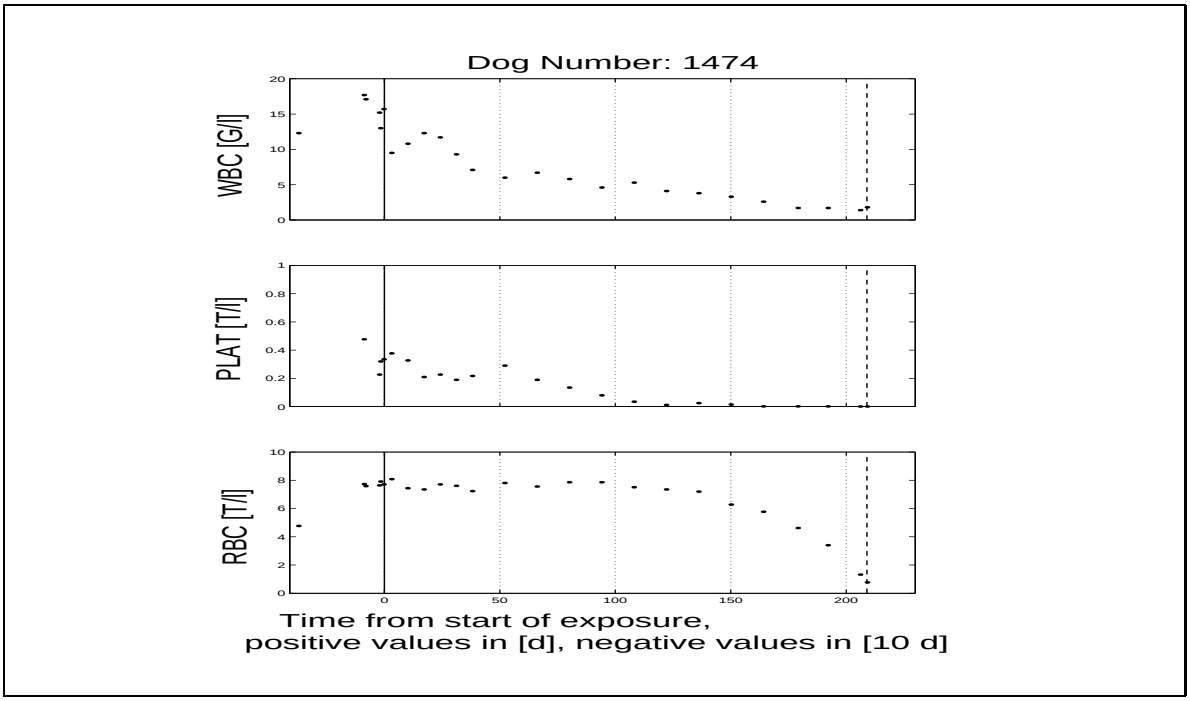

Figure 3.23: Bloodcount changes of a chronically irradiated dog with short survival time. Daily dose: 75mSv. WBC = white blood cell count. PLAT = platelet count. RBC = red blood cell count. - - - = termination of the experiment caused by death or removal from the radiation field. Data from Dr. Fritz and Dr. Seed, Argonne National Laboratory.

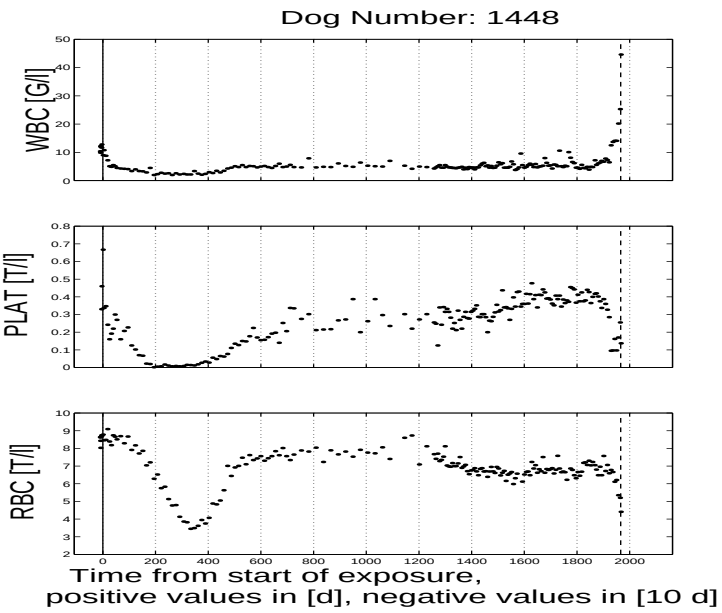

Figure 3.24: Bloodcount changes of a chronically irradiated dog with reconstitution of thrombocytopoiesis and erythropoiesis. Daily dose: 75mSv. WBC = white blood cell count. PLAT = platelet count. RBC = red blood cell count. - - - = termination of the experiment caused by death or removal from the radiation field. Data from Dr. Fritz and Dr. Seed, Argonne National Laboratory.

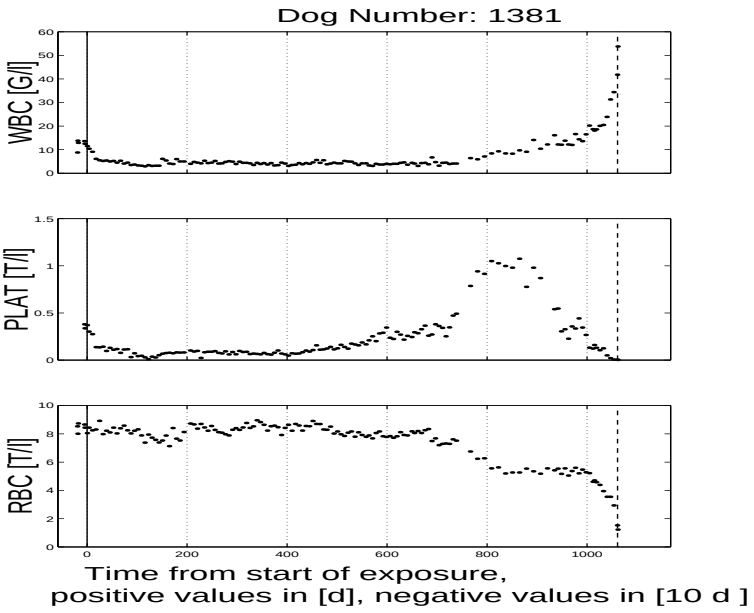

Figure 3.25: Changes in bloodcounts of a chronically irradiated dog developing leukemia. Daily dose: 127.5mSv. WBC = white blood cell count. PLAT = platelet count. RBC = red blood cell count. - - - = termination of the experiment caused by death or removal from the radiation field. Data from Dr. Fritz and Dr. Seed, Argonne National Laboratory.

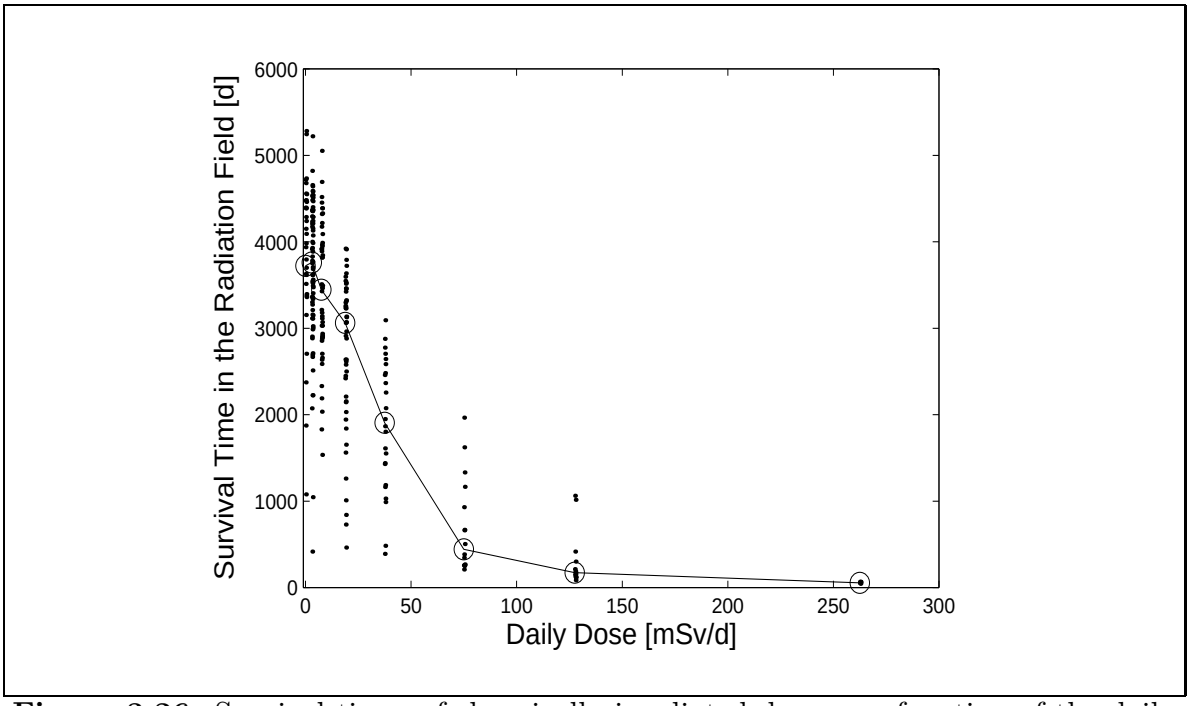

Figure 3.26: Survival times of chronically irradiated dogs as a function of the daily received dose. The survival times of control dogs were corrected by the average experimental radiation onset age of 400 days. Data from Dr. Fritz and Dr. Seed, Argonne National Laboratory.

3.3.2 Adaption of the Model to the Canine Thrombocytopoietic System

To analyze the platelet count dynamics of the dogs of the Argonne experiment the rodent model had to be adapted to the canine thrombocytopoietic system. This transformation was done by using the basic assumption, that cell kinetic processes in the dog require twice as much time as in rodents. Thus, the cell generation time was assumed to be $\approx 2 \cdot 10$ h $= 20$ h. The other kinetic parameters of the model were adapted in the same way. The model regulators were used in the same design as in the rodent model.

3.3.3 Modeling Excess Cell Loss

Damage of chronic irradiation to cells happens in general by causing defects in the DNA of the cell nucleus. These disturbances of the genome can lead to cell death or malfunction, which can be delayed to the time after one or more cellular divisions. These effects can be summarized by the assumption of the presence of a permanent

excess cell loss additional to the normal functional cell turnover in renewing tissues like the hematopoietic system. The normal cell turnover is represented by the term $-\lambda \cdot x(t)$. The excess cell loss is introduced to the differential equations as an additional loss term $-\varepsilon \cdot x(t)$ in the system equations:

$$\dot{x}(t) = u(t) + \alpha \cdot x(t) - \lambda \cdot x(t) - \varepsilon \cdot x(t), \quad x(0) = x^0 \tag{3.131}$$

Since it can be assumed, that the effect of cell loss is not constant from the beginning of exposure, but rises from zero to a constant value, ε is set up as a function of time in exponential form:

$$\varepsilon(t) = a + b \cdot e^{-c \cdot t} \tag{3.132}$$

with

$$\begin{aligned} &a = \varepsilon^* > 0, \text{ boundary value for } t \to \infty \\ &\quad = \text{ steady state value of } \varepsilon(t) \\ &b = -a \\ &c > 0 \text{ steepnes parameter of the excess cell loss function.} \end{aligned} \tag{3.133}$$

A value of $1/1000$ for the steepness parameter c showed good agreement of simulations and experimental data. The amount of excess cell loss in different cell populations depends on the radiation sensitivity. For this reason the excess cell loss rate ε is not the same for all compartments of the model. The general assumption on the radiation sensitivity of cell populations is summarized in figure 3.12. No exact data about the radiation sensitivity of the early cell populations in the megakaryocytic development line were available. Therefore the model for radiation induced permant excess cell loss is based on the following assumptions:

- The compartments PS, NC, C1 and C2 are set up with the same excess cell loss rates
  $\varepsilon^{PS}(t) = \varepsilon^{NC}(t) = \varepsilon^{C1}(t) = \varepsilon^{C2}(t) = \varepsilon(t)$.
- The EMB compartment is set up with an excess cell losss rate of

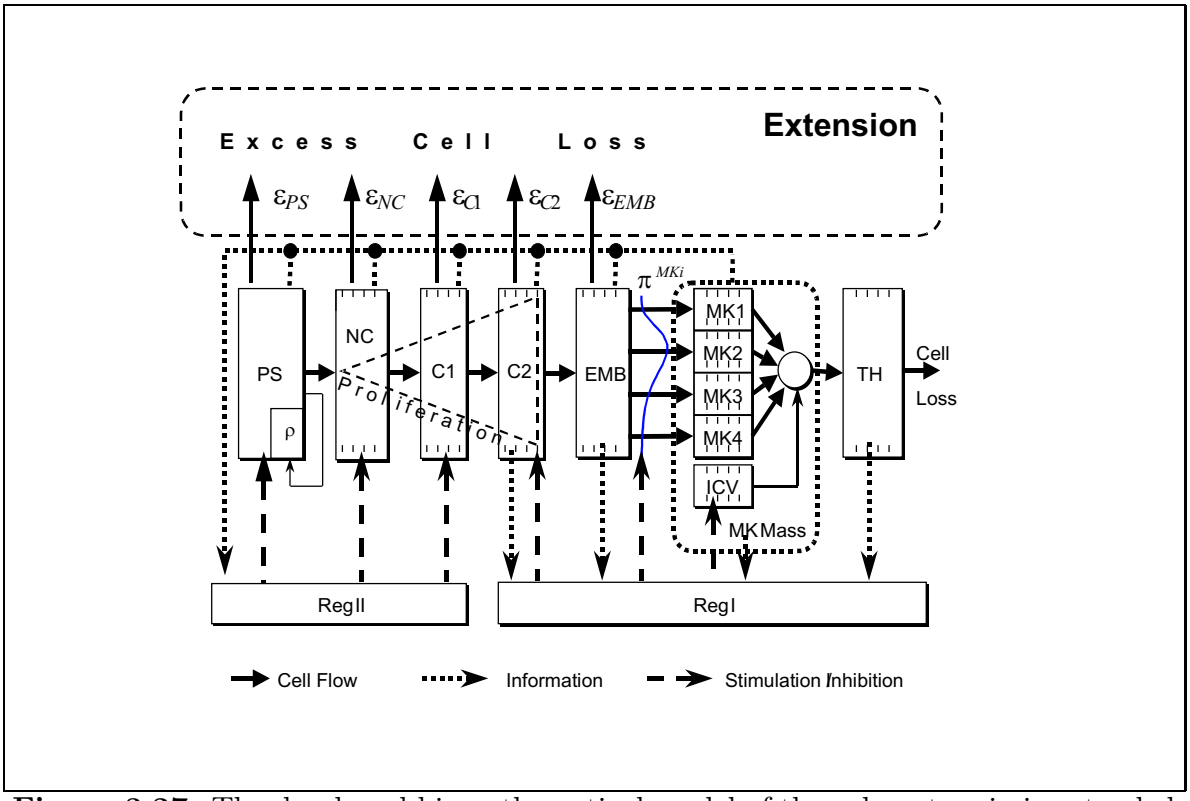

Figure 3.27: The developed biomathematical model of thrombocytopoiesis extended by elements for radiation induced excess cell loss. PS = pluripotent stem cells. PSinj = injured stem cells. NC = noncommitted progenitor cells. C1 = early committed progenitor cells. C2 = late committed progenitor cells. EMB = endoreduplicating precursor cells and megakaryoblasts. MK1...MK4 = maturing megakaryocytes. TH = thrombocytes. ICV = intra ploidy class volume. RegI, RegII = regulators. MkMass = megakaryocyte mass. ρ = self replication probability. π^{MKi} = probability for differentiation into the megakaryocyte compartment MKi. ε_{PS}, ε_{NC}, ε_{C1}, ε_{C2}, ε_{EMB} = radiation cnduced excess cell loss rates.

$$\varepsilon^{EMB}(t) = \tfrac{1}{3} \cdot \varepsilon(t).$$

- The megakaryocyte and thrombocyte compartments MK1...MK4 and TH are set up under the assumption of radioresistance. They receive no excess cell loss ($\varepsilon^{MK1}(t) = ... = \varepsilon^{MK4}(t) = \varepsilon^{TH}(t) = 0$).
- The intra ploidy class volume ICV is assumed to be not influenced by radiation exposure.
- Differentiation times are not assumed to be dependent from radiation exposure.
- Regulators are unchanged.

The model is adapted to chronic irradiation by application of the following changes in the system equations :

$$\dot{x}^{PS} = -\gamma^{PS} \cdot \lambda^{PS}_{active} \cdot x^{PS} + 2 \cdot \rho^{PS} \cdot \gamma^{PS} \cdot \lambda^{PS}_{active} \cdot x^{PS} - \varepsilon^{PS} \cdot x^{PS} \tag{3.134}$$

$$\dot{x}^{C}_{1} = u^{C} + \alpha^{C} \cdot x^{C}_{1} - \lambda^{C} \cdot x^{C}_{1} - \varepsilon^{C} \cdot x^{C}_{1} \tag{3.135}$$

$$\dot{x}^{C}_{2} = \lambda^{C} \cdot x^{C}_{1} + \alpha^{C} \cdot x^{C}_{2} - \lambda^{C} \cdot x^{C}_{2} - \varepsilon^{C} \cdot x^{C}_{2}$$

$$\ldots \qquad\qquad \ldots$$

$$\dot{x}^{C}_{5} = \lambda^{C} \cdot x^{C}_{4} + \alpha^{C} \cdot x^{C}_{5} - \lambda^{C} \cdot x^{C}_{5} - \varepsilon^{C} \cdot x^{C}_{5}$$

for the cell pools C where

C = NC, C1, C2, EMB.

Figure 3.27 shows the structure of the mathematical model for excess cell loss in thrombocytopoiesis.

3.3.4 Simulation Example

Figure 3.28 shows a simulation of the thrombocyte counts of the peripheral blood of a dog irradiated with 18.8 mSv/d gamma irradiation from a ^{60}Co source. The occurence of a new steady state value in the model thrombocyte counts is characteristic for the basic assumption of a permanent excess cell loss.

3.3.5 Examination of System Characteristics

Figure 3.29 shows the contents of the model cell numbers in the compartments PS and TH as a function of the steady state (boundary) excess cell loss rate ε^{*}. The shown lines are interpolated between values, which were calculated by long time simulations to achieve good approximations of the model steady state values. The figure shows two important changes in the thrombocytopoietic system under chronic radiation exposure:

- The content of the model stem cell compartment PS is more affected than the thrombocyte compartment TH.

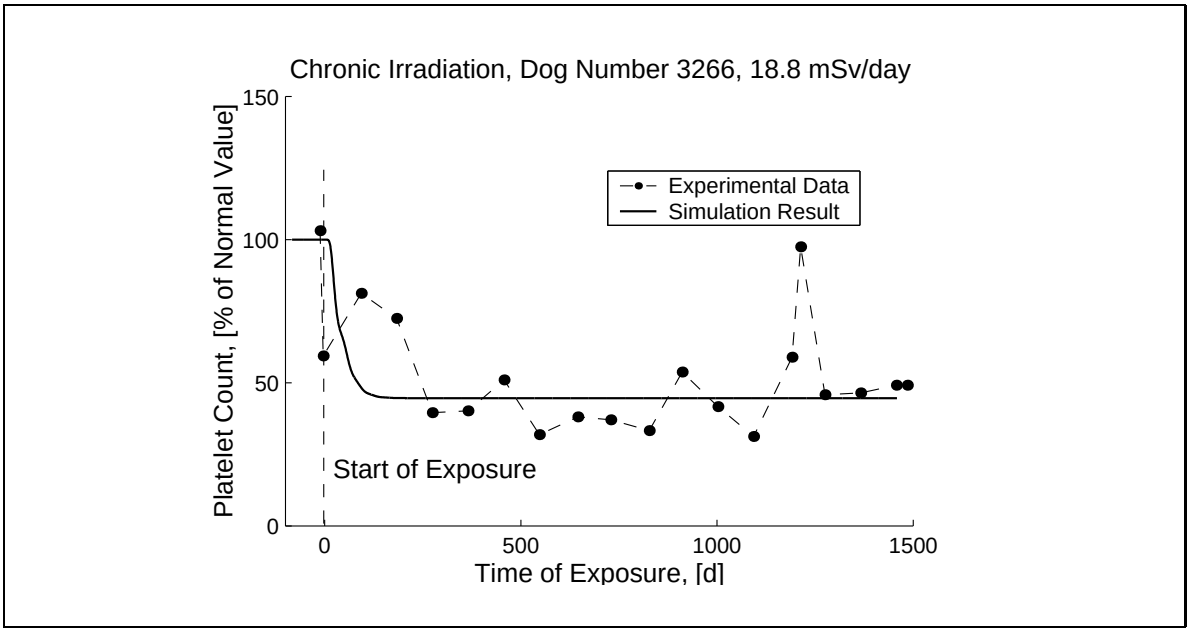

Figure 3.28: Experimental data and simulation result of the thrombocyte counts in the peripheral blood of a dog continously irradiated with 18.8 mSv/d from a ^{60}Co source. Data from Dr. Fritz and Dr. Seed, Argonne National Laboratory, USA.

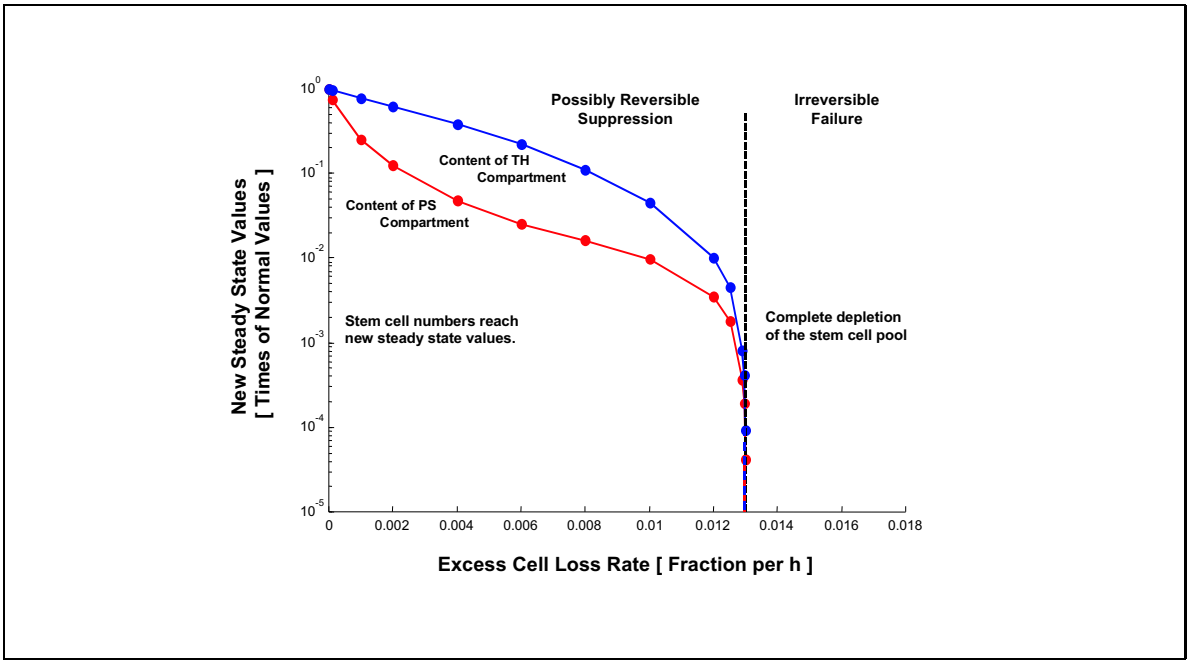

Figure 3.29: New steady state values of the model compartments PS and TH as a function of the steady state excess cell loss rate ε^*.

- The contents of the compartments drop dramatically near to a certain limit value of excess cell loss .

The conclusion that can be drawn from this facts is that the earlier stages of the hematopoietic system, especially the pluripotent stem cells, are stronger affected by radiation induced excess loss than it is recognized by the peripheral blood counts. In the case of low platelet counts the thrombocytopoietic system is already at high risk to fail if further stresses appear.

The very sensitive state of the hematopoietic system in case of low platelet counts can be analyzed further if the cell loss rate is a changing variable. The mathematical technique for this problem is stochastic simulation.

3.3.6 Stochastic Simulation of Permanent Excess Cell Loss

In the previous simulations it was assumed, that the parameters of the model are not additionally influenced from other physiological disturbances. This is not true for real biological systems or organisms. Variance can be of great importance in areas, where the characteristics of systems are dominated by nonlinearity. In such areas very small changes of variables can cause dramatic changes in the whole system. The analysis of the new steady state model cell numbers in the TH and the PS compartment as a function of the excess cell loss rate showed such a small region with very dramatic changes in cell numbers. If the constant excess cell loss rate ε^* is replaced by a probability variable which changes in time, it is possible to simulate the consequences of such a stochastically varying value.

3.3.6.1 Observed Survival Times in Experimental Animals

Indications for nonconstant and rather stochastic characteristics of the disturbed hemopoietic system can be found for example in observations of the Argonne dogs. Figure 3.30 shows the thrombocyte counts of selected dogs, which were not observed to develop radioresistancy with long time recovery of thrombocytopoiesis. The thrombocyte counts stop at the death times of the dogs. As can be seen the survival times of these dogs are widely distributed, and death in general appears in connection with a rapid drop in platelet counts. The question arises if and how this can be explained

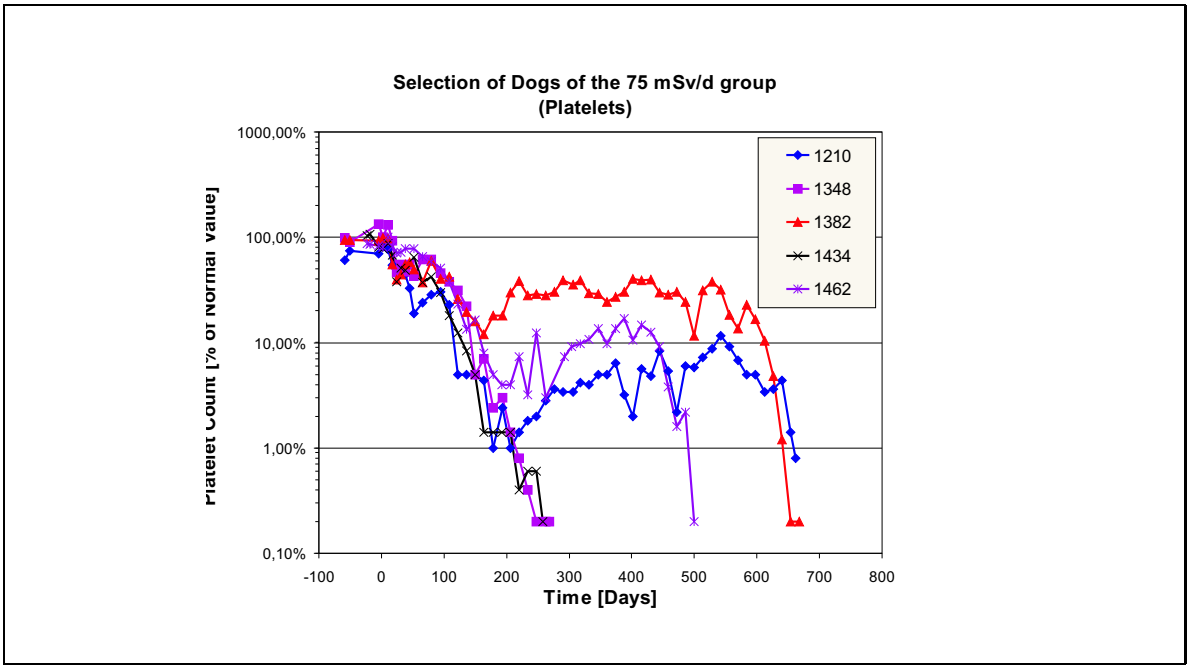

Figure 3.30: Platelet counts of several selected dogs of the 75 mSv/d group of the Argonne Experiment.

with the help of the proposed model of thrombocytopoiesis under permanent excess cell loss.

3.3.6.2 Explanatory Stochastic Approach

The assumption of constant biological parameters, like described above, is not true for real biological systems. Variation of parameters could be an explanatory approach, for example, for the widely distributed survival times observed in animal experiments (figure 3.30). In order to test the influence of stochastic disturbances to the model dynamics it is necessary to perform stochastic simulations, in which constant parameters are extended by a stochastic disturbance. Written in the syntax of the proposed model equations, ε^* is replaced by

$$\varepsilon^*(t) = \varepsilon^* + \omega^{(\mu,\sigma)}(t) \tag{3.136}$$

where

$$\omega^{(\mu,\sigma)}(t) = \omega_i^{(\mu,\sigma)} \quad if \quad t_{i-1} \leq t < t_i \tag{3.137}$$

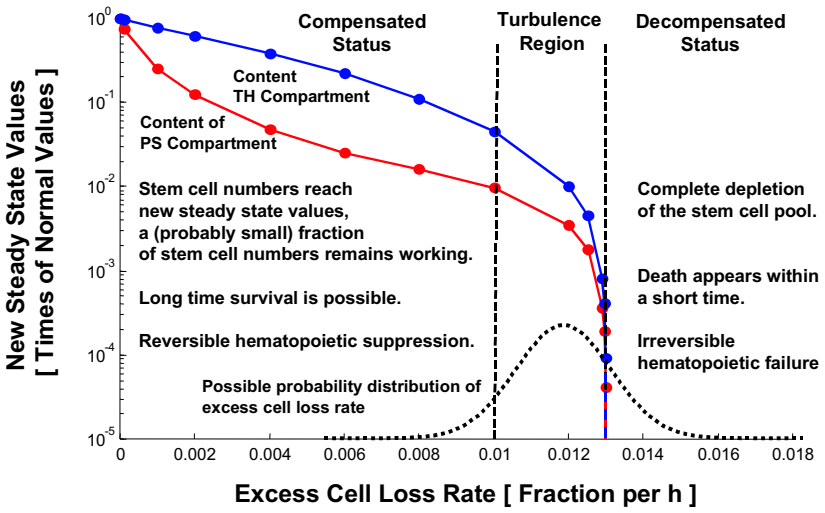

Figure 3.31: New model steady state values as a function of the excess cell loss rate and the assumption of a stochastically varying excess cell loss rate with a possible probability distribution.

and

$$(\omega_i^{(\mu,\sigma)})_{i=1...n} = \text{ normal distributed random numbers of } N(\mu,\sigma)\ . \tag{3.138}$$

3.3.6.3 Stochastic Simulations

For examination of the reactions of the model to stochastic changes in the excess cell loss rate the time points for change

$$t_i = i \cdot 1000\,h \quad i = 1...n \tag{3.139}$$

were used. The used parameters of the normal distribution were

$$\mu = 0.01 \tag{3.140}$$
$$\sigma = 0.001\ .$$

Figure 3.32 shows the content of the TH compartment of 4 stochastic simulations with

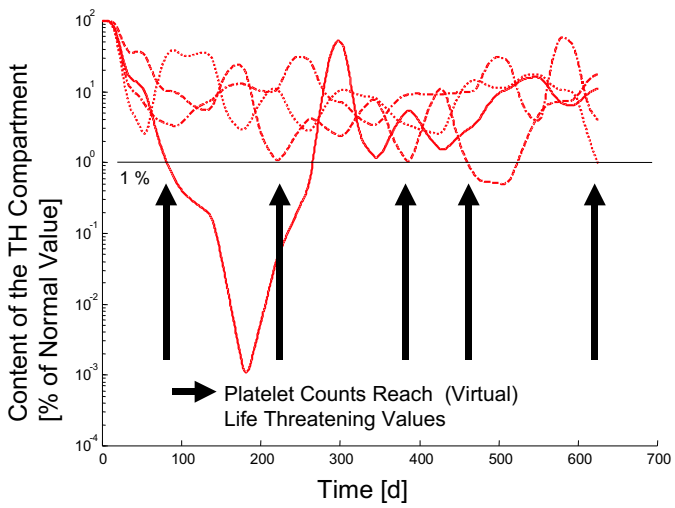

Figure 3.32: Several simulation results under the assumption of a stochastically distributed permanent excess cell loss. The different dotted and continous lines represent the different simulations. The arrows mark points where the (simulated) platelet counts reach (virtual) life threatening values.

the given distribution parameters. The lines of the platelet counts show the strong variations of the (simulated) platelet count. It can be recognized, that a coefficient of variation of 10% in the excess cell loss rate can result in a drop of platelet counts down to 1% or even lower. The simulated system can recover to higher values. This recovery would of course not be possible for an experimental animal, which would have a high probability to die from spontaneous bleeding at such a low platelet level.

3.3.7 Estimation of Radiation Induced Average Excess Cell Loss Rates

With the extended model of thrombocytopoiesis for permanent excess cell loss it is possible to estimate the excess cell loss rate ε^* from experimental data. This is done by least square fitting of the simulated platelet count as a function of time against experimental data. A trust region based optimization algorithm was used for optimization . In several fitting procedures a value of 0.001 for the steepness parameter c of the excess cell loss function $\varepsilon(t)$ was determined to give good approximations for simulations of all dose groups. Figures 3.33a-f and 3.34 show the experimental data and the simulation results, which were determined by least square fitting. Table 3.4

summarizes the dose rates and the corresponding excess cell loss rates ε^*.

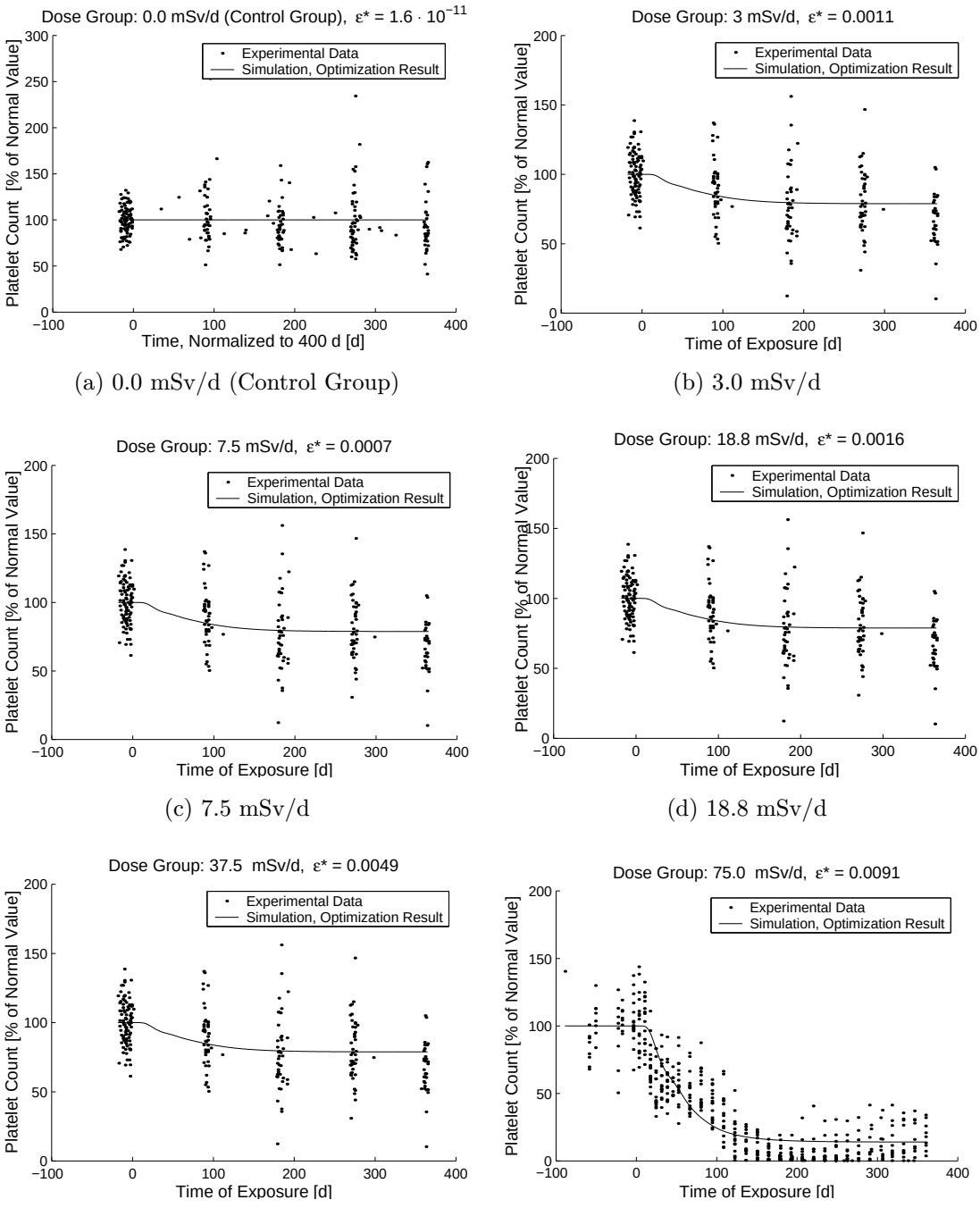

(a) 0.0 mSv/d (Control Group)

(b) 3.0 mSv/d

(c) 7.5 mSv/d

(d) 18.8 mSv/d

(e) 37.5 mSv/d

(f) 75.0 mSv/d

Figure 3.33: Platelet counts of chronically irradiated and control dogs. Dose rates 0.0-75.0 mSv/d. Experimental data and simulation of the fitting result. Excess cell loss rate ε^* given in [1/h], estimated by least square optimization.

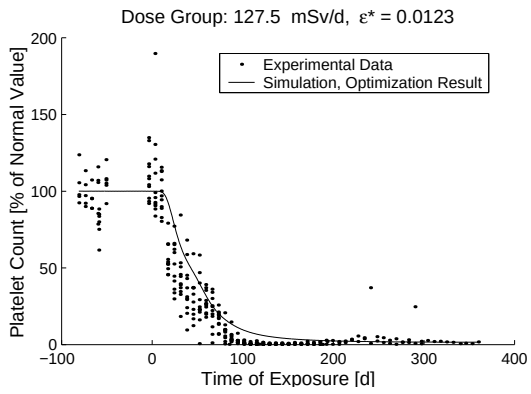

Figure 3.34: Platelet counts of chronically irradiated dogs. Dose rate 127.5 mSv/d. Experimental data and simulation of the fitting result. Excess cell loss rate ε^* given in [1/h], estimated by least square optimization.

Dose [mSv/d]	ε^* [Fraction of cells lost per h]	ε^* [% of cells lost per h]
0.0 (control)	$1.6 \cdot 10^{-11}$	$1.6 \cdot 10^{-9}$
3.0	0.0011	0.11
7.5	0.0007	0.07
18.8	0.0016	0.16
37.5	0.0049	0.49
75.0	0.0091	0.91
127.5	0.0123	1.23

Table 3.4: Daily dose rates applied in the Argonne experiment and estimated excess cell loss rates. Dose in [mSv/d]. Estimated excess cell loss rates ε^* in [Fraction of cells lost per h] and [% of cells lost per h].

3.4 Excess Cell Loss and Microdosimetric Radiation Effects

In modern dosimetry the common abstract size "dose" which indicates the amount of energy absorbed by a mass unit is replaced by methods which put more emphasis on the discrete character of the energy deposition events of radiation.

Ionizing radiation desposits energy in discrete packages. The mechanisms of energy transfer are based on interactions with atoms of the irradiated structure. Thus, not only the total amount of energy absorbed per mass (i.e. dose) but the characteristics of these discrete interaction may influence the effect of ionizing radiation to biological cells and tissues or other structures.

For this reason the estimated excess cell loss rates are compared to microdosimetric discrete energy deposition events.

3.4.1 Average Number of Particle Traversals per Cell

One method to characterize the effects of ionizing irradiation on the level of biological cells is the number of particle traversals per cell and time unit. These characterization becomes important in connection with cellular repair mechanisms [26].

3.4.1.1 Calculation of the Mean Energy Deposition per Particle Traversal per Cell of ^{60}Co Based on Microdosimetric Spectra

Following the microdosimetric spectrum of ^{60}Co gamma radiation [43] for volume diameters in the order of magnitude of cells the inear energy transfer (LET) of the Compton electrons, which are induced in a cascade of photon-electron scattering processes (see 3.4.3) of the γ-photons of ^{60}Co , has a mean value of ≈ 0.3 keV $\cdot\mu$m^{-1}:

$$y_{\gamma,\bar{^{60}Co}} \approx 0.3\,keV \cdot \mu m^{-1} \tag{3.141}$$

For calculation of the energy hit size per cell a spherical cell with a diameter of

$$d_{cell} \approx 10\,\mu m \tag{3.142}$$

or radius

$$\begin{aligned} r_{cell} &\approx \frac{1}{2} \cdot 10\,\mu m \\ &\approx 5\,\mu m \end{aligned} \tag{3.143}$$

is assumed. The mean traversal length through the cell $\bar{s}$ is calculated as:

$$\begin{aligned} \bar{s} &= 2 \cdot \frac{1}{r} \cdot \int_0^{r_{cell}} \sqrt{r^2 - x^2}\, dx \\ &= 2 \cdot \frac{1}{r} \cdot \left[\frac{1}{2} (x \cdot \sqrt{r^2 - x^2} + r^2 \cdot arcsin\left(\frac{x}{r}\right) \right]_0^r \\ &= 1.5780 \cdot r \\ &\approx 7.890\,\mu m \end{aligned} \tag{3.144}$$

Thus, the average particle traversal energy deposition per cell is calculated as

$$\begin{aligned} E_{cell} &\approx 7.890 \mu m \cdot 0.3\,keV \cdot \mu m^{-1} \\ &\approx 2.367\,keV \\ &\approx 3.7872 \cdot 10^{-16}\,J\ . \end{aligned} \tag{3.145}$$

The average partical traversal dose by an estimated cell mass of 1 ng is

$$\begin{aligned} z_{cell} &\approx 3.7872 \cdot 10^{-16}\,J \cdot (ng)^{-1} \\ &\approx 3.7872 \cdot 10^{-16}\,J \cdot (10^{-12} kg)^{-1} \\ &\approx 3.7872 \cdot 10^{-4}\,J \cdot kg^{-1} \\ &\approx 3.7872 \cdot 10^{-4}\,Gy\ . \end{aligned} \tag{3.146}$$

Dose [mSv/d]	$n_{cell-traversals}$/d	$\Delta t[h]$
0.0 (control)	0	-
3.0	7.812	3.072
7.5	19.53	1.229
18.8	48.96	0.490
37.5	97.65	0.246
75.0	195.3	0.123
127.5	332.0	0.072

Table 3.5: Daily dose rates of the Argonne experiment in mSv/d, overall average number of particle traversals per cell per day $n_{cell-traversals}$/d, mean duration between cellular hits Δt in h.

3.4.1.2 Calculation of the Mean Number of Particle Traversals Per Cell for a Given Dose

If it is assumed that all energy of a received dose is transmitted to the cellular tissue, the overall average number of particle traversals per cell at a dose of 1 Gy can be calculated as:

$$\bar{n} = \bar{n}_{traversals/cell,1\,Gy} \approx 2.6405 \cdot 10^3 \tag{3.147}$$

The corresponding values for the Argonne dose rates are shown in table 3.5. Additionally, the mean durations Δt between the single hits are given.

The calculated mean numbers of particle traversals should not be interpreted in the way that every cell receives exactly these values, since the hit numbers are distributed by random. The statistical distribution for the number of hits per cell is the Poisson distribution, which is given by the equation

$$p(n) = e^{-\bar{n}} \cdot \frac{\bar{n}^n}{n!} \tag{3.148}$$

where

$$p(n) = \text{ probability of exactly n hits} \tag{3.149}$$

$$\bar{n} = \text{ overall average number of hits per cell .} \tag{3.150}$$

Figure 3.35 shows the cumulative density functions of the Poisson distributions for

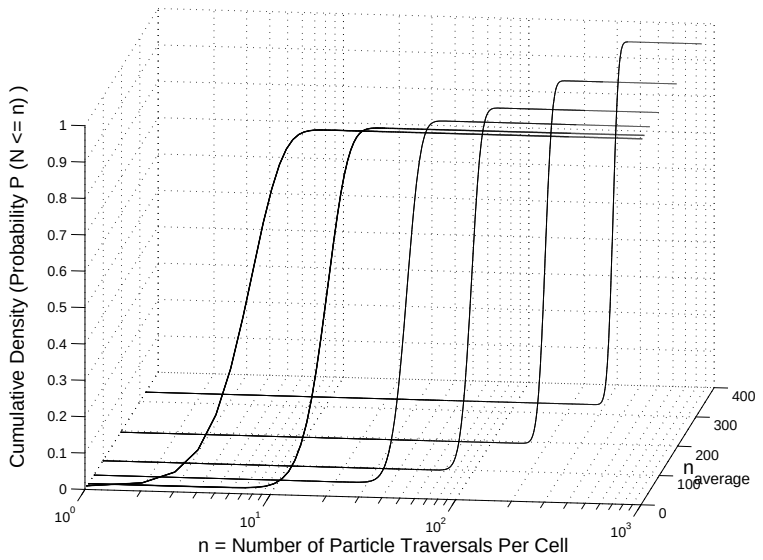

Figure 3.35: Cumulative Poisson density functions of the received hit numbers per cell. distributions calculated for the daily doses of the Argonne experiment.

the numbers of received particle traversals per cell. The distribution parameters are calculated according to the daily doses of the Argonne dogs.

Figure 3.36 shows the excess cell loss rate in %/d as a function of the (microdosimetric) average number of particle traversals per cell and day.

3.4.2 Calculations Based on Received Photon Numbers

In the Argonne experiment a sealed ^{60}Co radiation source was used. Therefore, the absorbed energy in the tissue of the dogs was transferred by γ irradiation. Seen from the physical viewpoint, γ irradiation consists of photons.

In the following section the numbers of absorbed γ photons are calculated for the dose ranges of the Argonne experiment.

3.4.2.1 Calculation of the Received Photon Number per Dose

The dogs of the Argonne experiment described above were irradiated with γ-rays emitted by a ^{60}Co radiation source. Per nuclear reaction ^{60}Co emittes two γ photons $\gamma_{0,1}$ and $\gamma_{0,2}$ with the energies

$$E_{\gamma_{0,1}} \approx 1.33\,MeV \tag{3.151}$$

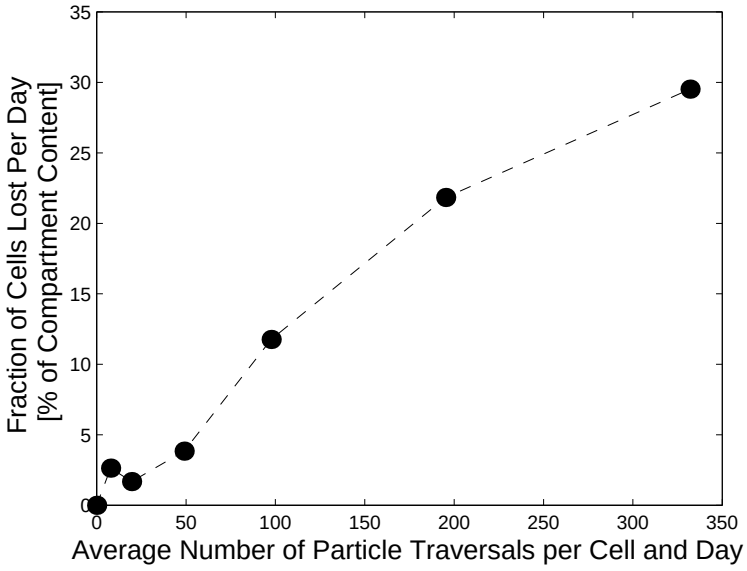

Figure 3.36: Estimated excess cell loss rate ε^* in per cent of lost cells per day as a function of the average number of particle traversals per cell and day.

$$E_{\gamma_{0,2}} \approx 1.17\,MeV \tag{3.152}$$

[54] [59]. The mean photon energy E_{γ_0} is

$$\begin{aligned} E_{\gamma_0} &= \frac{E_{\gamma_{0,1}} + E_{\gamma_{0,2}}}{2} \\ &= 1.25\,MeV\ . \end{aligned} \tag{3.153}$$

A sealed radiation source was used for the Argonne dog experiment . This means, that the received energy is transferred only by photons. If the received energy dose

$$D_{received} = 1\,Gy = 1\frac{J}{kg} \tag{3.154}$$

one can calculate the number of photons, which are necessary to carry this dose of 1 Gy as

$$\begin{aligned} N_{\gamma_{0,1\,Gy}} &= \frac{D_{received}}{E_{\gamma_0}} \\ &= \frac{1\,Gy}{1.25\,MeV} \\ &= \frac{1\frac{J}{kg}}{1.25 \cdot 1.602 \cdot 10^{-19} C \cdot 10^6 V} \end{aligned} \tag{3.155}$$

$$= \frac{1\frac{J}{kg}}{1.25 \cdot 1.602 \cdot 10^{-13} J}$$
$$= \frac{4.9936 \cdot 10^{12}}{kg}$$
$$\approx \frac{5 \cdot 10^{12}}{kg} \ .$$

3.4.2.2 Calculation of the Number of Elementary Reaction Products per Photon Based on the G Value

The number of molecules or radicals generated by a certain radiation type can be calculated from the photon energy with the so called G-value [55]:

$$G = \frac{\text{number of produced molecules or radicals}}{100 \text{ eV transferred energy}} \tag{3.156}$$

For ^{60}Co, the mean G value over all types of molecules and radicals equals about 7:

$$G_{^{60}Co} \approx \frac{7}{100 \text{ eV transferred energy}} \tag{3.157}$$

Thus, the number of reaction products for the mean photon energy of ^{60}Co is calculated as

$$N_{r,photon} = E_{\gamma_0} \cdot G_{^{60}Co} \tag{3.158}$$
$$= 1.25\, MeV \cdot \frac{7}{100 \text{ eV transferred energy}}$$
$$= 8.75 \cdot 10^4 \ .$$

3.4.2.3 Calculation of the Number of Elementary Reaction Products per kg Tissue Based on the G Value

The number of reaction products generated by 1 Gy irradiation in 1 kg tissue from a ^{60}Co source is calculated by:

$$N_{r,1\,Gy} = N_{r,photon} \cdot N_{\gamma_0,1\,Gy} \tag{3.159}$$
$$= 8.75 \cdot 10^4 \cdot \frac{5 \cdot 10^{12}}{kg}$$

$$= 4.375 \cdot 10^{17} \cdot \frac{1}{kg}$$

3.4.2.4 Calculation of the Number of Elementary Reaction Products per Cell at 1 Gy Based on the G Value

If the mean mass of a cell is assumed to be about

$$m_{cell} \approx 1\,ng \tag{3.160}$$

the average number of elementary reaction products per cell from a received dose of 1 Gy can be calculated by the mass ratios:

$$\begin{aligned} N_{r,1\,Gy,cell} &= N_{r,1\,Gy} \cdot \frac{m_{cell}}{1\,kg} \\ &= 4.375 \cdot 10^{17} \cdot \frac{1\,ng}{1\,kg} \\ &= 4.375 \cdot 10^{5} \end{aligned} \tag{3.161}$$

3.4.2.5 Calculations on the Argonne Experiment

In the Argonne experiment dogs were irradiated continously at different dose rates. If D_i denotes the received daily dose, then the number of generated reaction products per day $N_{r,cell,d}$ satisfies the equation:

$$N_{r,cell,i,d} = D_i \cdot N_{r,1\,Gy,cell} \tag{3.162}$$

The results for the different dose rates from 0-127.5 mSv/d are shown in table 3.6.

3.4.3 Calculations Based on the Photon-Electron Transfer

The most important mechanisms of radiation matter interaction are based on the interaction of photons with the shell electrons of the atoms. The most frequent photon electron interactions (in the dose range of the Argonne Experiment) are the Compton effect and the photo electric effect. Electrons are set free and transfer their energy multiple hits which can cause ionization of numerous molecules. In the following

Dose [mSv/d]	$N_{r,cell}$/d
0.0 (control)	0
3.0	$1.313 \cdot 10^3$
7.5	$3.281 \cdot 10^3$
18.8	$8.225 \cdot 10^3$
37.5	$1.640 \cdot 10^4$
75.0	$3.281 \cdot 10^4$
127.5	$5.578 \cdot 10^4$

Table 3.6: Daily dose rates of the Argonne experiment in mSv/d and and corresponding calculated number of elementary reaction products per day ($N_{r,cell}$/d).

section the radiation induced numbers of molecular events caused by these electrons are calculated based on these effects.

3.4.3.1 Calculation of the Photon-Electron Energy Transfer to Primary Electrons based on Compton and Photo Electric Effect

For photon energies in the area between 0.1-3 MeV photon matter interaction happens nearly exclusively by the Compton effect (photon scattering by shell electrons with energy transfer) [49]. Below this energy range the photo-electric effect appears. For photon energies below 50 keV the photo-electric effect is the dominant interaction process [49]. The remaining energy is carried by a photon of less energy, which again can cause another Compton electron. This repeats, until the energy of the photon is to low for the Compton effect. The remainder of the photon energy then is transferred to another electron within one hit by a photo electric reaction. For a γ photon of the energy $E_{\gamma_0} = 1.25$ MeV the mean remainder energy of the scattered photon is $\approx 50\%$ [56]. For the scattered photon one can calculate an energy of

$$\begin{aligned} E_{\gamma_1} &= 0.5 \cdot E_{\gamma_1} \\ &= 0.625 MeV \ . \end{aligned} \tag{3.163}$$

For the Compton electron, which receives the lost energy, the result is

$$\begin{aligned} E_{e_1^-} &= E_{\gamma_0} - E_{\gamma_1} \\ &= 0.625 MeV \ . \end{aligned} \tag{3.164}$$

i	type	pet [%]	E_{γ_i} [MeV]	$E_{e_i^-}$ [MeV]	$E_{\gamma_i}/E_{\gamma_0}$	$n_{mol-hits,i}$
1	Compton	50	0.6250	0.6250	0.5000	10417
2	Compton	60	0.3750	0.2500	0.3000	4166
3	Compton	65	0.2438	0.1312	0.1950	2187
4	Compton	70	0.1706	0.0731	0.1365	1218
5	Compton	78	0.1331	0.0375	0.1065	625
6	Compton	80	0.1065	0.0266	0.0852	443
7	Compton	85	0.0905	0.0160	0.0724	267
8	photo electric	-	0	0.0905	0	1508
					Sum	20831
					Energy	$= 20831 \cdot 60$ eV
						= 1.249860 MeV

Table 3.7: Cascade of photon-electron scattering processes of 1 ^{60}Co γ photons. i = process number. type = type of scattering process. pet = photon energy transfer $E_{\gamma_{i-1}}$ to E_{γ_i} in %. E_{γ_i} = energy of Compton photon in [MeV]. $E_{e_i^-}$ = energy of Compton electron in [MeV]. $n_{mol-hits}$ = calculated number of molecular energy deposition events.

For the second Compton process the mean energy transfer to the scattered photon is about 60% :

$$\begin{aligned} E_{\gamma_2} &= 0.6 \cdot E_{\gamma_1} \\ &= 0.6 \cdot 0.625 MeV \\ &= 0.375 MeV \end{aligned} \tag{3.165}$$

and the electron receives:

$$\begin{aligned} E_{e_2^-} &= E_{\gamma_1} - E_{\gamma_2} \\ &= 0.625 MeV - 0.375 MeV \\ &= 0.25 MeV \end{aligned} \tag{3.166}$$

A chain of Compton processes is assumed, until the remaining energy of the Compton photon is below 0.1 MeV, according to [49]. The result of this cascade of Compton processes is shown in table 3.7.

Dose [mSv/d]	$N_{mol-hits,cell}$/d
0.0 (control)	0
3.0	$3.13 \cdot 10^2$
7.5	$7.81 \cdot 10^2$
18.8	$1.96 \cdot 10^3$
37.5	$3.91 \cdot 10^3$
75.0	$7.82 \cdot 10^3$
127.5	$1.33 \cdot 10^4$

Table 3.8: Daily dose rates of the Argonne experiment in mSv/d and corresponding calculated number of molecular energy deposition events per cell and day ($N_{mol-hits,cell}$/d).

3.4.3.2 Calculation of the Number of Molecular Energy Deposition Events of the Primary Electrons Based on Compton and Photo Electric Effect

As described before, the energy of the Compton and photo electric electrons is transferred to the surrounding tissue by a number of elementary energy deposition events. These molecular hits in general dissociate water molecules and generate free radicals (fragments of molecules). Following [44], the average energy transfer ΔE of one hit of a fast electron in tissue is ≈ 60 eV. The number of single molecular-hit events per electron are calculated as

$$n_{mol-hits,i} = \frac{E_{e_i^-}}{\Delta E} \tag{3.167}$$
$$n_{mol-hits,i} = \frac{E_{e_i^-}}{60\,eV}\ .$$

The calculated molecular hit numbers are shown in table 3.7. One 1.25 MeV photon generates a number of

$$n_{mol-hits,\gamma} = 20831 \tag{3.168}$$

microhits in tissue. Since for a dose of 1 Gy a photon number of

$$N_{\gamma_0,kg} \approx \frac{5 \cdot 10^{12}}{kg} \tag{3.169}$$

was calculated, the corresponding number of micro hits caused by 1 Gy γ irradiation from a ^{60}Co source in tissue is

$$\begin{aligned} n_{mol-hits,1\,Gy} &= n_{mol-hits,\gamma} \cdot N_{\gamma_0,kg} \\ &= 20831 \cdot \frac{5 \cdot 10^{12}}{kg} \\ &= 1.042 \cdot 10^{17} \cdot \frac{1}{kg} \ . \end{aligned} \tag{3.170}$$

That means for an average cell of mass 1 ng an average number of molecular hits of:

$$\begin{aligned} n_{mol-hits,1\,Gy,cell} &= 1.042 \cdot 10^{17} \cdot \frac{1}{kg} \cdot 1ng \\ &= 1.042 \cdot 10^{17} \cdot \frac{1}{kg} \cdot 10^{-12} \cdot kg \\ &= 1.042 \cdot 10^{5} \ . \end{aligned} \tag{3.171}$$

With the help of this value the average numbers of molecular hits per cell and day in the Argonne dog experiment can be calculated. The results are summarized in table 3.8.

Dose [mSv/d]	n_1	Δt [h]	n_2	n_3	ε^* $[\frac{1}{h}]$
0.0 (control)	0	-	0	0	$1.6 \cdot 10^{-11}$
3.0	7.812	3.072	$1.313 \cdot 10^3$	$3.13 \cdot 10^2$	0.0011
7.5	19.53	1.229	$3.281 \cdot 10^3$	$7.81 \cdot 10^2$	0.0007
18.8	48.96	0.490	$8.225 \cdot 10^3$	$1.96 \cdot 10^3$	0.0016
37.5	97.65	0.246	$1.640 \cdot 10^4$	$3.91 \cdot 10^3$	0.0049
75.0	195.3	0.123	$3.281 \cdot 10^4$	$7.82 \cdot 10^3$	0.0091
127.5	332.0	0.072	$5.578 \cdot 10^4$	$1.33 \cdot 10^4$	0.0123

Table 3.9: Dose = daily dose rates of the Argonne experiment in mSv/d n_1 = corresponding overall average number of hits per cell per day $n_{cell-traversals}$/d. Δt = average duration between two hits per cell in hours. n_2 = number of elementary reaction products per cell per day calculated from the microdosimetric G-value ($N_{r,cell}/d$). n_3 = number of molecular hits per cell per day calculated from the photon-scattering cascade ($n_{mol-hits,cell}/d$). ε^* = estimated excess cell loss rates given as fraction of cells lost per h.

3.4.4 Summarized Results of the Microdosimetric Calculations

Table 3.9 summarizes the results of the estimations of excess cell loss rates and the results of the different microdosimetric methods to describe the effects of chronic irradiation on the cellular level. The calculations were performed for the dose groups of the Argonne experiment. Shown are the average daily dose, the number of particle traversals per cell and day (cell hits), the average time between these hits, numbers of molecular reactions calculated by different methods and the model based estimated excess cell loss rates.

Chapter 4

Discussion

Contents

4.1 Modeling Thrombocytopoiesis in Rodents

In section 3.1 a biomathematical model of thrombocytopoieis was constructed to reproduce the steady state cell production and the regulation dynamics of the megakaryocyte-platelet renewal system in rodents. The compartment structure of the model reflects the current biological concepts of hematopoiesis and thrombocytopoiesis in mammalians. The kinetic parameters of the model were calculated from experimental data of animal experiments as far as available. Where no data were available, parameters were chosen in a physiological reasonable way to fit to other experimentally derived parameters. The model is set up in a modular approach which makes it easier to modify and extend.

4.1.1 Comparison to Models of Other Authors

Wichmann et al. [98] describe a model of thrombocytopoiesis which consists of compartments for stem cell numbers, megakaryocyte numbers, megakaryocyte volume, thrombocyte numbers and thrombopoietin. Pluripotent stem cells, progenitors and precursors are pooled together in one stem cell compartment. Special characteristics of pluripotent stem cells are not included.

Selivanov and Lanin [86] use compartments for earliest megakaryocyte precursor cells, later megakaryocyte precursor cells, megakaryocyte numbers and volume and give more emphasis to age structure characteristics. A compartment describing the special characteristics of pluripotent stem cells is not part of their model.

Eller et al. [24] include compartments for committed progenitors, megakaryocyte numbers, thrombocyte numbers, chalones and thrombopoietin, but not pluripotent stem cells and megakaryocyte volume or ploidy.

The model of Kodym [52] includes compartments for early committed progenitors, late committed progenitors, endoreduplicating megakaryocytes, four ploidy-classes of the maturing megakaryocytes and thrombocytes. A pluripotent stem cell compartment is not implemented.

In contrast to this previous work the presented model is explicitely constructed to fulfill the following criteria:

- The model reflects the physiological realities of thrombocytopoiesis and hematopoiesis. No artificial compartments whithout biological correlates were included into the model structur.

- The special characteristics of the pluripotent stem cell compartment like self reproduction probability and mitotic activity were explicitely set up in the model. This is essential for the simulation of stem cell recovery after total body irradiation (TBI).

- The model reflects the heterogeneity of the megakaryocyte population. This is necessary for accurate enough simulations of the short time pattern of thrombocyte counts after TBI. The accuracy is needed for the application of nonlinear optimization routines (least-square fitting of model thrombocyte counts against experimental data) to estimate remaining stem cell numbers after TBI.

4.1.2 Approaches to Validation and Verification of the Model

Validation and verification was done in two steps. First, the steady state model was compared to experimental cell concentration data. In the next step the dynamics of the model were compared to experiments on imposed disturbances of thrombocytopoiesis.

4.1.2.1 Verification and Validation of the Steady State System

The steady state (model) cell numbers were compared to experimentally derived cell numbers of the rat. The explicit calculations were performed in section 3.1.5.1. Model cell numbers and corresponding model cell concentrations were calculated based on cell turnover rates and other kinetic parameters of the model. The experimental cell concentrations were taken from data of different authors described in the literature. The techniques of the experiments depend on the type of cells. Morphologically observed data are available for differentiated cells, such as megakaryocytes and platelets. Cell concentrations of earlier development stages of the thrombocytopoietic system have to be detected by cell culture techniques which only can give indirect information. Thus, they provide less accuracy. Deviations of one order of magnitude between experiments

are quite normal. This is very important for interpretation of the validation calculations in section 3.1.5.1. Comparison of model and experimental cell numbers show that the correlating cell concentrations of the model and of the experiments are all in the same order of magnitude.

Thus, the model assumptions for the undisturbed system are compatible to the physiology of thrombocytopoiesis like known from experiments.

4.1.2.2 Verification and Validation of the Disturbed System

Validation of the model dynamics in the case of disturbances was done by simulation of different experiments and comparison of the simulation results to experimental data. Simulations were performed for exchange and hypertransfusions with platelet poor or enriched blood, administration of cytotoxic agents, and recovery after total body irradiation. The simulation results and the experimental data are shown explicitely in section 3.1.5.2.

The simulation results show that the model is able to reproduce completely different disturbances to the thrombocytopoietic system satisfactory to be used as a valuable tool.

4.1.2.3 Possibilities of Deviations between Model and Reality

Of course, some deviations of model cell numbers, simulation results, and experimental data can be recognized. There are many possible reasons for deviations between model dynamics and physiological reality:

- Deviation of experimental and "real" cell numbers:
  The proposed model reflects the development of platelets from the earliest stem cell populations. In contrast to differentiated cells which can be examined very precisely by morphologic experimental setups, the early development stages of hematopoiesis and thrombocytopoiesis are known from indirect experiments, such as in-vitro cell culture experiments or labeling experiments. These experimental techniques always imply the danger to produce unprecise results or experimental artefacts.

- Deviation of the structure of "real world" and model regulation:
  The regulators of the model are based in general on experimental observations, physiological assumptions and mathematical reasons of stability. Not all assumptions which were necessary in the feedback regulations to reproduce compensation dynamics of the thrombocytopoietic system can be verified by experimental results. Thus, it is possible that some structural aspects of the regulation mechanisms are not correct or are missing in the model.

- Deviation of "real world" and model regulation functions:
  There is no guarantee that the model regulation functions reflect exactly the compensation mechanisms of the thrombocytopoietic system. The functions used in the model were selected as mathematical and physiological reasonable solutions with respect to numerical stability of the model. Biology surely has a lot more possibilities for "physiological" feedback functions.

4.2 Model Based Analysis of the Hematological Effects of Acute Irradiation

Section 3.2 analyzed the application of model based methods to the hematopoietic effects of chronic irradiation.

4.2.1 A Model Based Method for Estimation of Surviving Fractions of Stem Cells from Blood Counts

In section 3.2.2 the basic model was extended by a compartment for an injured stem cell population in order to simulate acute irradiation effects to hematopoiesis. Based on this model, a method for the estimation of remaining stem cell numbers from platelet counts in the blood after TBI was developed. The model was coded in MATLAB® and included into a nonlinear optimization routine. Mathematically speaking, the estimation method is a model based least square estimator for surviving fractions of stem cells. The estimation routine worked well in most cases regarding convergence behaviour and estimation times.

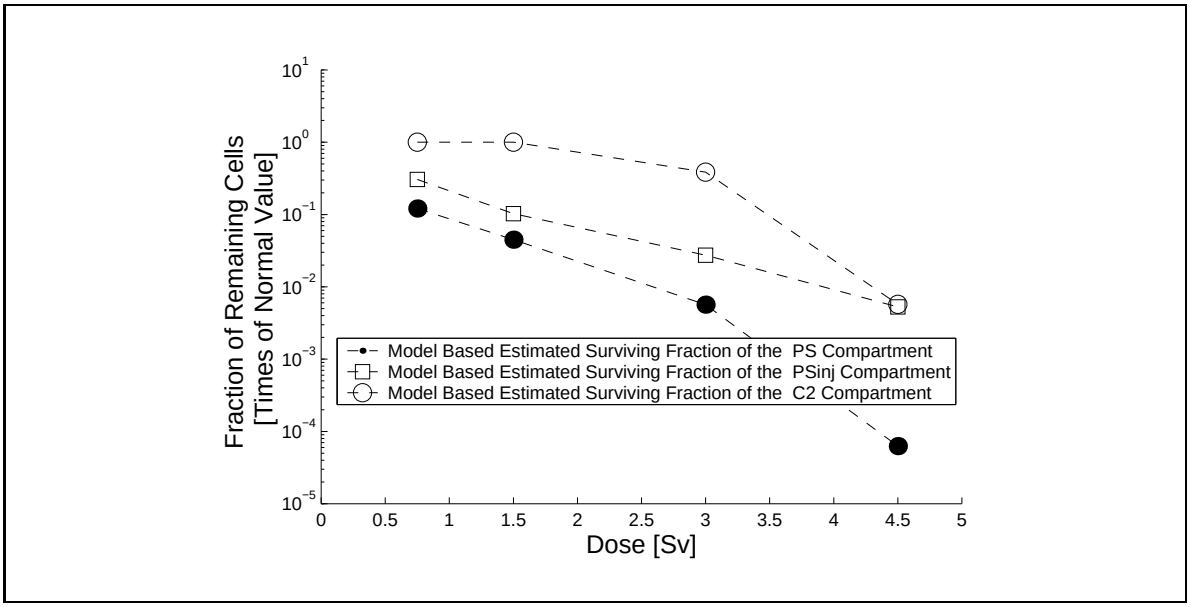

Figure 4.1: Model based estimated fractions of surviving cells in rats as a function of the received dose. Data from Stein [87].

The application of the biomathematical model of thrombocytopoiesis to analyze radiation effects opens the possibility to calculate survivng fractions of stem cells by using exclusively data of the peripheral blood counts.

Pluripotent stem cells are distributed throughout the complete skeleton and are difficult to identify. The model based estimation opens a very elegant method to analyze the effects of irradiation to these cell populations. Further, it allows the retrospective evaluation of data of experiments and accidents, where no modern techniques of bone marrow analysis were performed.

4.2.2 Estimation Results for Rat Data

In section 3.2.5 surviving fractions for stem cells were (model based) estimated from data of X-ray irradiated rats of experiments done by Stein [87]. The results are summarized in figure 4.1. There are no data for direct comparison of the model based estimated surviving fractions of pluripotent stem cells to experimentally determined surviving fractions of pluripotent stem cells in rats. For this reason, the model based estimated surviving fractions of pluripotent stem cells of rats are compared to empirical surviving fractions of CFU-S in mice. To calculate values for comparison, the

Source	Dose [Sv]	S_{PS}	S_{CFU-S}	Comments
Stein	0.75	0.12	0.39	
Stein	1.5	0.045	0.15	
Stein	3.0	0.0057	0.024	
Stein	4.5	0.0001	0.0036	
Stein	6.0	0.0007	0.00055	data not sufficient
Ebbe	6.5	0.00063	0.00030	different setup

Table 4.1: Comparison of model based estimations and experimental based calculations of surviving fractions of stem cells. Dose = received dose in Sv. $S_{PS} = S_{PS,model,X-ray,rat}$ = model based estimated pluripotent stem cell numbers in rats. $S_{CFU-S} = S_{CFU-S,calc.,X-ray,mouse}$ = experimentally determined numbers of CFU-S in mice.

empirical dose survival relationship

$$S = 1 - (1 - e^{-\frac{D}{D_0}})^n \tag{4.1}$$

where

$S =$ surviving fraction of cells

$D =$ received dose

$D_0 =$ dose for reduction of S to 0.37

$n =$ extrapolation number

is used. The extrapolation number n represents the idea of multi-hit models [42] [9] [57]. Like D_0, it is determined by fitting of the dose survival model equation 4.1 against experimental data. A review on radiation sensitivities of bone marrow cells [53] gives D_0 values of about 0.8 Gy and n values of 1.0 for CFU-S in mouse bone marrow.

Table 4.1 compares the values of the different methods for determination of surviving fractions at different dose rates. The data for the row at 6.0 Sv were not sufficient for a satisfactory estimation, since the experimental animal died within a short time. The data for the 6.5 Sv data are taken from an other experimental setup. Therefore, the last two rows of the table for the doses 6.0 Sv and Sv Gy were not used for further evaluations.

Figure 4.2 shows the correlation of the surviving fractions of model stem cells for

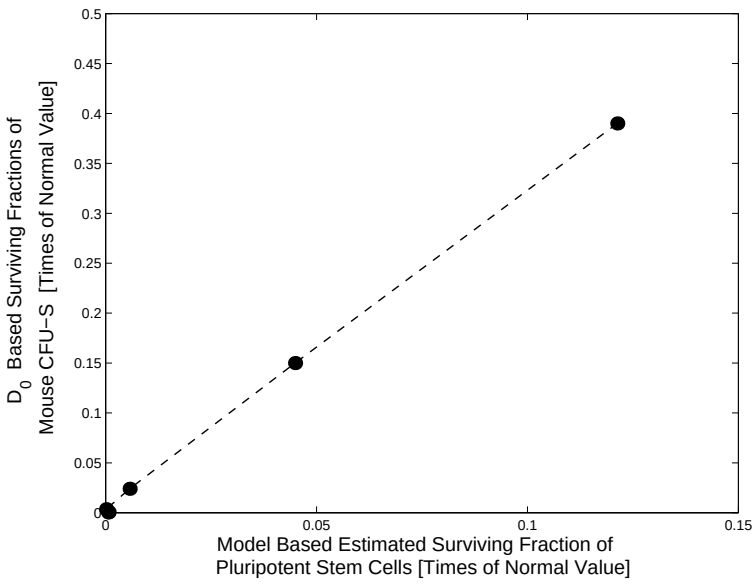

Figure 4.2: Scatter plot of model based estimated surviving fractions of pluripotent stem cells in rats and D_0 based experimentally derived surviving fractions of mouse bone marrow CFU-S at equal received doses.

the doses 0.75 - 4.5 Sv estimated from rat data $S_{PS,model,X-ray,rat}$ and the surviving fractions of CFU-S for the same doses calculated using equation 4.1.

It can be recognized that the estimated surviving fractions differ in their absolut values. On the other hand, the different estimation approaches result in proportional survival fractions for the different methods.

Reasons for the non-matching in absolute values, but proportionality can be:

- Deviations in the measured doses between the experiments.
- Different radion sensitivities between bone marrow cells in rats and mice.
- Deviations between model and physiology of thrombocytopoiesis. Such a deviation can be, for example, differing numbers of cell divisions in the model and in reality.

It can be assumed that the deviations are a result of combinations of the above listed reasons.

The obvious proportionality of the results shows that it is possible to make quantifying estimations of surviving fractions of pluripotent stem cells in rats after TBI by

using exclusively data of the blood counts. Thus, using the model method can give assistance to assess surviving fractions of hematopoietic stem cells without cytological bone marrow examinations.

4.2.3 Estimation Results for Human Data

The examinations in section 4.2.2 showed the correlation between the model based stem cell estimations and the experimental results. For human radiation accident victims, the basis for diagnosis and treatment are response categories (RCs). These RCs were developed by an interdisciplinary team of international radiation accident experts under the project name METREPOL (medical treatment protocols). Thus, a point of interest is to examine the correlation between the severity of the acute radiation syndrome described by the RCs and the damage of the stem cell pool.

Figure 4.3 shows the relationship of the estimated remaining fractions of pluripotent and injured (model) stem cell numbers and the METREPOL response categories.

In response category 4 the estimations for two cases resulted in values which are of orders of magnitude like found in RC1. The reason is the short time span of the data. The very severly affected patients (cases 1012 and 1026) died within a short time after irradiation. As a consequence, the available time span of data is about 20 days. Since platelets and megakaryocytes have transit times of 8 - 10 days, this duration is too short for reasonable estimations of the PS and PSinj compartments. One patient (case 3088) lived longer and a better estimation of stem cell numbers was possible.

4.3 Model Based Analysis of the Hematological Effects of Chronic Irradiation

The application of the biomathematical model of thrombocytopoiesis to analyze the effects of chronic irradiation resulted in an model for radiation induced permanent excess cell loss in the proliferating parts of thrombocytopoiesis (section 3.3.3).

The model explains the development of suppressed steady state cell numbers in the thrombocytopoietic system (section 3.3.4). Of course this steady state effect sometimes

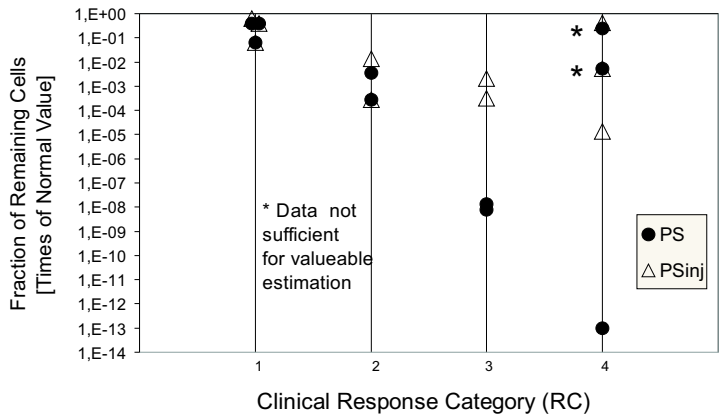

Figure 4.3: Model based estimation results of stem cell numbers in patients of different clinical response categories (see text) after irradiation accidents.

can be overlaied by other effects. Such effects are, for example, the development of acquired radioresistance or development of leukemia (section 3.3.1).

The analysis of the compartment contents of the model as a function of the excess cell loss rate demonstrated the existence of a certain critical value of the excess cell loss rate (section 3.3.5). Near to this value, the cell numbers of the thrombocytopoietic system and of the stem cell pools can drop to life threatening values. Comparison of the contents of the thrombocyte (TH) and pluripotent stem cell (PS) compartments (figure 4.4) shows that the remaining fractions of pluripotent stem cells are far below remaining fractions of thrombocytes (relative to normal values). From the medical viewpoint this means that in the case of radiation induced suppressed platelet counts, the stem cell system is affected in a significant more severe degree than would perhaps be assumed by interpretation of thrombocyte counts..

Stochastic simulations with small variances showed the dramatic dynamics of the thrombocytopoietic system in an area near to the critical value (section 3.3.6). Thus, stochastic interpretations can give an explanatory approach to widely distributed survival times in experimental animals.

Pathophysiological interpretations of the model analysis shown in figure 4.4 resulted in the assumption of the presence of different states of the hematopoietic system under the stress of chronic irradiation:

- In the first area the thrombocytopoietic system is able to compensate the excess cell loss. Further, it is not affected by small stochastic variations of the excess

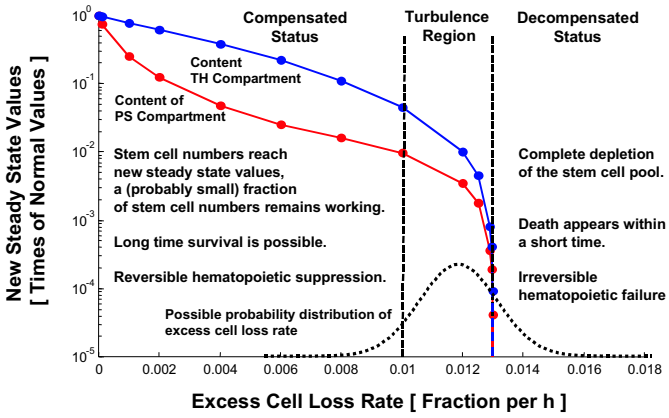

Figure 4.4: New model steady state values of the TH and PS compartments as a function of the excess cell loss rate.

cell loss rate. Thus, this area was interpreted as a state of compensated platelet production.

- Near to the critical value of the excess cell loss rate, there exists an area where the thrombocytopoietic system is very sensitive to small stochastic variations of the excess cell loss rate. According to the unpredictable stochastic system failure, this states of the system are assigned to a turbulence region.

- If the excess cell loss rates exceedes the critical value, this leads to an depletion of the thrombocytopoietic proliferation pools, failure of platelet production, and, as a consequence, to the death of the organism by bleeding.

4.4 Excess Cell Loss and Microdosimetric Radiation Effects

A model based least-square estimator for the estimation of excess cell loss rates from experimental data was implemented with nonlinear optimization algorithms (section 3.3.7). Using the data of dogs which were permanently exposed to defined daily radiation doses of a ^{60}Co source, explicite excess cell loss rates for each dose group were estimated.

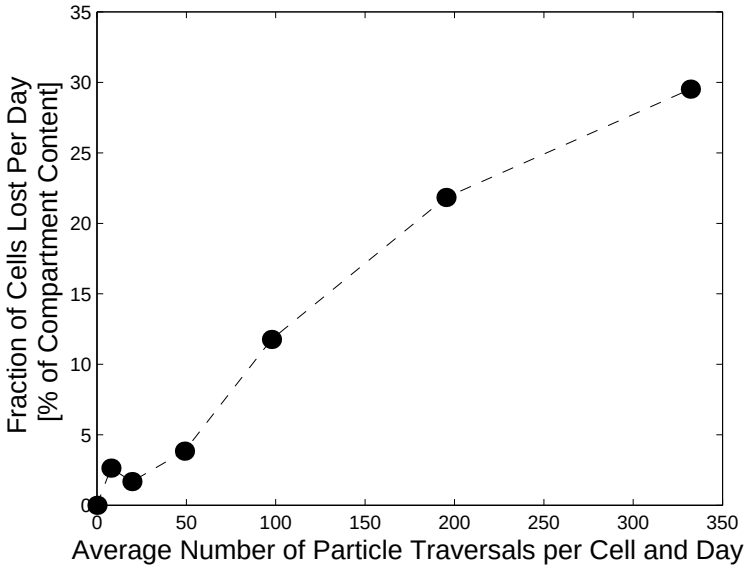

Figure 4.5: Model based estimated excess cell loss rates ε^* based on data of the Argonne experiment as a function of the calculated average number of particle traversals per cell and day.

In section 3.4 the average numbers of particle traversals per cell per day were calculated for the dose groups of the Argonne experiment following Feinendegen [26]. The calculations are based on the linear energy transfer (LET), microdosimetric event spectra in tissue [43], specific energies of the ^{60}Co photons, and daily received radiation doses of the dogs.

In the investigated dose area from 3.0 mSv/d to 127.5 mSv/d the correlation of the excess cell loss rate and the average number of particle traversals per cell was almost linear. Figure 4.5 shows the estimated excess cell loss rates plotted over the average number of particle traversals per cell. A nearly linear relationship between the number of average particle traversals per cell per day and the estimated average excess cell loss rates can be observed in the dose area of 3.0 - 127.5 mSv/d.

In the sections 3.4.2.2 and 3.4.3 numbers of radiation induced molecular reactions per cell and day were calculated using different aproaches based on the G-value and the photon-electron scattering process by the Compton effect. The G-value based calculated values were between $1.3{\cdot}10^3$-$5.6{\cdot}10^4$ reaction products per cell and day for the dose rates 3.0-127.5 mSv/d of the Argonne experiment. The Compton effect based calculated values were between $3.13{\cdot}10^2$-$1.33{\cdot}10^4$ molecular hits per cell and day. Following Feinendegen [26], it has been estimated that about 10^3 molecular

attacks per cell per minute are produced by normal cell mebatolism. This equals to a "background" radical attack number of $10^3 \cdot 60 \cdot 24 = 1.44 \cdot 10^6$ per cell and day. The interesting point is that the radiation induced values are 1-2 orders of magnitude below the values caused by normal metabolism. The fact that an excess cell loss is detected, shows the special quality of of the effects of ionizing radiation.

The connection of model based estimation of excess cell loss rates in hematopoietic cell pools on the one hand and microdosimetric calculations on the other hand defines a completely new method for the in-vivo analysis of effects of chronic irradiation. At the moment there exist no standard methods for the estimation of excess cell loss rates by biological techniques.

4.5 Next Steps

One interesting application of the presented modeling work could be, for example, to determine the correlation between estimated model pluripotent stem cell numbers and numbers of CD34 positive cells in bone marrow transplantations. The assumptions and parameters of the pluripotent stem cell compartment are derived from CFU-S cells. The CFU-S are only detected by animal experiments with mice. Human bone marrow cells which are histogenetically close to the pluripotent stem cell are CD34 positive cells. It is assumed that the pluripotent stem cells are a subset of the CD34 positive cells. Thus, the numbers of CD34 cells should be proportional to the number of pluripotent stem cells. This hypothesis could be tested using data of the recovery of patients after bone marrow transplantations.

Another possible application is to use the entire model or parts of it for quantifications of the short time response patterns in thrombocyte counts of humans after accidental radiation exposure. Thus, the model should, in connection with models of other hematopoietic cell lines, provide a method for early diagnosis of the severity of the degree of the hematopoietic radiation syndrome. With this function the model will be part of a medical assistance system for the acute radiation syndrome.

Regarding the area of chronic irradiation effects other hypothesis, such as stochastic variation of self replication probabilities, could be tested.

A mathematically interesting point would be to examine the confidence intervals of the constructed estimators. Since solutions of the system equations have to be performed numerically, confidence intervals can not be derived analytically from the model equations.

4.6 Conclusion

The developed biomathematical models and estimation routines in this thesis show how the connection of biomedical research and applied mathematics can result in completely new methods to gain information and new knowledge. Looking back to the objectives of this thesis one can summarize the results as follows.

- A model of thrombocytopoiesis, reflecting the megakaryocyte/platelet renewal system from the stage of the pluripotent stem cells to the blood platelets, was developed. The model contains compartments for pluripotent stem cells, non-committed progenitor cells, early and late committed megakaryocyte precursor cells, endoreduplicating cells, megakaryocytes in four ploidy groups and thrombocytes. The developed model is capable to reproduce thrombocytopoiesis in steady state and under different imposed disturbances (exchange transfusion, administration of cytostatic substances) in a satisfactory quality.

- To simulate acute irradiation effects to hematopoiesis, the developed basic model was extended by a compartment for injured stem cells which are impaired in their proliferative potential by radiation. Further, a model based least-square estimator for stem cell numbers was implemented. The quality of the estimation method was validated by comparison to data from experiments on rats. Model based estimations of surviving fractions of pluripotent stem cells were proportional to experimental results on CFU-S in bone marrow of irradiated mice.

- Model based estimations of surviving fractions in radiation accident patients were used to examine the relationship of the degree of damage of the hematopoietic stem cell pool and the clinical response categories (RCs) of the acute irradiation syndrome. The estimations showed a dramatic decrease of stem cell surviving fractions with rising severity degree of the response category.

- The model was extended for simulation of permanent radiation induced excess cell loss. Simulations showed that the extended model is capable to reproduce the damaging effects of chronic irradiation to the hematopoietic stem cell pools. The possibility of new steady states of platelet numbers during chronic irradiation was shown.

- Examination of the characteristics of the model and pathophysiological interpretations of the results delivered new explanatory approaches for experimentally observed biological phenomena. Examples of randomly distributed survival times were reproduced by stochastic simulations. A least-square estimation method was set up to estimate excess cell loss rates from experimental data of chronically irradiated dogs.

- The received dose rates of the dogs of the used ^{60}Co γ source were transformed to the mean number of particle traversals (micro-hits) per cell and day and other microdosimetric sizes. The number of micro-hits per day was compared to the model based estimated excess cell loss rates in the dogs. In the examined dose area of 3.0 - 127.5 mSv/d a nearly linear relationsship between the average number of micro-hits (per cell and day) and the excess cell loss rate was observed.

The results clearly justify the model technique and the assumptions made for the different research questions. New insights in the way ionising radiation affects the mammalian and human organism could be elaborated.

Chapter 5

Summary

This thesis presents the application of biomathematical models of the megakaryocyte-platelet system to be used in the analysis of radiation effects on hematopoiesis and thrombocytopoiesis.

The basic structure of the used biomathematical models of thrombocytopoiesis follows the currently accepted biological model of hematopoiesis and thrombocytopoesis in mammalians and humans. It contains compartments for pluripotent stem cells, noncommitted progenitor cells, committed progenitor cells, endoreduplicating precursor cells, megakaryocytes in the most important four ploidy groups 8N, 16N, 32N, and 64N, average megakaryocyte volume within the ploidy groups and platelets. Regulatory functions were included to represent the compensatory feedback mechanisms of the megakaryocyte-platelet system.

The compartments, the regulator structure and the cell-kinetic parameters of the model are derived from biological experiments such as in-vivo labeling with radioactive DNA precursors, cell culture experiments, flow cytometry and others. For evaluation of experiments and for building suitable submodels mathematical techniques were developed and implemented with numerical software packages.

As a first step a model of thrombocytopoiesis in rodents was developed. The model was validated for steady state cell numbers and compensation dynamics after several imposed disturbances. For analyzing the effects of acute irradiation to the hematopoietic system the basic rodent model was extended for simulation of acute irradiation effects and included into an estimation method which is able to calculate remaining stem cell numbers based on the response patterns of platelet counts in the peripheral blood after irradiation. The calculation method is in its mathematical structure a least square estimator based on nonlinear optimization methods. Several experiments performed with rats were evaluated. It was clearly shown that the depression of platelet counts in rats after total body irradiation is a function of the damage of the stem cell pool.

For analyzing hematopoietic radiation effects on humans the cell kinetic parameters of the model were transformed to fit the human thrombocytopoietic system. Further a development-specific damage function for the megakaryocytes had to be set up. Estimation of stem cell numbers was done using the techniques which were developed for the rodent model. Analysis of patient data from radiation accidents resulted in a clear correlation of the severity of the hematopoietic radiation syndrome described by clinical response categories and the degree of the estimated damage of the stem cell pool represented by surving fraction of pluripoten stem cells.

For application to chronic irradiation effects the model was transformed by calculating new cell kinetic parameters for dogs and extended by excess cell loss rates in the model equations of the radiosensitive cell pools. Simulations of experimental results of chronically irradiated dogs showed the existence of new steady-state values in the thrombocyte counts of irradiated dogs. Analysis of the model cell numbers in dependency of the excess cell loss rate can be summarized in the existence of a critical limit value. Approximation of this limit value results in a dramatic drop in (model) cell numbers. Introducing the excess cell loss rate as a stochastic variable shows the existence of a turbulence region near to the limit value, in which small changes of the excess loss rate can lead to a sudden failure of the hematopoietic system. Model based estimations of the excess cell loss rate from experimental thrombocyte counts were compared to microdosimetric quantities.

The developed models of thrombocytopoiesis with extensions for several kinds of external disturbances proofed to be capable to reproduce the real physiological processes and to fulfill the objectives of this thesis. The special feature of the proposed biomathematical methods is the possibility to assess in vivo the stem cell damage caused by acute and chronic irradiation by using exclusively peripheral platelet counts.

Because of this advantage the models are planned to be used to build a module of an assistance system for the medical management of radiation accident victims.

Bibliography

[1] Blackett N: Erythropoiesis in the rat under continuous gamma-irradiation at 45 rads/day. Br J Haematol, 13: 915–923 (1967)

[2] Boll I: Knochenmarkuntersuchungen. In: Boll I, Heller S (eds.), Praktische Blutzelldiagnostik, Springer, Berlin, pp. 274–353 (1991)

[3] Boll I, Domeyer C, Buehrer C: Human megakaryoblastic proliferation and differentiation events observed by phase-contrast cinematography. Acta Haematol, 97: 144–152 (1997)

[4] Bond J, Fliedner T, Archambeau J: Mammalian Radiation Lethality, Academic Press, London, pp. 17–26 (1965)

[5] Bond J, Fliedner T, Archambeau J: Mammalian Radiation Lethality, Academic Press, London, pp. 29–37 (1965)

[6] Bond J, Fliedner T, Archambeau J: Mammalian Radiation Lethality, Academic Press, London, pp. 159–230 (1965)

[7] Bond J, Fliedner T, Archambeau J: Mammalian Radiation Lethality, Academic Press, London, pp. 15–17 (1965)

[8] Bond J, Fliedner T, Archambeau J: Mammalian Radiation Lethality, Academic Press, London, pp. 231–275 (1965)

[9] Bond J, Fliedner T, Archambeau J: Mammalian Radiation Lethality, Academic Press, London, pp. 50–60 (1965)

[10] Bond J, Fliedner T, Archambeau J: Mammalian Radiation Lethality, Academic Press, London, pp. 61–100 (1965)

[11] Bronstein I, Semendjajew K: Laplace Transformation, Teubner, Leipzig, pp. 634–648 (1987)

[12] Calabresi P, Parks Jr. R: Alkylating agents, antimetabolites, hormones, and other antiproliferative agents. In: Goodman L, Gilman A (eds.), The Pharmacological Basics of Therapeutics, MacMillan, New York, pp. 1254–1307 (1975)

[13] Calabresi P, Parks Jr. R: Chemotherapy of neoplastic diseases. In: Goodman L, Gilman A (eds.), The Pharmacological Basics of Therapeutics, MacMillan, New York, pp. 1248–1253 (1975)

[14] Carnes B, Fritz T: Responses of the beagle to protracted irradiation. i. effect of total dose and dose rate. Radiat Res, 128: 125–132 (1991)

[15] Carnes B, Fritz T: Continuous irradiation of beagles with gamma rays. Radiat Res, 136: 103–110 (1993)

[16] Chabner B, Wilson W: Pharmacology and toxicity of antineoplastic drugs. In: Beutler E, Lichtmann M, Coller B, Kipps T (eds.), Williams Hematology, McGraw-Hill, New York, pp. 143–155 (1995)

[17] Coleman T, Branch M, Grace A: Optimization Toolbox For Use With MATLAB, Version 2, The MathWorks INC., Natick MA, pp. 1.1–4.138 (1999)

[18] Ebbe S: Postirradiation thrombocytopoiesis: Suppression, recovery, compensatory states, and macromegakaryocytosis. In: Levine R, Williams N, Levin J, Evatt B (eds.), Megakaryocyte Development and Function, Alan R. Liss, New York, pp. 71–89 (1986)

[19] Ebbe S, Phalen E: Does autoregulation of megakaryocytopoiesis occur? Blood Cells, 5: 123–138 (1979)

[20] Ebbe S, Stohlman Jr. F: Megakaryocytopoiesis in the rat. Blood, 26: 20–35 (1965)

[21] Ebbe S, Stohlman Jr. F, Donovan J, Howard D: Platelet survival in rats with transfusion-induced thrombocytosis. J Lab Clin Med, 68: 813–823 (1966)

[22] Ebbe S, Yee T, Carpenter D, Phalen E: Megakaryocytes increase in size within ploidy groups in response to the stimulus of thrombocytopenia. Exp Hematol, 16: 55–61 (1988)

[23] Ebbe S, Yee T, Phalen E: 5-fluorouracil-induced thrombocytosis in mice is independent of the spleen and can be partially reproduced by repeated doses of cytosine arabinoside. Exp Hematol, 17: 822–826 (1989)

[24] Eller J, Gyoeri I, Zoellei M, Krisza F: Modelling thrombopoiesis regulation. In: Witten H (ed.), Mathematical Models in Medicine, Pergamon Press, Oxford, pp. 841–848 (1988)

[25] Feinendegen L: Tritium-Labeled Molecules in Biology and Medicine, Academic Press, London, pp. 163–235 (1967)

[26] Feinendegen L, Loken M, Booz J, Muehlensiepen H, Sondhaus C, Bond V: Cellular mechanisms of protection and repair induced by radiation exposure and their consequences for cell system responses. Stem Cells, 13(suppl 1): 7–20 (1995)

[27] Fenton R, Longo D: Cell biology of cancer. In: Fauci A, Braunwald E, Isselbacher K, Wilon J, Martin J, Kasper D, Hauser S, Longo D (eds.), Harrisons Principles Of Internal Medicine, MacGraw-Hill, New York, pp. 505–512 (1998)

[28] Fliedner T, Calvo W, Tang P: Realitaeten in der Blutbildung am Beispiel des Megakaryozyten-Blutplaettchen-Systems. In: Gross R (ed.), Modelle und Realitaeten in der Medizin, Schattauer, Stuttgart, pp. 65–78 (1983)

[29] Fliedner T, Kindler H, Densow D, Baranov A, Guskova A, Szepesi T: The Moscow-Ulm radiation accident clinical history database. In: MacVittie T, Weiss J, Browne D (eds.), Advances in Treatment of Radiation Injuries, Pergamon Press, Oxford, pp. 271–279 (1996)

[30] Fliedner T, Nothdurft W, Tibken B, Hofer E, Weiss M, Kindler H: Haemopoietic cell renewal in radiation fields. Adv Space Res, 14: 541–554 (1994)

[31] Fliedner T, Steinbach K: Repopulating potential of hematopoietic precursor cells. Blood Cells, 14: 393–410 (1988)

[32] Fliedner T, Steinbach K, Raffler H: Erholungsvorgaenge im Stammzellenbereich des Knochenmarkes nach Strahleneinwirkung. In: Messerschmidt O, Moehrle G, Zimmer R (eds.), Strahlenschutz in Forschung und Praxis, vol. XVIII, Georg Thieme, Stuttgart, pp. 4–20 (1977)

[33] Fliedner T, Tibken B, Hofer E, Paul W: Stem cell responses after radiation exposure: A key to the evaluation and prediction of its effects. Health Phys, 70: 787–797 (1996)

[34] Gerhardts M: Ein Mathematisches Modell zur Granulopoese beim Menschen. Ph.D. thesis, Medizinische Fakultaet der Universitaet Koeln, pp. 19–24 (1991)

[35] Graessle D: Mathematische Modellierung der Thrombopoese. Master's thesis, Fakultaet fuer Mathematik und Wirschaftswissenschaften der Universitaet Ulm, pp. 45–94 (1998)

[36] Harker L: Kinetics of thrombopoiesis. J Clin Invest, 47: 458–465 (1968)

[37] Harker L: Platelet production and its regulation. In: Paulus J (ed.), Platelet Kinetics, North Holland Publishing Company, Amsterdam, pp. 202–211 (1971)

[38] Heimpel H, Pruemmer O: Bedeutung und Effizienz der Blutzelldiagnostik. In: Boll I, Heller S (eds.), Praktische Blutzelldiagnostik, Springer, Berlin, pp. 6–35 (1991)

[39] Hendry J, Lajtha L: The response of hemopoietic colony-forming units to repeated doses of X-ray. Radiat Res, 52: 309–315 (1972)

[40] Hjort P, Paputchis H: Platelet life span in normal, spleenectomized and hyperspleenic rats. Blood, 15: 45–51 (1959)

[41] Hodgson G, Bradley T, Fartin R, Sumner M, Fry P: Recovery of proliferating haemopoietic progenitor cells after killing by hydroxyurea. Cell Tissue Kinet, 8: 51–60 (1975)

[42] Hug O, Kellerer A: Treffertheorie und alternative Deutung der Dosiswirkungsbeziehungen. In: Hug O, Kellerer A (eds.), Stochastik der Strahlenwirkung, Springer, Berlin, pp. 1–33 (1966)

[43] International Commission on Radiation Units and Measurements: Report 36, Microdosimetry, International Commission on Radiation Units and Measurements, Bethesda, Maryland, pp. 46–52 (1983)

[44] International Commission on Radiation Units and Measurements: Report 36, Microdosimetry, International Commission on Radiation Units and Measurements, Bethesda, Maryland, pp. 18–19 (1983)

[45] Jacquez J: Compartmental Analysis in Biology and Medicine, Elsevier, Amsterdam, pp. 1–12 (1972)

[46] Junqueira L, Carneiro J, Schiebler T, Peiper U, Schneider U: Histologie, Springer, Berlin, pp. 41–91 (1986)

[47] Kalina I, Mackova N, Brezani P, Ondrussekova A: Chronic irradiation effects with daily dose rate 0.5 Gy on haematopoiesis: 1. haematopoietic cell changes in bone marrow. Radiobiol Radiother, 23: 277–282 (1982)

[48] Kalina I, Praslicka M, Marko L, Krasnovska V: Effect of continuous irradiation upon bone marrow haemopoietic stem cells in mice. Folia Biol, 45: 279–283 (1975)

[49] Kiefer J: Biologische Strahlenwirkung, Birkhaeuser, Basel, pp. 43–44 (1989)

[50] Kimura H, Segal G, Lee M, Adamson J: Megakaryocytopoiesis in the rat: Response to thrombocytopenia induced by exchange transfusion. Exp Hematol, 13: 1048–1054 (1985)

[51] Kipps T: The cluster of differentiation (CD) antigens. In: Beutler E, Lichtmann M, Coller B, Kipps T (eds.), Williams Hematology, McGraw-Hill, New York, pp. 113–140 (1995)

[52] Kodym R: A mathematical model, describing the kinetic behaviour of the thrombopoietic system in mice and rats. Alternatives to Laboratory Animals, 22: 269–284 (1994)

[53] Kovalev E, Darenskaya N, Smirnova O: Analysis of experimental and clinical data. In: Reeves G (ed.), AFRRI Contract Report 96-1, Estimation of Radiation Risk Based on the Concept of Individual Variability of Radiosensitivity, Armed Forces Radiobiology Research Institute, Maryland, USA, pp. 123–198 (1996)

[54] Krieger H: Strahlenphysik, Dosimetrie und Strahlenschutz, Grundlagen, Teubner, Stuttgart, vol. 1, pp. 47–48 (1998)

[55] Krieger H: Strahlenphysik, Dosimetrie und Strahlenschutz, Grundlagen, Teubner, Stuttgart, vol. 1, pp. 248–249 (1998)

[56] Krieger H: Strahlenphysik, Dosimetrie und Strahlenschutz, Grundlagen, Teubner, Stuttgart, vol. 1, pp. 123–124 (1998)

[57] Krieger H: Strahlenphysik, Dosimetrie und Strahlenschutz, Grundlagen, Teubner, Stuttgart, vol. 1, pp. 258–266 (1998)

[58] Krueger G: Java 1.1, Addison-Wesley, Bonn, pp. 5–7 (1997)

[59] Kuchling H: Taschenbuch der Physik, Harri Deutsch, Thun, pp. 653–654 (1989)

[60] Kuter D, Rosenberg R: Regulation of megakaryocyte ploidy in vivo in the rat. Blood, 75: 74–81 (1990)

[61] Lamerton L: Radiation biology and cell population kinetics. Phys Med Biol, 13: 1–14 (1968)

[62] Lamerton L, Pontifex A, Blackett N, Adams K: Effects of protracted irradiation on the blood-forming organs of the rat. Part I: Continuous exposure. Br J Radiol, 33: 287–301 (1960)

[63] Lepore D, Harris R, Penington D: Megakaryoblast precursors in rodent bone marrow: specificity of acetylcholinesterase staining. Br J Haematol, 58: 473–481 (1984)

[64] Loetter M, Heyns A, Badenhorst P, Wessels P, van Zyl J, Kotze H, Minnar P: Evaluation of mathematic models to assess platelet kinetics. J Nucl Med, 27: 1192–1201 (1986)

[65] Long M, Gragowski L, Heffner C, Boxer L: Phorbol diesters stimulate the development of an early murine progenitor cell - the burst-forming unit-megakaryocyte. J Clin Invest, 76: 431–438 (1985)

[66] Long M, Williams N: Immature megakaryocytes in the mouse: Morphology and quantitation by acetylcholinesterase staining. Blood, 58: 1032–1039 (1981)

[67] Mazur E, Arriaga M, South K, Cohen J: Polyploidization of human megakaryocytes in culture. In: Levine R, Williams N, Levin J, Evatt B (eds.), Prog Clin Biol Res, Megakaryocyte Development and Function, vol. 215, Alan R. Liss, New York, pp. 193–199 (1986)

[68] McIntosh J, McIntosh R: Mathematical Modelling and Computers in Endocrinology, Springer, Berlin, pp. 115–142 (1980)

[69] Messner H, Fauser A, Lepine J, Martin M: Properties of human pluripotent hemopoietic progenitors. Blood Cells, 6: 595–607 (1980)

[70] Metcalf D, Moore M: Haemopoietic cells. In: Neuberger A, Tatum E (eds.), Frontiers Of Biology, vol. 24, North-Holland Publishing Company, Melbourne, pp. 1–163 (1971)

[71] Mueller I: Zur Zytokinetik des Megakaryozytensystems von bestrahlten und unbestrahlten Ratten und des Menschen. Ph.D. thesis, Institut fuer Haematologie Freiburg i. Br. der Gesellschaft fuer Strahlenforschung mbH, Leiter: Prof. Dr. T.M. Fliedner, pp. 15–56 (1967)

[72] Nakahata T, Gross A, Ogawa M: A stochastic model of self-renewal and commitment to differentiation of the primitive hemopoietic stem cells in culture. J Cell Physiol, 113: 455–458 (1982)

[73] Neumann K, Morlock M: Operations Research, Hanser, Muenchen, pp. 536–584 (1993)

[74] Nothdurft W: Bone marrow. In: Scherer E, Streffer C, Trott K (eds.), Medical Radiology, Radiopathology of Organs and Tissues, Springer, Heidelberg, pp. 113–169 (1991)

[75] Odell T, Jackson C, Friday T: Megakaryocytopoiesis in rats with special reference to polyploidy. Blood, 35: 775–782 (1970)

[76] Odell T, Jackson C, Friday T, Charsha D: Effects of thrombocytopenia on megakaryocytopoiesis. Br J Haematol, 17: 91–101 (1969)

[77] Odell Jr. T, Murphey J: Effects of degree of thrombocytopenia on thrombocytopoietic response. Blood, 44: 147–156 (1974)

[78] Penington D, Olsen T: Megakaryoctes in states of altered platelet production: Cell numbers, size and DNA content. Br J Haematol, 18: 447–463 (1970)

[79] Pontifex A, Lamerton L: Effects of protracted irradiation on the blood-forming organs of the rat. Part II: Divided doses. Br J Radiol, 33: 736–747 (1960)

[80] Quesenberry P: Hemopoietic stem cells, progenitor cells, and cytokines. In: Beutler E, Lichtmann M, Coller B, Kipps T (eds.), Williams Hematology, McGraw-Hill, New York, pp. 211–228 (1995)

[81] Redfern D, Campbell C: Ordinary Differential Equations, Springer, New York, pp. 105–121 (1998)

[82] Schermer S: Blut und blutbildende Organe. Blut. In: Cohrs P, Jaffe R, Meessen H (eds.), Pathologie der Laboratoriumstiere, Pergamon Press, Oxford, pp. 176–235 (1958)

[83] Seed T, Fritz T, Tolle D, Poole C, Lombard L, Doyle D, Kaspar L, Cullen S, Carnes B: Survival patterns and hemopathological responses of dogs under continuous gamma irradiation. In: Broerse J, MacVittie T (eds.), Responses of Different Species to Total Body Irradiation, Martinus Nijhoff, Boston, pp. 137–159 (1984)

[84] Seed T, Kaspar L: Acquired radioresistance of hematopoietic progenitors (granulocyte/monocyte colony-forming units) during chronic radiation leukemogenesis. Cancer Res, 52: 1469–1476 (1992)

[85] Seed T, Tolle D, Fritz T, Cullen S, Kaspar L, Poole C: Haemopathological consequences of protracted gamma irradiation in the beagle. In: Late Biological Effects of Ionizing Radiation, International Atomic Energy Agency, Vienna, pp. 531–545 (1978)

[86] Selivanov V, Lanin V: Mathematical model of megakaryocytopoiesis. Ontogenez, 17: 270–277 (1984)

[87] Stein G: Zytologische Fruehveraenderungen der Knochenmarkzellsysteme bei Ratten nach einmaliger Roentgen-Ganzkoerperbestrahlung in Abhaengigkeit von

Zeit und Dosis. Ph.D. thesis, Zentrum fuer Klinische Grundlagenforschung der Universitaet Ulm, Leiter Prof. Dr. T.M. Fliedner, pp. 42–43 (1972)

[88] Stein G: Zytologische Fruehveraenderungen der Knochenmarkzellsysteme bei Ratten nach einmaliger Roentgen-Ganzkoerperbestrahlung in Abhaengigkeit von Zeit und Dosis. Ph.D. thesis, Zentrum fuer Klinische Grundlagenforschung der Universitaet Ulm, Leiter Prof. Dr. T.M. Fliedner, pp. 72–83 (1972)

[89] Stryckmans P, Cronkite E, Fliedner T, Ramos J: DNA synthesis time of erythropoietic and granulopoietic cells in human beings. Nature, 211: 717–720 (1966)

[90] Suda J, Suda T, Ogawa M: Analysis of differentiation of mouse hemopoietic stem cells in culture by sequential replating of paired progenitors. Blood, 64: 393–399 (1984)

[91] The MathWorks: NAG® Foundation Toolbox for Use with MATLAB® , The MathWorks INC., Natick MA, pp. i.1–i.10 (1995)

[92] The MathWorks: MATLAB® , The Language of Technical Computing, The MathWorks INC., Natick MA, pp. 1.1–1.9 (1998)

[93] The MathWorks: Optimization Toolbox for Use with MATLAB® , The MathWorks INC., Natick MA, pp. 1.1–1.2 (1999)

[94] The MathWorks: Using SIMULINK® , The MathWorks INC., Natick MA, pp. 1.1–1.15 (1999)

[95] Trinchieri G: The hematopoietic system and hematopoiesis. In: Knowles D (ed.), Neoplastic Hematopathology, Williams and Wilkins, Baltimor, pp. 1–25 (1992)

[96] Vassort F, Frindel E, Tubiana N: Effects of hydroxyurea on the kinetics of colony forming units of the bone marrow in the mouse. Cell Tissue Kinet, 4: 423–431 (1971)

[97] Vogel H, Niewisch H, Matoli G: The self-renewal probability of hemopoietic stem cells. J Cell Physiol, 72: 221–228 (1968)

[98] Wichmann H, Gerhardts M, Spechtmeier H: A mathematical model of thrombopoiesis in rats. Cell Tissue Kinet, 12: 551–567 (1979)

[99] Williams N, Jackson H: Regulation of the proliferation of murine megakaryocyte progenitor cells by cell cycle. Blood, 52: 163–170 (1978)

[100] Yeager A, Levin J, Levin C: The effects of 5-fluorouracil on hematopoiesis: Studies of murine megakaryocyte-CFC, granulocyte-macrophage-CFC, and peripheral blood cell levels. Exp Hematol, 11: 944–952 (1983)

Acknowledgements

This interdisciplinary work would not have been possible without the help of many people.

I would like to thank Prof. T.M. Fliedner for the continuous support and confidence in my work. I am especially grateful to Prof. Fliedner for all the fruitful and stimulating discussions, which opened my eyes to see mathematics from completely different perspectives.

I would like to thank Prof. H. Wolff for his uncomplicated support and for finding the time for refreshing discussions, in addition to his numerous responsibilities as the head of the University of Ulm.

Further, I would like to thank Prof. L. Feinendegen for his constructive discussions of the assessment of excess cell loss based on the dosimetric background and for his continous encouragement.

For the support regarding the biological background of radiation effects I would like to thank Prof. W. Nothdurft.

The Research Institute for Applied Knowledge Processing (FAW) at the University of Ulm contributed in many ways to this thesis. I would like to thank especially Prof. F. Radermacher, Mr. P. Spiertz, Dr. T. Rose, and the infrastructure team of the FAW for providing an excellent working environment.

For the continous support I would like to thank my past and present colleagues of our project team: Carola, Christian, Colette, Conny, Dirk, Evelyn, Hauke, Iris, Knut, Melanie, Robert, Steffie, Viola, and Yilmaz.

Special thanks I would like to tell to all the people at the FAW, who made life and work a pleasure, especially the 10.00 o'clock coffee club: Anja and Susi (ladies first!), and Harald.

For his support in writing this thesis and the discussions regarding all areas of life I would like to thank Ralf.

Last, but not least I would like to thank my family, including uncle Hans, for making this thesis possible.